

**Estimation of Reservoir Properties from Seismic
Attributes and Well Log Data using Artificial
Intelligence**

BY

MOHAMED SITOUAH

A Thesis Presented to the
DEANSHIP OF GRADUATE STUDIES

KING FAHD UNIVERSITY OF PETROLEUM & MINERALS

DHAHRAN, SAUDI ARABIA

In Partial Fulfillment of the
Requirements for the Degree of

MASTER OF SCIENCE

In

GEOPHYSICS

June 2009

Estimation of Reservoir Properties from Seismic Attributes and Well Log Data using Artificial Intelligence

By

MOHAMED SITOUAH

A Thesis Presented to the
DEANSHIP OF GRADUATE STUDIES
KING FAHD UNIVERSITY OF PETROLEUM & MINERALS
DHAHRAN, SAUDI ARABIA
In Partial Fulfillment of the
Requirements for the Degree of

MASTER OF SCIENCE

In
GEOPHYSICS


June 2009

KING FAHD UNIVERSITY OF PETROLEUM AND MINERALS
DHAHRAN 31261, SAUDI ARABIA
DEANSHIP OF GRADUATE STUDIES

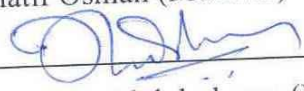
This thesis, written by Mohamed Sitouah under the direction of his thesis advisor and approved by his thesis committee, has been presented to and accepted by the Dean of Graduate Studies, in partial fulfillment of the requirements for the degree of MASTER OF SCIENCE IN GEOPHYSICS

Thesis Committee



Prof. Gabor Korvin (Advisor)

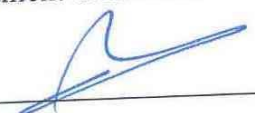

Dr. Abdulatif Al-Shuhail (Co-Advisor)


Dr. Abdulatif Osman (Member)


Dr. Abdulazeez Abdulraheem (Member)


Dr. Azedine Zerguine (Member)


Dr. Abdulaziz Al-Shaibani
Department Chairman


Dr. Salaam Zummo
Dean of Graduate Studies

18/14/09
Date

Dedicated

To my Loving Parents and my loving wife

ACKNOWLEDGEMENT

All gratitude belongs to Almighty Allah SWT the lord of the universe, who teaches man what he knows not. I thank Allah for having spared my life over the years and for bestowing on me His uncompromising blessings.

First, I like to acknowledge the opportunity given to me by King Fahd University of Petroleum and Minerals and especially Department of Earth Sciences to pursue my master degree in a harmonious environment with state-of the-art facilities.

My thanks are due to Dr.Al-Shaibani the Chairman of ESD, for his support and help.

My immense appreciation and gratitude goes to my thesis advisor Prof. Gabor. Korvin and co-advisor Dr. Abdulatif Al-Shuhail, for their guidance, encouragement and support during the research. Most important of all were their enthusiastic approach towards research and their readiness and eagerness to help me at any times. Additionally their innovative thinking and valuable suggestions greatly inspired me. I thank them, as they are indeed not only advisors but fathers to reckon with.

My sincere gratitude is due to my thesis committee members: Dr.Abdulatif. Osman, Dr. Abdulazeez. AbdulaReheem and Dr. Azedine. Zerguine. Their constructive and positive criticism and suggestions were extremely helpful and an immense privilege.

I also want to acknowledge the support and suggestions of my friends and colleagues: Maamer Al-Djabri, Ali Al-Rayeh and Fayçal Belaid.

TABLE OF CONTENTS

DEDICATE.....	iii
ACKNOWLEDGMENT.....	iv
TABLE OF CONTENT.....	v
LIST OF TABLES.....	ix
LIST OF FIGURES.....	x
THESIS ABSTRACT	xv
ملخص الرسالة.....	xvii
CHAPTER ONE	
Introduction.....	1
1.1 Overview	1
1.2 Problem Statement	3
1.3 Thesis Objectives.....	4
1.4 Thesis Organization	4
1.5 Literature review.....	5
CHAPTER TWO	
Geological Setting of Study Area	7
2.1 Overview	7
2.2 Regional Geological description of the basin	9
2.2.1 The Southern accident atlas:.....	9
2.2.2 The Paleozoic of the Sahara:	9
2.2.3 The Lower and the Middle Jurassic (Lias-Dogger).....	9
2.2.4 The Upper Jurassic.....	10
2.2.5 The Lower Cretaceous.....	11
2.2.5.1 Barremian.....	11
2.2.5.2 Aptian.....	11
2.2.5.3 Albian.....	11
2.2.5.4 Cenomanian.....	12
2.2.5.5 Turonian.....	12
2.2.5.9 Eocene.....	13
2.2.5.10 The Quaternary	13

2.3 Local geological framework.....	16
2.4 The Geological Structure of the Study Area	18
2.5 Geological History of the Study Area	19
2.6 The characteristics of the Source Rock.....	20
2.7 Sedimentary facies Analysis	23
2.7.1 Fluvial-channel lag deposit	24
2.7.2 Point bar deposit.....	24
2.7.3 Channel bar sedimentary	24
2.7.4 Over bank deposit.....	25
2.7.5 Crevasse splay deposit	25
2.8 Reservoir Properties.....	25
2.9 Cap rock characteristics	30
2.10 Migration System	31
CHAPTER THREE	
3.1 Introduction	32
3.2 Definitions	32
3.4 Classification of Seismic Attributes	34
3.4.1 Geometrical attributes (reflection configuration).....	34
3.4.2 Physical attributes (reflection characteristics)....	35
3.4.3 Pre-stack Attributes	35
3.4.5 Instantaneous Attributes.....	36
3.4.7 Reflection Attributes	36
3.4.8 Transmissive Attributes	36
3.5 Hilbert Transform.....	38
3.5.1 Definition of the Hilbert Transform	38
Figure 3.2 Hilbert Filter.....	39
3.5.2 Properties of Hilbert Transform	39
3.5.3 Discrete Hilbert Transform	40
Figure 3.3 Impulse Response of Hilbert Transform	43
3.6 Computation of Seismic Attributes.....	44
3.6.1 Formulation of Seismic Attributes	45
CHAPTER FOUR	
Artificial Neural Networks.....	52

4.1 Definition	52
4.2 Historical background of Neural Networks.....	52
4.2 Comparison between Artificial neurons and Human.....	56
4.3.1 a simple neuron	57
4.3.2 Firing rules	58
4.3.3 How the firing rule works	59
4.4 Neural network structure	60
4.4.1 Feed-forward networks	61
4.4.2 Adaptive networks	62
4.5 The Mathematical Model (figure 4.5)	64
4.6 Multilayer Perceptron Neural Network (MLP)	70
4.6.1 The Network Performance	75
4.6.2 Testing (Generalizing).....	76
4.6.3 Advantages and disadvantages of MLP	77
4.7 General Regression Neural Networks.....	79
4.7.1 Advantages and disadvantages of GRNN	83
CHAPTER FIVE	
5.1 Overview	84
5.2 DATA ANALYSIS	85
5.3 Experimental Results Using Multilayer Perception and General Regression Neural Networks	87
5.3.1 Porosity Estimation Results From Well Logs.....	87
5.3.2 Permeability Estimation Results From Well Logs	92
5.3.3 Porosity Estimation Results From Seismic Attributes.....	97
5.3.4 GRNN MODEL FOR POROSITY	107
5.3.5 GRNN MODEL FOR PERMEABILITY	109
5.4 Predicting Porosity and Permeability using Well logs and Seismic Attributes.....	111
5.4.1 GRNN MODEL FOR POROSITY	112
5.4.2 GRNN MODEL FOR PERMEABILITY	115
5.5 Prediction of Lithofacies Using ANNs.....	117
Figure 4.14b Facies Predictions using ANNs.....	118
5.6 Predicting the Spatial Distribution of Porosity, Permeability and Lithofacies	119

5.6.1 Porosity Models	120
5.6.2 Permeability Models.....	122
5.6.3 Lithofacies models	124
CHAPTER SIX	
6.1 Summary.....	128
6.2 Conclusions	129
References	131

LIST OF TABLES

Table 2.1: The main reservoirs in the study area and their Properties.....	26
Table4.1: The truth table.....	59
Table 5.1: Statistics of the combined wells 1 and 2 (Training set).....	86
Table 5.2: Statistics of the combined wells 1 and 2 (Testing set).....	86
Table 5.3 Results Summary for MLP and GRNN models.....	96
Table 5.4 Statistical Properties of the Seismic Attributes (Training set).....	97
Table 5.5 Statistical Properties of the Seismic Attributes (Testing set).....	97
Table 5.6 Statistical Analysis for Seismic and Logs (Training data).....	111
Table 5.7 Statistical Analysis for Seismic and Logs (Testing data).....	112

LIST OF FIGURES

Figure 2.1: Satellite Image of the Study area.....	7
Figure2.2: Geographical Map of the Study Area.....	8
Figure 2.3: Origin of Sands of Lower Cretaceous.....	10
Figure 2.4: Regional geological Map showing the geological time of each zone.....	14
Figure 2.5: Stratigraphic Colum of the Northeast of Sahara showing the main lithology in each stage.....	15
Figure 2.6: Maturation in the Lower Silurian Radioactive Clays.....	22
Figure 2.6 b: TOC Distribution in the Lower Silurian Radioactive Clays.....	23
Figure.2.7a: Porosity Distribution within lower Ordovician.....	27
Figure 2.7 b. Porosity Distribution within upper Ordovician.....	28
Figure 2.7c: Porosity distribution within Triassic.....	29
Figure 2.8: Distribution of Clay & Evaporate deposits from Triassic & Liassic.....	31
Figure 3.1: Seismic attributes Classification.....	37
Figure .3.2: Hilbert Filter.....	39
Figure 3.3: Impulse response of Hilbert Transform.....	43
Figure.4.1: Comparison between Artificial neurons and Human neurons.....	57

Figure 4.2: a simple neuron	58
Figure 4.3: Feed Forward Networks Structure.....	61
Figure 4.4: Supervised Learning Scheme	64
Figure 4.5: Mathematical model of ANNs	65
Figure 4.6: Pure linear function.....	67
Figure 4.7: Threshold function.....	68
Figure 4.8: Sigmoid Function	69
Figure 4.9: Tangent Hyperbolic Function for $a=1$	70
Figure 4.10: Multilayer Perceptron with two hidden layers.....	71
Figure.4.11 Typical GRNN architecture.....	79
Figure.4.12: Radial Basis Transfer Function for one input.....	81
Figure.4.13: Radial Basis Transfer Function for multi inputs.....	82
Figure 5 .1a: Training core porosity vs predicted porosity using MLP.....	88
Figure 5.1b: Testing core porosity vs predicted porosity using MLP.....	89
Figure 5.2a: Training core porosity vs predicted porosity using GRNN.....	90
Figure 5.2b: Testing core porosity vs predicted porosity using GRNN.....	91
Figure 5.3a: Training core permeability vs predicted permeability using MLP.....	93
Figure 5.3b: Testing core permeability vs predicted permeability using MLP.....	94

Figure 5.4a: Training core permeability vs predicted permeability using GRNN.....	95
Figure 5.4b: Testing core permeability vs predicted permeability using GRNN.....	96
Figure 5.5: Base map of the study area.....	98
Figure 5.6: 3D Seismic Volume of the study site.....	99
Figure 5.7: Top of T1 on base map.....	100
Figure 5.8a: 3D Volume of Instantaneous Frequency.....	101
Figure 5.8b: 3D Volume of RMS amplitude.....	102
Figure 5.9a: Time slice of the Instantaneous Frequency at 2ms.....	103
Figure 5.9b: Time slice of the Instantaneous Frequency at 8ms.....	103
Figure 5.9c: Time slice of the Instantaneous Frequency at 12ms.....	104
Figure 5.9d: Time slice of the Instantaneous Frequency at 20ms.....	104
Figure 5.10a: Time slice of the Instantaneous Phase at 2ms.....	105
Figure 5.10b: Time slice of the Instantaneous Phase at 6ms.....	105
Figure 5.10c: Time slice of the Instantaneous Phase at 10ms.....	106
Figure 5.10d: Time slice of the Instantaneous Phase at 12ms.....	106
Figure 5.11a :Training core porosity vs predicted porosity using GRNN.....	107
Figure 5.11b :Testing core porosity vs predicted porosity using GRNN.....	108
Figure 5.12c :Training core permeability vs predicted permeability using GRNN.....	109
Figure 5.12d: Training core permeability vs predicted permeability using GRNN.....	110

Figure 5.13a Training core porosity vs predicted porosity using GRNN (Logs + Attributes).....	113
Figure 5.13b Testing core porosity vs predicted porosity using GRNN (Logs + Attributes).....	114
Figure 5.13c Training core permeability vs predicted permeability using GRNN (Logs + Attributes).....	115
Figure 5.13d: Testing core permeability vs predicted permeability using GRNN (Logs + Attributes).....	116
Figure 5.14a: Facies Description of Well-1 and Well-2.....	117
Figure 5.14b: Facies Predictions (in column # 4) using ANNs.....	118
Figure 5.15: Seismic Interpretation of T1, SI and Dev reservoirs in the study area.....	119
Figure 5.16a: Histogram of the porosity distribution.....	120
Figure 5.16b: Porosity distributions in the 3D model for SI reservoir.....	121
Figure.5.16c: Porosity (10% - 30 %) distribution in the 3D model for SI reservoir.....	121
Figure 5.17 Histogram of permeability distribution.....	122
Figure 5.17 a. Permeability Distribution in 3D model for SI reservoir.....	123
Figure 5.17b: Permeability (10-300 mD) distribution for SI reservoir.....	123
Figure 5.18: Histogram of facies distribution	124
Figure 5.18a: Facies model of SI and Dev reservoirs.....	125
Figure 5.18b: Channel lag distribution for SI Reservoir	126
Figure 5.18.c. Point bar distribution for SI Reservoir	126
Figure 5.18d: Over bank distribution for SI Reservoir	127

THESIS ABSTRACT

NAME: Mohamed Sitouah

TITLE OF STUDY: Estimation of Reservoir Properties from
Seismic Attributes and Well Log Data
Using Artificial Intelligence

MAJOR FIELD: Geophysics

DATE OF DEGREE: June, 2009

Permeability, Porosity and Lithofacies are key factors in reservoir characterizations. Permeability, or flow capacity, is the ability of porous rocks to transmit fluids, porosity, represent the capacity of the rock to store the fluids, while lithofacies, describe the physical properties of rocks including texture, mineralogy and grain size. Many empirical approaches, such as linear/non-linear regression or graphical techniques. Were developed for predicting porosity, permeability and lithofacies. Recently, researches used another tool named Artificial Neural Networks (ANNs) to achieve better predictions. To demonstrate the usefulness of Artificial Intelligence technique in geoscience area, we describe and compare two types of Neural Networks named Multilayer Perception Neural Network (MLP) with back propagation algorithm and General Regression Neural Network (GRNN), in prediction reservoir properties from seismic attributes and well log data.

This study explores the capability of both paradigms, as automatique systems for predicting sandstone reservoir properties, in vertical and spatial directions. As it was expected, these computational intelligence approaches overcome the weakness of the standard regression techniques.

Generally, the results show that the performances of General Regression neural networks outperform that of Multilayer Perceptron neural networks. In addition, General Regression Neural networks are more robust, easier and quicker to train. Therefore, we believe that the use of these better techniques will be valuable for Geoscientists.

ملخص الرسالة

الإسم الكامل : محمد ستواح

عنوان الرسالة: تقدير خصائص المكامن من المعطيات السيزمية و بيانات الآبار باستخدام الذكاء الصناعي

التخصص: جيزفيزياء

تاريخ الشهادة: جوان ٢٠٠٩

المسامية، النفاذية والسحن الصخري هي عوامل رئيسية في تحديد خصائص المكامن. النفاذية ، أو تدفق القدرة ، هو قدرة الصغور لنقل السوائل ، المسامية ، تمثل قدرة الصخر لتخزين السوائل ، بينما السحن الصخري فهو وصف الخصائص الفيزيائية للخور من الملمس حجم الحبوب والمعادن . توجد الكثير من الطرق التجريبية للتنبأ بالنفاذية، المسامية و السحن الصخري ، مثل الانحدار الخطي و الانحدار اللاخطي و كذا الطرق البيانية. هذه الطرق أثبتت محدوديتها في هذا المجال عندما يتعلق الأمر بتنبأ خصائص المكامن الغير متجانسة حيث أن التغيرات في خصائص المكامن تجعل من الصعوبة بمكان التنبأ بخصائصه.

مؤخرا ، استخدم أداة أخرى للبحوث اسمها الشبكات العصبية الاصطناعية (ANNs) لتحقيق مستوى أفضل من التوقعات. لإثبات جدوى تقنية الذكاء الاصطناعي في مجال علوم الأرض ، قمنا بإجراء مقارنة بين نوعين من الشبكات العصبية النوع الأول يسمى (GRNN) و الثاني (MLP) .و ذلك باستعمال المعطيات السيزمية و تسجيل بيانات المكامن.

في هذا البحث تم تناول قدرة كلتا الشبكتين العصبيتين على تنبأ بعض خصائص المكامن البترولية كالمسامية، النفاذية و السحن الصخري. عموما نتائج هذه الدراسة أثبتت نجاعت و قدرة الشبكة العصبية المسماة (GRNN) على تنبأ خصائص المكامن و بدقة عالية تفوق تلك التي تم تقديرها باستعمال الشبكة الثانية المسماة (MLP) .بالاضافة

الى أن الشبكة العصبية (GRNN) أكثر سرعة و أكثر قوة. لهذا نعتقد أن استعمال هذه التقنيات المتطورة سيساعد أكثر في تطوير المكامن البترولية و يعطي نظرة أوضح للجیولوجیین و الجیوفیزیائیین في تقدير حركة السوائل داخل المكن.

CHAPTER ONE

Introduction

1.1 Overview

Reservoir characteristics can be divided into three groups: geological characteristics (structure and seal, lithology, diagenesis), engineering data (well spacing, well-bore integrity, etc.) and rock-fluid properties (porosity, permeability, resistivity, etc.), (see James and Lawrence , 2002). Porosity, permeability and lithofacies are key factors for reservoir modeling. Permeability is the ability of the porous rock to transmit fluid, it depends on the statistics of the pore throat diameters rather than of the pore size, and is related to effective porosity rather than the total porosity.

Lithofacies identification is a primary task in reservoir characterization; it is achieved by studying a combination of petrophysical and petrographical properties of the rock. In general, when core samples are taken from rocks, they are described and classified into categories called “Facies” or “Lithofacies”. Such lithofacies represent a well defined rock type (e.g. sandstone, limestone, dolomite, etc.). To build a 3D geological model for a reservoir, accurate knowledge of permeability, porosity and lithofacies is required. The best method to get accurate values for these three factors is to measure them directly in the laboratory; however, this method has some disadvantages: its high cost, being time consuming, and incomplete representation of the total depth range. For these reasons geologists often core only a few out of all

wells and even then only a small portion of the well. Geologists generally use a statistical approach, such as linear or non-linear multiple regressions (Wendt et al., 1981; Jensen et al. 1985) to correlate different reservoir properties (such as: porosity and permeability). In these approaches, a linear or non-linear relationship is assumed between permeability and other reservoir properties. However, these techniques have proved inadequate for certain geological problems like heterogeneous reservoirs (Moline and Bahr, 1995).

Recently, geoscientists have utilized methods of Artificial Intelligence (AI), especially Neural Networks (NNs), to predict reservoir properties. Neural Networks have been widely used in many fields of science and engineering (e.g. in economy to predict chaotic stock market behavior, or to optimize financial portfolios). In Petroleum Industry, Neural Networks have been used to predict fracture intensity (Boevner et al., 2003; Ouenes et al., 1998), for field development (Dorusamy, 1997), for litho-facies analysis (Tanmbasu et al., 2004), to predict irreducible water saturation (Goda et al., 2007), to predict drilling hydraulics in real time (Fruhworth et al., 2007), and for other purposes, such as to optimize hydraulic fracture designs, characterize oil and gas reservoirs, optimize drilling operation, interpret well logs, generate virtual magnetic resonance logs, and to select candidate wells for reservoir stimulation.

Artificial Neural Networks are powerful tools for modeling nonlinear, complex systems. They are distributive, parallel systems, very useful to deal with pattern recognition problems. They are able to predict complex relationships between several variables (e.g. between well log data and seismic attributes, permeability, porosity and rock types). However, Neural Networks are black-box models that use activation functions of a predefined form (but with parameters adjusted through learning) and a predefined

architecture (number of hidden layers, number of neurons in each layer), without duly considering the specific properties of the phenomena being modeled.

Computer scientists in the field of Machine Learning and Data Mining have found several alternative methods to get over the limitations of Neural Networks. One of the popular methods is Adaptive Neural Fuzzy Inference System (ANFIS), which is a new framework, dealing with prediction and classification problems.

1.2 Problem Statement

Permeability, porosity and rock types are important reservoir properties to build a 3D geological model. The best way to get information about these factors would be to measure them in laboratories, however this procedure is costly and time consuming.

Well log and core data are local measurements that may not reflect the reservoir behavior as a whole. In addition, well log data do not cover the whole area of the field whereas 3D seismic covers larger areas. Changes in the lithology and fluids result in changes in amplitude, wavelet shape, lateral coherence, and other seismic attributes. These attributes can provide information for the construction of reservoir models. Neural Networks for quantitative analysis of reservoir properties from well logs have been demonstrated in several practical applications (e.g. Huang et al., 1996; Huang and Williamson, 1997; Zhang et al., 2000; Helle et al., 2001), a simple and accurate alternative for converting well logs to common reservoir properties such as porosity and permeability. Multilayer perceptron (MLP) with back-propagation algorithm has been the popular tool for most practical applications over the last decade. However, one major problem encountered in the back-propagation algorithm is its slow convergence during learning and the local minima problem which may reduce the network performance.

Thus, to overcome the drawbacks of multi-layer perceptron neural networks, we are interested in designing and investigating some more adequate intelligent system techniques which have been proposed as an improvement to neural networks, and can be utilized in estimation of porosity and permeability.

1.3 Thesis Objectives

The main objective of this research work is to explore new techniques developed by computer scientist particularly neural networks to predict reservoir properties such as porosity, permeability and rock types in vertical and spatial directions from well log data and seismic attributes. This study aims to develop the best approach for the estimation of these properties. More specifically this work aims to achieve the following

1. Investigate and develop a multi layer perceptron (MLP) to estimate porosity and permeability from well log data.
2. Investigate the suitability of estimating porosity and permeability from well logs using general regression neural network (GRNN).
3. Compare the above two techniques and choose the better one.
4. Estimate porosity and permeability from seismic attributes using the selected algorithm.
5. Build a 3D model for the properties estimated by the selected neural network.

1.4 Thesis Organization

In the introductory Chapter one, I highlight the motivation behind this work. Chapter two describes the geological setting of the study area and the main reservoirs. Chapter three

deals with seismic attributes calculation and analysis. The main technique, neural networks are discussed in detail in Chapter four. In Chapter five I discuss the results provided by MLP and GRNN and investigate the performance of both techniques in estimating reservoir properties. Finally, conclusions and recommendations will be given in Chapter six.

1.5 Literature review

Porosity, permeability and lithofacies are very important factors in geological modeling. Many empirical approaches are available to estimate these reservoir properties such as linear/non-linear multiple regression. Recently, geoscientists benefited from the fast development in computer science, and used other, non standard approaches to solve complicated geological problems, related to reservoir heterogeneity (e.g.: permeability and lithofacies distributions). The following discussion focuses on the use of Artificial Neural Networks (NNs) in prediction reservoir properties.

Mohaghegh et al. (1991, 1997) designed a Neural Network model for permeability determination from well log data. Smith et al. (1991) used a distributed Neural Network to identify the presence of lithographic facies types in an oil well, using only the readings obtained by a log probe. Hsien-Cheng et al. (1991) presented a hybrid system consisting of three adaptive resonance-theory NNs and a rule-based expert system to identify lithofacies from well log data. Rogers et al. (1992) also determined lithology from well logs using NNs. Huang (1996) used NNs to predict permeability in a venture gas field offshore eastern Canada. Olson (1998) used NNs to predict porosity and permeability in a low permeability gas reservoir based on well log data. Garrouch et al. (1998) used a

back-propagation NN to estimate tight gas sand and permeability from porosity, mean pore size and mineralogical data. Tamhane (2000) presented an overview of soft computing technologies for reservoir characterization, including Neural Networks, fuzzy logic and evolutionary algorithms. Soto et al. (2000, 2001) developed an integrated concept of multi-variant statistical analysis, Neural Networks and Fuzzy Logic to predict reservoir properties on uncored wells. Jong et al. (2004) combined fuzzy logic and neural networks to predict reservoir porosity and permeability from well log data.

Tanwi et al. (2004) integrated core data and log data for facies analysis using NNs. Ferraz and Garcia (2005) made a comparative study of four different techniques: traditional discriminant analysis, neural networks, fuzzy logic and neuro-fuzzy system, to determine the rock's lithofacies. El-shafei and Hamada (2007) used NNs to identify the Hydrocarbon Potential of shaly sand reservoirs.

CHAPTER TWO

Geological Setting of Study Area

2.1 Overview

The study area is situated in the North East of the Algerian Sahara (Figures 2.1 and 2.2).

The exploration area is 4353.46KM² and its surface altitude is about 230M.



Figure 2.1 Satellite Image of the Study area (Google Earth)

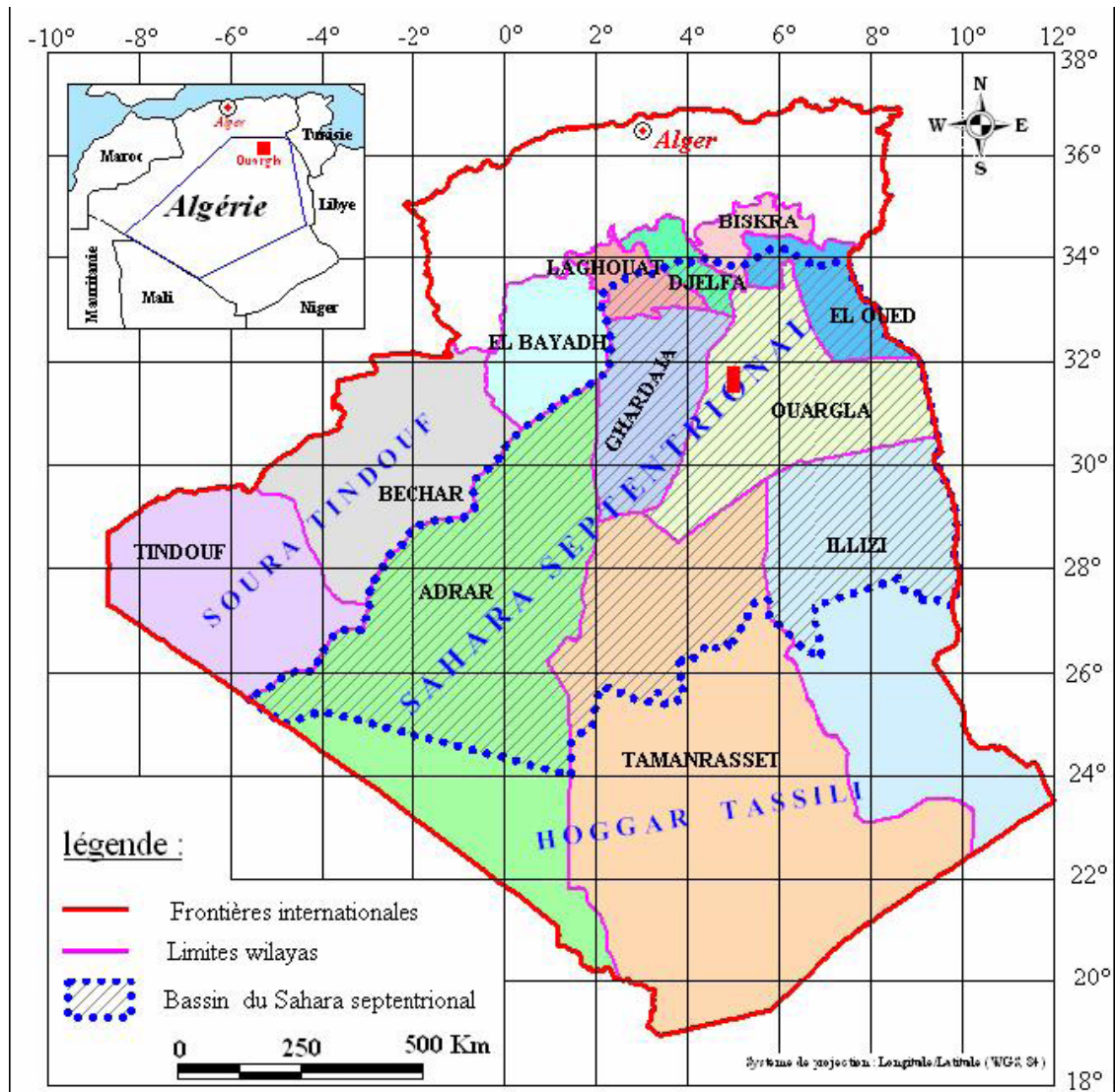


Figure2.2 Geographical Map of the Study Area (Bellaoueur.A, 2008)

2.2 Regional Geological description of the basin

There have been a great number of published articles and reports on the geology of the sedimentary basin of the Sahara (Busson, 1970; Conrad, 1969 and Dubief, 1959).

The study is located in the sedimentary basin of Oued Mya, North-Eastern Sahara, whose large geologic features are given below.

2.2.1 The Southern accident atlas:

It separates the Maghrebian mobile zone from the remainder of Western Africa. The rigid shield is made of sedimentary and eruptive, folded and metamorphosed rocks.

2.2.2 The Paleozoic of the Sahara:

It corresponds to the deposits of periglacial desert climate. Around the outcrops of the base, sandy and schist layers of Tassilis are staged. The Hercynian movements caused the erosion of the shield, then settled a great continental period during the Triassic (Busson, 1970). The Triassic is divided into large distinct lithological units which can be: salty, argillaceous, argilo-sandy or carbonate. The thickness of these various formations varies mainly where salty benches are intercalated. The thickness of Triassic shaly-sand increases towards the North-West (150-180 m) and decreases in the zones of Hassi Messaoud and R. El Baguel. Triassic has a thickness of 700 m in the N-E of Ghadamès and which reaches 1300 m in H. Messaoud.

2.2.3 The Lower and the Middle Jurassic (Lias-Dogger)

It consists of mainly evaporate layers primarily made up of salt, anhydrite and clays which are superimposed in marine layers and which are presented in the form of limestones and clays with anhydrite benches. The Middle Jurassic is characterized by a

transgression covering all the basin of the Great Eastern Erg and the deposits are thick there.

2.2.4 The Upper Jurassic

It is characterized by a relative permanence of the marine mode with sediments of confined surroundings. In the Western part of the basin, the marine mode shows a certain regression. The passage of the upper Jurassic to the lower Cretaceous is characterized by terrigenous contributions having for origin the feeder reliefs located at the South of the Saharan basin (Hoggar) (Figure.2.3) (Busson, 1970).

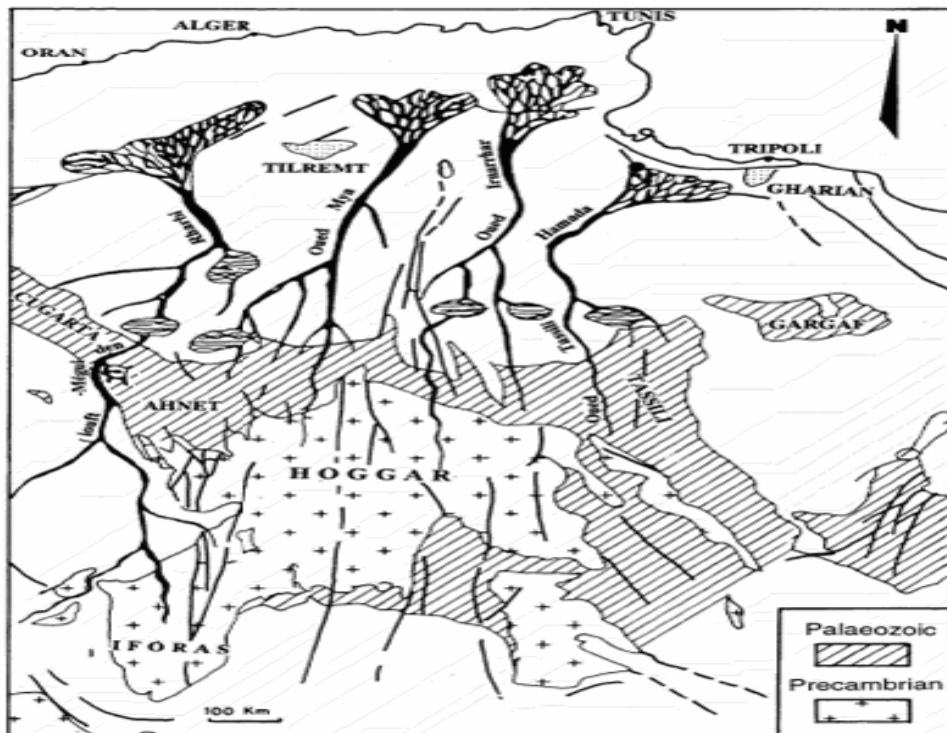


Figure 2.3 Origin of Sands of Lower Cretaceous (Ouaja, 2003)

2.2.5 The Lower Cretaceous

The study of core data (Busson, 1970) made possible to specify the succession of paleogeography in the lower Cretaceous. It consists of fluvio-deltaic layers which are in lithological and sedimentary contrast with the marine deposition of the upper Jurassic . It include the following:

2.2.5.1 Barremian

It is characterized by a spreading of the detrital formations of the Lower Cretaceous into the Low-Sahara. These formations arise in the form of fine to coarse sandstones and of clays coming apparently from the South (Hoggar) (Figure.2.3). The intercalations of carbonates are very few and confined in the North-East of the Algerian Sahara.

2.2.5.2 Aptian

It is a good lithological reference marker in the surveys. It is represented in most of the Low-Sahara, by 20 to 30 m of dolomite alternating with beds of anhydrite, clays and lignite.

2.2.5.3 Albian

It is characterized by a remarkable return of sedimentation. This stage gathers the mass of sands and clays lain between the Aptian bar and the overlying argillaceous horizon allotted to Cenomanian. It has been noticed that the change of the sedimentary mode and the arrival of clastic rock mass occurred during the Albian (Fabre, 1976).

2.2.5.4 Cenomanian

It is formed by an alternation of benches of dolomite, dolomitic limestone, clays and evaporates (anhydrite or salt).

Its facies varies:

- a- In the South of the basin, clays and evaporate.
- b- In North, the dolomite and limestone benches are dominant.

Moreover, the thickness increases along South-North direction from 50 m in Tademaït to 350 m in the Low-Sahara. The presence of many benches of evaporates and clays make Cenomanian sediments impermeable (Bel and Cuche, 1969). The lower and the middle Cenomanian are argillaceous in Tinrhert and Lower-Sahara, whereas the upper Cenomanian is a calcareous (Busson, 1970).

2.2.5.5 Turonian

It is presented in three different facies, from the South to the North:

- a- In the South of the parallel of El Goléa, it is marly-limestone
- b- Between El Goléa and Djamaâ, it is primarily calcareous.
- c- In the North of Djamaâ, it is again marly-limestone.

Its average thickness varies between 50 and 100 m. However, it increases in the area of the chotts, where it exceeds 300 m (Bel and Cuche, 1969).

2.2.5.6 Santonian

It subdivides into two facies. Lower Santonian with Laguna sedimentation characterized by argillaceous and salty formations with anhydrite, it is an impermeable formation (Busson, 1970). Upper Santonian, which is a permeable carbonated formation.

2.2.5.9 Eocene

from the lithological point of view, we distinguish between two different sets:

- a- **At the base:** The carbonated Eocene is formed primarily by dolomites and limestones with some intercalations of marls, clays and even of anhydrite and marls. The thickness of this formation varies between 100 and 500 m, the maximum thickness being in the zone of the Low-Sahara.
- b- **At the top:** The Eocene evaporitic is formed by an alternation of limestone, anhydrite and marls. Its thickness reaches a hundred meters under Chotts (Bel and Cuhe, 1969).

The Eocene constitutes the last marine episode of the Algerian Sahara (Busson, 1970).

2.2.5.10 The Quaternary

The continental Tertiary sector of the Sahara can be relatively thick (150 m). It is presented in the form of a sandy and argillaceous facies with gypsum. In the Lower-Sahara, (lacustrine sedimentation) is presented in the form of sandy and argillaceous series known as the Continental Terminal (Me-Pliocene) in which the thickness can reach, in the area of Chotts Algéro-Tunisian, a few hundred meters. We identify there, in the area of Oued Rhir, two aquiferous levels within sands which are separated by an argillaceous layer in the medium of Oued Rhir. The unit is overcome by Plio-Quaternary argilo-sandy and gypseous formations which results from medium sedimentation in lake during the phase of draining lagoons of the chotts (Busson, 1970).

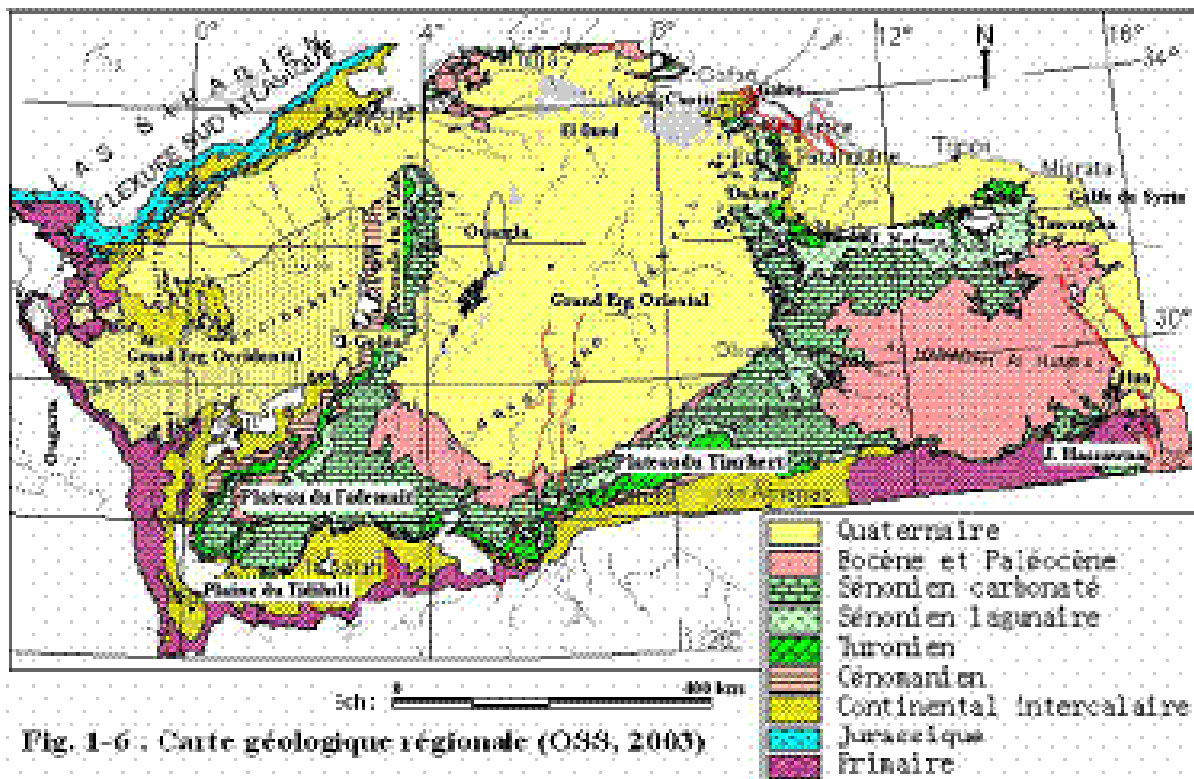


Figure 2-4 Regional geological Map showing the geological time of each zone

(OSS, 2003)

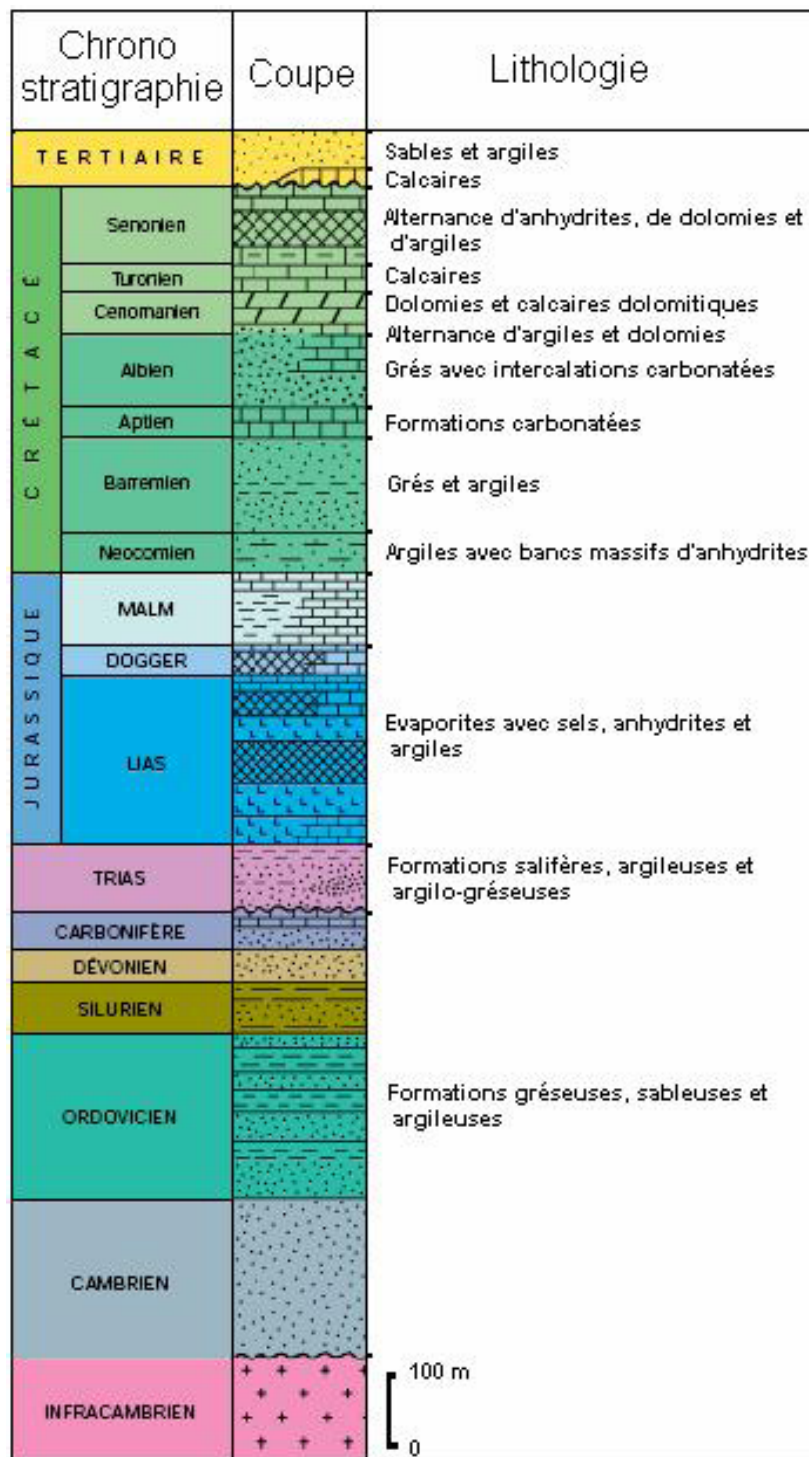


Figure 2.5 Stratigraphic Column of the Northeast of Sahara showing the main lithology in each stage ((Bellaoueur.A, 2008)

2.3 Local geological framework

The exploration area is 4353.46KM² and its surface altitude is about 230m. The surface slope of the block dips down from west to east, the central and west area are dunes and dune ridges, and the east is desert.

The seismic and drilling was started in 1970's. Now there are 7900km² 2D-seismic and 266km² of 3D seismic data. Totally there are 62 wells drilled in this block, from among them 20 are production wells. The oil fields were discovered between 1970 and 1984, with a daily oil production of 624 m³/d (3925bbl/d).

According to the regional geological analysis and drilled formations in this basin the strata sequence is Precambrian basement, Palaeozoic Cambrian (which is constituted by one set of volcanic and meta sandstone with stable sedimentary facies), marine facies sandstone and mudstone of Ordovician, clay shale of Silurian, sand-shale interbedding of Devonian; sandstone/shale/gypsum-salt rock of Triassic in Mesozoic, gypsum-salt rock/calcareous rock with shale of Jurassic, sandstone/calcareous rock/gypsum rock of Cretaceous; the development of Cenozoic is not entire, it is mainly sand-mud rock of Miocene and Pliocene of Tertiary. The main targets of exploration are Triassic, Devonian and Ordovician.

The Triassic

It has been divided into 6 layers from bottom to top.

1. SI: interbedding of fine to medium sandstone with maroon and celadon mudstone.

2. Volcanic effusive rock: andesite, basalt.
3. T1: consists of gray and maroon fine-to medium sandstone, its bottom contains granules; the maroon barrier bed on its top is split from T2. It is the production layer of this area.
4. T2: consists of brown and crimson-pearl silt and fine sandstone, its top is pelite siltstone.
5. Argillaceous: mainly maroon mud stone.
6. S4: interbedding of white and pink salt rock with maroon and celadon mud stone.

From the cross plane of well, the longitudinal distribution character of Triassic strata shows the trend of gradually thickening from west to east, and sharply thinning from south to north. The thickness of SI in Triassic changes between 12-96m, the northwest is thicker than the southeast part and in the central part of this Block, the thickness distribution is more stable, generally between 70-80m. The thicknesses of volcanic effusive rock changes between 0-110m, its distribution characteristic shows that the southern part is thicker than the northern part. The thickness of T1 in Triassic changes between 0-78m, its northern thickness is larger than of the southern part. Note the absence of T1 in well-4B and well-5. The thickness of T2 in Triassic changes between 9-66m and its thickness distribution shows more stability in the central and the eastern area, and it increases to northwest.

The thickness of the Devonian changes between 9-66m, and its thickness distribution shows that the thickest part is located along the well-5 well-1 Line and the strata sharply thin down to the east.

2.4 The Geological Structure of the Study Area

This block is geographically located in the north of OUED MYA Basin with more flattening stratum and simple structure. Tectonically, this basin is located in the North Africa platform. The structural system with SSW-NNE trend controls the areal structure unit. Because of the Hercynian uplift, the strata of Paleozoic have been eroded. The structure system trending SSW-NNE was formed by the Australian compression structure movement in the end period of Lower Cretaceous. That movement controls the distribution of structural traps. All the monoclines in this area are distributed from Southwest to East North and show the complication caused by two set of fractures trending in North East and East West.

Interpretation of 237 profiles indicated the existence of the structures below:

The top Triassic (S4), bottom Triassic (Hercynian surface SI), lower Ordovician (O).

32 traps have been discovered in this area, 27 traps confirmed and 5 new traps discovered. The structural traps are mainly attached with fracture belt, and show the distribution in form of pinch-and-swell. I list below some of the structures which are traversed by wells.

Well-4 Structure

It is a fault anticline structure with drilling history. Its south and east regions are sheltered by the normal faults trending NE and NW and the structure appears clearly on the 2D

seismic profiles LINE97-NGS-2 and LINE97-NGS-6. Now there are 11 controlled survey lines, and 3 wells were drilled, out of which 2 wells have oil production history.

Well-5 Structure

It is an anticline structure with drilling history. Its east region is sheltered by a normal fault trending NE; the axial direction is NE-SW and the structure is shown clear on the 2D seismic profiles LINE97-NGS-1 and LINE97-NGS-10. Now there are 14 controlled survey lines, and 5 wells were drilled, 4 having oil production history.

Well-1B Structure

This trap is located to the south of Well-1B with distance of 2Km, its eastern region is sheltered by the north south fault and its south is sheltered by the east fault, thereby it forms a faulted anticline and its structural area is about 6.17Km^2 , the structural ~~amplitude~~ closure is about 30ms two-way time.

2.5 Geological History of the Study Area

Sedimentary evolution of this area is a marine and continental facies. Sedimentary association developed from Precambrian basement which consists mainly of volcanic rocks and metamorphic quartz sandstone in Precambrian. This area was an open sea deposition during Ordovician and Silurian periods, mainly developed marine facies (quartz sandstone, mudstone and shale). Mudstone and shale developed from lower Silurian is the main hydrocarbon source rock in this area. Sea water gradually shrunk during Devonian period, developed a neritic shelf facies deposition; after that, the strata uplifted and suffered from erosion due to Hercynian uplift. In Carboniferous, Permian, this area integrally sank and undertook sedimentation, mainly of fluvial type. The

direction of main source material is SW—NE. The Devonian formation and overlying Triassic formation present an unconformable contact.

2.6 The characteristics of the Source Rock

The main source rock in the study area is the hot shale mudstone and shale in lower Silurian. Its distribution keeps stable in the whole area, with a thickness of 40—60m . Hot shale mudstone and shale (radioactive black shale) contain high abundance of organic matter (TOC, generally about 4—10%). The kerogen is of type-2 which leads to oil generation.

The lower Silurian clays are essentially grey to black clays, radioactive at the base. They are present over the whole Saharan Platform. At a few places they have been removed away by the Hercynian erosion phases (Figure 2.6a). The radioactive clays were deposited immediately after the late Ordovician glacial period and correspond to the first significant Paleozoic marine transgression. Radioactivity is mainly due to a high uranium concentration. Thicknesses vary from 10 m to 100m with the maxima located in the basins of Ahnet, Ghadames, Illizi, Oued Mya, Mouydir, to the north of Timimoun Basin (Guern El Mor trough) and in the Benoud and Sbaa troughs (Figure 2.6 b). The total organic carbon (TOC) varies from 1% to 11% but reaches 20% in some cases. The richest zones are located in the vicinity of Hassi Rmel and Hassi Messaoud structures, in the north-east of the Triassic province (El Borma and north of Ghadames Basin), to the west of Illizi Basin, in the Sbaa trough and in the NE of the Grand Erg occidental. Organic matter is of marine origin (algae, chitinozoa, graptolites; amorphous sapropelic organic matter). The resulting source rock is of excellent quality and its hydrocarbon potential is often in excess of 60 Kg HC/t as it is the case for the lower Silurian formations of the

Saharan Platform The separate evolution of each basin means that residual hydrocarbon potentials vary from basin to basin. They are controlled by the state of maturation reached in the radioactive clays. Kerogen maturation is the gas window (dry gas and condensate) for the basins of Timimoun, Ahnet, Bechar and Mouydir, in the central and northern parts of the Reggane and Tindouf Basins, in the centre of Ghadames Basin and Oued Mya , and in the centre and the NW of the Sbaa trough. In other parts the same kerogen is in the oil window, as in the rest of the Triassic province, in Illizi Basin, in the south of the Reggane and Tindouf basins, in the east of Reggane in the vicinity of Ougarta and finally in the SE of the Sbaa trough. In other cases the kerogen is not mature (for example: in the south east of the Sbaa trough close to the Azzene uplift).

The mudstone and shale of the upper Ordovician is considered as a source rock for this basin. Its organic matter content (TOC) is about 1-5%. The lower Ordovician (Shal d'Azel and d'El Gassi) can also be considered as a source rock.

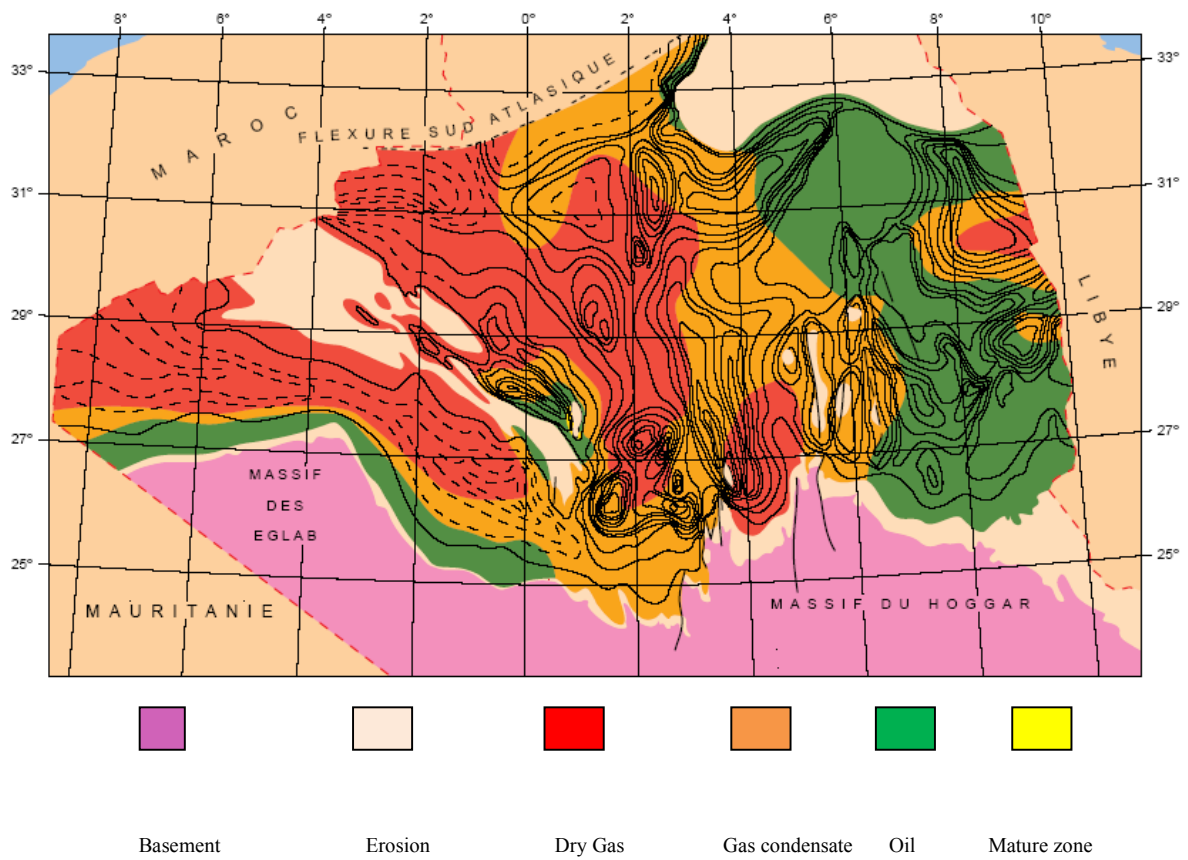


Figure 2.6 Maturation in the Lower Silurian Radioactive Clays (Geology of Algeria)

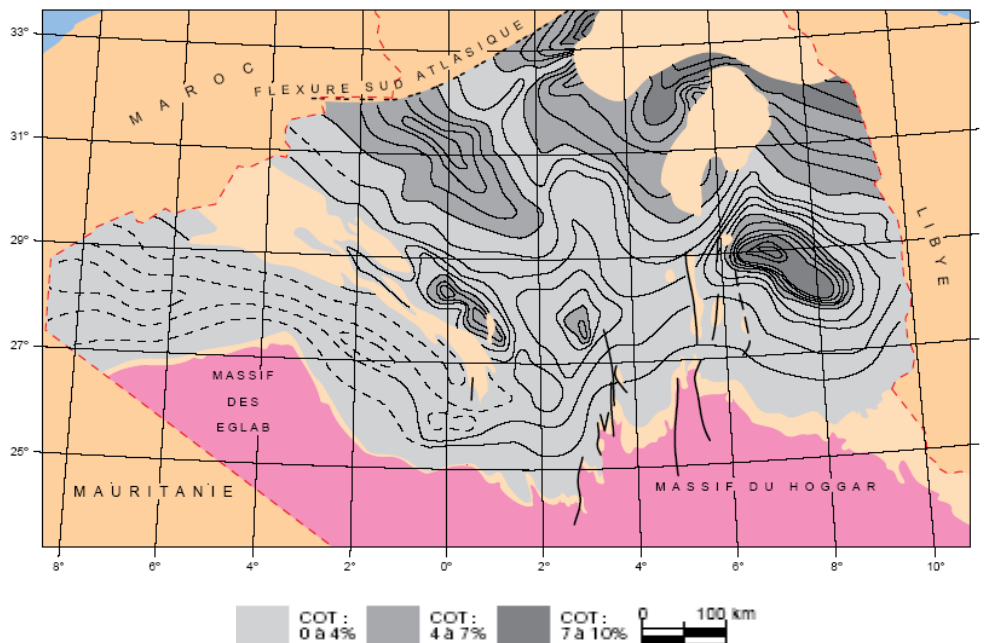


Figure 2.6 b. TOC Distribution in the Lower Silurian Radioactive Clays (Geology of Algeria)

2.7 Sedimentary facies Analysis

From bottom to top, sedimentary cap rock in this area is composed of deep, shallow sea and continental facies strata. In Ordovician, marine sedimentary facies are mainly quartz sandstone, mudstone and shale. Mudstone and shale are the main hydrocarbon source rocks. The reservoir in this area is buried deeply and its porosity is low. Its lithology is relative compact, so the effective reservoir storage place is formed only by fractures. Lower Devonian (under Hercynian unconformity), is a neritic shelf fades sedimentary, its thickness ranges from 0 to 239m. Reservoir lithology in the Devonian is medium to fine grained sandstone, with porosity 4—20 % (average 12 %) and low permeability is 0.03 — 100 md.

In Silurian, marine sedimentary facies mainly consist of a stable distribution of mudstone, dolomitic mudstone and argillaceous limestone.

In this area, Triassic is the main target layer and it is deposited in fluvial environment. According to layer's color, depositional structure, lithology assembly and electrical characteristics the classification can be as follows:

1. **SI layer:** It is mainly braided river sedimentation, it can be divided into over bank deposit, channel bar sedimentary, fluvial-channel lag deposit.
2. **T1, T2 layers:** They are meandering river sedimentary, they can be divided to point bar deposit, over bank deposit, crevasse splay deposit and fluvial-channel lag deposit.

2.7.1 Fluvial-channel lag deposit

It is medium to fine grained sandstone interbedded by argillaceous siltstone. Degree of roundness is high. Gamma ray (GR) values range 20-160 API and resistivity response shows large values, generally from 1 to 30Ω.m, resistivity curve appears as zigzag.

2.7.2 Point bar deposit

It is meandering river sediments with medium to fine grained sandstone. The degree of roundness is high. Gamma ray (GR) values range 30-50 API, resistivity value is low, generally from 3 to 10Ω.m, resistivity curve is zigzag.

2.7.3 Channel bar sedimentary

It is braided river sedimentation with medium to fine grained sandstone. The degree of roundness is high. Gamma ray (GR) values range 20-40 API with high resistivity, generally from 10 to 50Ω.m. Resistivity curve is shown as zigzag or bell shape. Sand body maturity of this sedimentary micro-facies is high, this sedimentary formation is the

main reservoir.

2.7.4 Over bank deposit

It is mudstone and silty mudstone, frequently has a massive structure, parallel and small-sized cross bedding. Gamma ray (GR) values range 70-120 API with low resistivity values, generally from 1 to 4 Ω m. Resistivity curve is box shaped

2.7.5 Crevasse splay deposit

It is an argillaceous siltstone, silty mudstone, with little sandstone at the bottom. Frequently shows massive structure, sometimes shows parallel and small-sized cross bedding. Gamma ray (GR) value is high, from 60 to 100 API with large resistivity values range, generally from 2 to 100 Ω m. Resistivity curve is dentate.

2.8 Reservoir Properties

The main reservoirs (T1, TSI, Lower Devonian, Upper and Middle Ordovician) with their properties are summarized in the table below.

Table1.The main reservoirs in the study area and their properties.

Reservoir		Thickness	Lithology	Porosity and Permeability
Triassic	T1, sandstone	<75	medium to fine sandstone	Φ : 2~17 % (average=10 %) K: 0.1~300md (max500md)
	TSI Sandstone	<95	coarse to fine Sandstone	Φ : 1~14 % (average= 8 %) K: 0.04~200md(max800md)
Lower Devonian		<240	medium to fine Sandstone	Φ : 4~20 % (average= 12 %) K:0.03~100md(max200md)
Upper Ordovician		<20	Quartz sandstone	Φ : 2~10 % (average= 6 %) K: 0.02~3md(100md)
Middle Ordovician		150	Quartz sandstone	Φ : 2~11 % (average= 7 %) K: 0.03~8md(max200md)

Figures 2.7a , 2.7b and 2.7 c illustrate porosity distribution within the lower Devonian , the upper Devonian and Triassic reservoirs in the Sahara platform (south of Algeria)

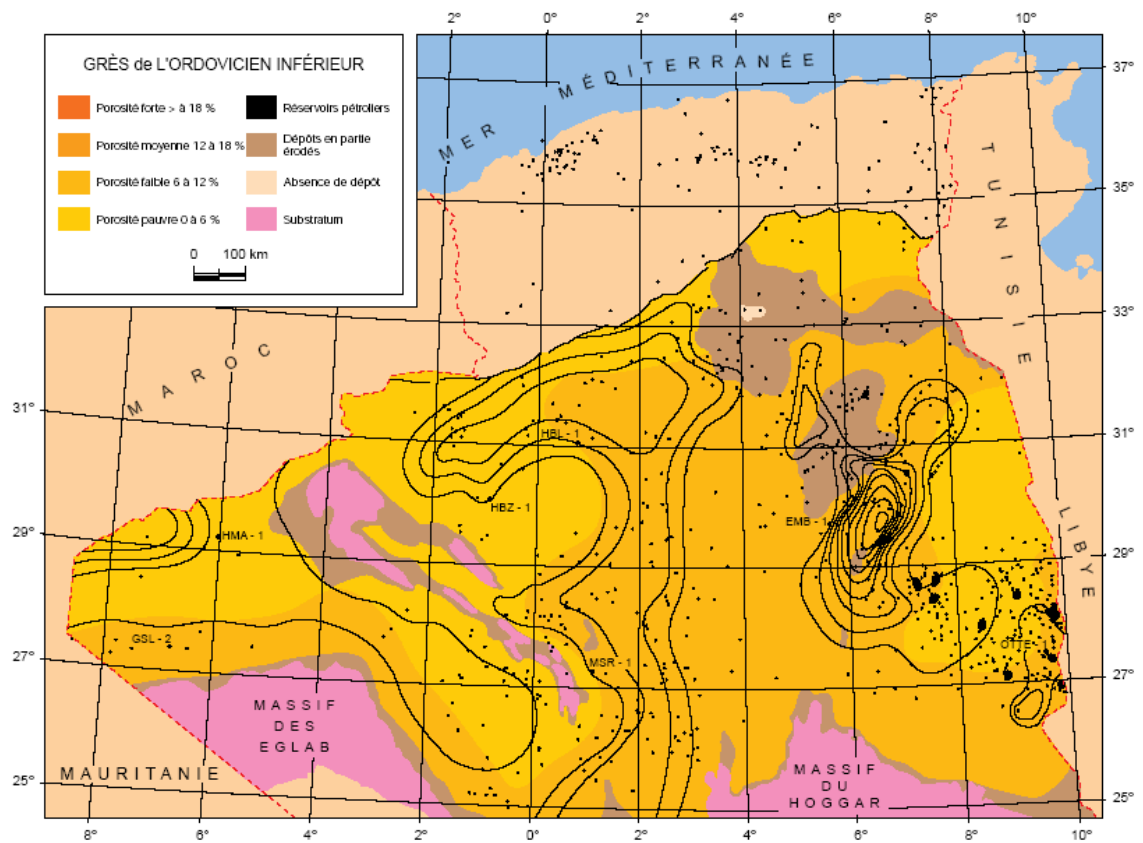


Figure.2.7a. Porosity Distribution within lower Ordovician (Geology of Algeria)

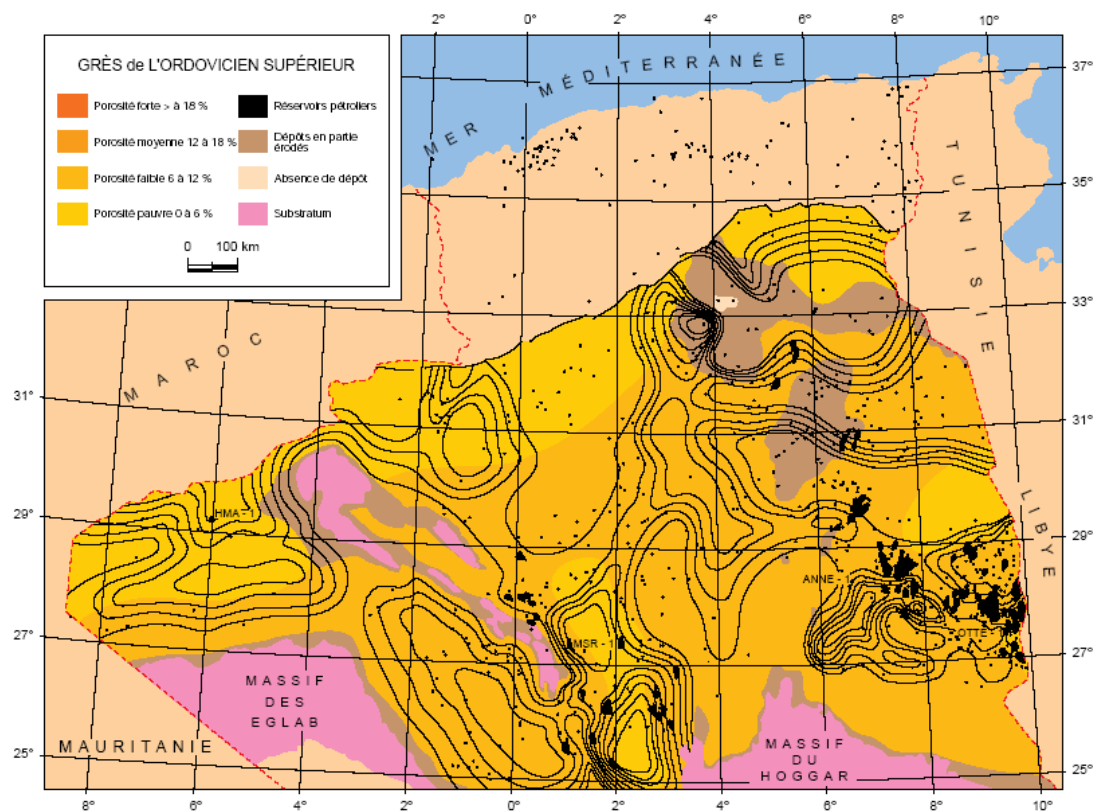


Figure 2.7 b. Porosity Distribution within upper Ordovician (Geology of Algeria)

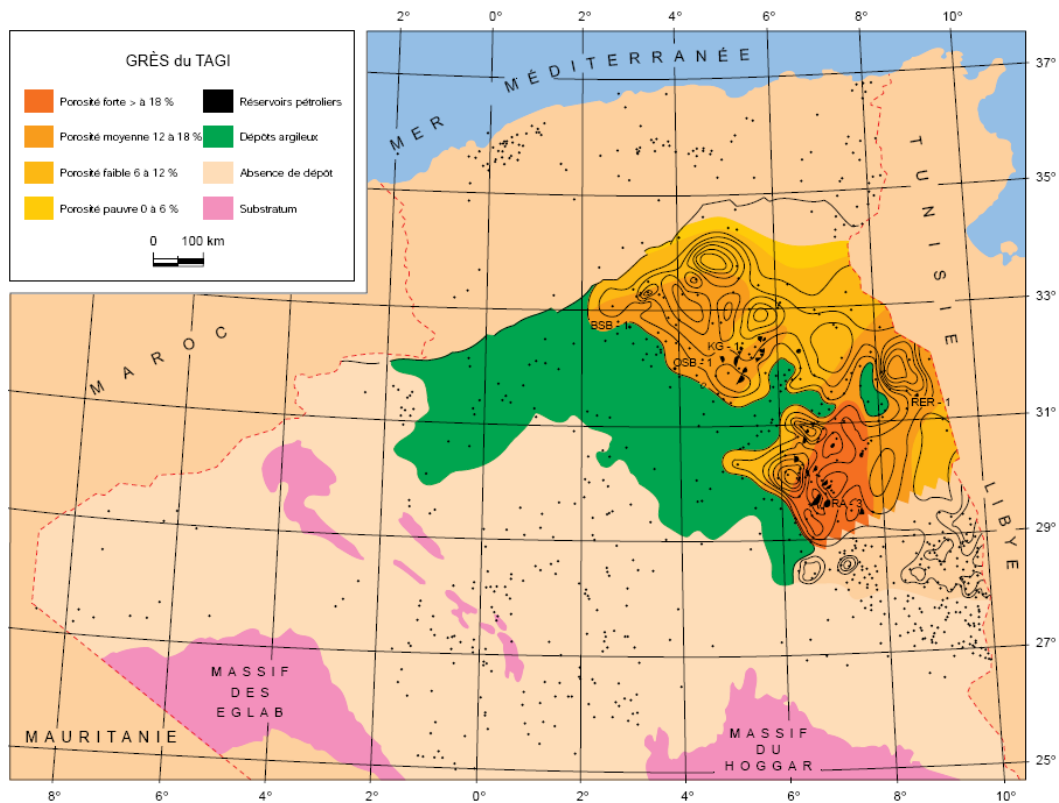


Figure 2.7c. Porosity distribution within Triassic (Geology of Algeria)

The Triassic (TSi) sandstone lithology is fine to coarse grained sandstone and it is the main production formation. TSi sand layer is the lower Triassic, the Hercynian erosion plane landform controls Triassic Si sedimentary, it is the most favorable oil-gas accumulation formation. Its main source material direction is SW—NE. The thickest of TSi layers in this block is 95m, it is a braided river sedimentation formation with a net thickness of sandstone generally 20-30m. TSi sandstone porosity is medium, with medium pore size, permeability is not high but the existence of micro-fractures has made a great improvement in reservoir properties, note (Table.1) that the highest permeability value is about 800mD.

Triassic T1: It is a meandering river deposit; its lithology is fine to medium grained

sandstone. T1 material source is from Hassi R'Mel ancient highland, with a thickness of 75m (the net thickness of the sandstone is 10-20m). The reservoir porosity is low to medium with low permeability which was improved by the micro-fractures.

Devonian layer: This section is mainly shallow marine and continental shelf sediments. It develops as offshore bar and underwater channel-mouth bar sand bodies. The oil production from this reservoir is low.

Ordovician: Little oil and gas have been discovered in the northeast section of this area.

2.9 Cap rock characteristics

The Mesozoic cap rocks correspond to the Triassic and Liassic clays and evaporites. In the Triassic basin they act as cap rocks for the sandstone reservoirs and in some cases, through an unconformity surface, for the Paleozoic reservoirs.

Due to their thickness, in excess of 2000 m, and their lithology they are classified as "super seals". The cover consists of a number of sub-units. The "argillaceous Triassic" is made of salty clays. Unit "S4" is a salty interval. The "argillaceous Liassic" is generally overpressured. Unit "S3" is a Liassic interval, formed of salt and shale. It is followed by units S1 and S2 which consist of salts, anhydrites and clays, topped by the Liassic B dolomitic horizon and terminated by the upper Liassic anhydritic clays (Figure 2.8). Due to pinchouts only the upper units are found on the borders of the Triassic basin. The gypsum-salt rock of the Upper Triassic, the gypsum-salt rock, mud stone and limestone of Jurassic-Cretaceous are good cap rocks in the study area.

The thickness of these rocks is up to 1000m.

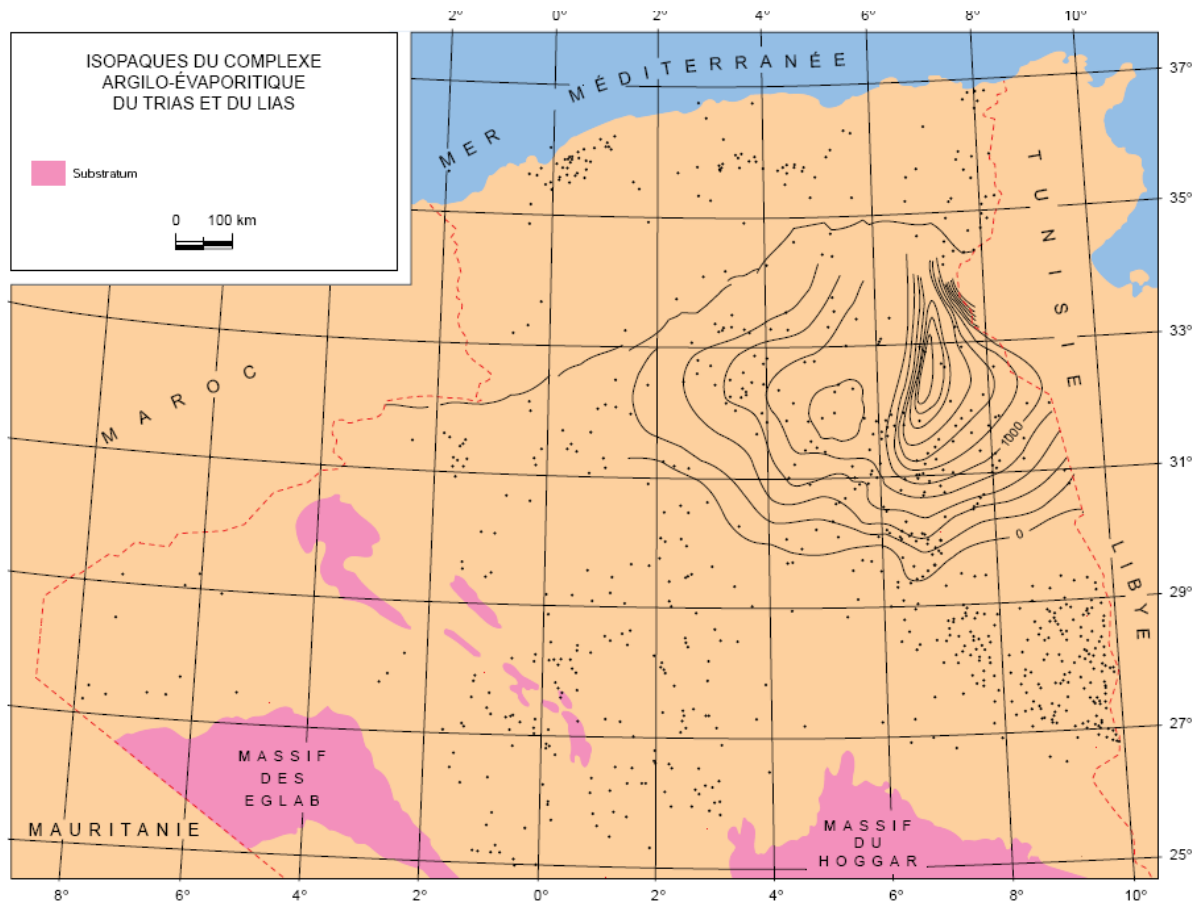


Figure 2.8 . Distribution of Clay & Evaporate deposits from Triassic & Liassic
(Geology of Algeria)

2.10 Migration System

The oil and gas accumulation of this area has a direct relation with the Hercynian unconformity plane and fault zone. The Hercynian movement in the Devonian caused an erosion of the study area, and formed a local Hercynian unconformity plane. Additionally, Australian structure movements formed a series of SSW – NNE direction compresso-shear fault structural zones in early Cretaceous (Australia rifted away from Africa), the long fracture extension and fault horizon reached Silurian, interconnected the hydrocarbon source rock and overlaying sandstone rock reservoir.

CHAPTER THREE

SEISMIC ATTRIBUTES CALCULATIONS AND ANALYSIS

3.1 Introduction

Seismic Reservoir Characterization (SRC) is a branch of Reservoir Geophysics, which provides reservoir description using 2-D or 3-D seismic reflection methods. The main objective of Seismic Reservoir Characterization is to predict and estimate reservoir properties using 3-D seismic attributes as the main source of estimation of reservoir parameters in the sparse inter-well area.

Generally, porosity, permeability, rock type, pore fluid, pore shape, burial depth (temperature and pressure), consolidation (compaction and cementation) and geological age are the most important rock properties to be considered in any description of the reservoir. However, only some of these properties have a considerable effect on the dominant component in the seismic response (namely: the velocity).

3.2 Definitions

Seismic attribute is any characteristics, qualitative or quantitative, measured, calculated or inferred from seismic data, representing all the parameters of the trace complex, geometrical configurations of seismic events and their spatial variations. Taner et al. (1979) defined seismic attributes as all the information obtained from seismic data, either by direct measurements or by logical or experience-based reasoning. They relate to

basic information from the seismic data, time, amplitude, frequency and attenuation. The attributes provide alternative representations of seismic data and can be used for geological and petrophysical characterization. These attributes can be classified in a way that allows one to make the most of their usefulness in seismic.

Generally, the calculation of seismic attributes is based on data represented in time. Therefore, conventional sections (CDP stack), the migrated sections before or after stack are given as input for this calculation. The attributes derived from the migrated sections in time, due to the accurate positioning of reflectors, may be more beneficial for the objectives of the seismic interpretation.

Seismic attributes were introduced in the 1970's as useful tool to help interpret the seismic data in a quantitative way. Walsh (1971) published the first paper under the title of "Color Sonograms". In the same period, Nigel Anstey published "Seiscom 1971" and he introduced the concept of reflection strength and mean frequency. Realizing the potential for extracting useful instantaneous information, Taner, Koehler and Anstey turned their attention to wave propagation and simple harmonic motion (Taner, 2000). Neidell proposed the use of the Hilbert transform to derive the kinetic portion of the energy flux. In the mid 70's three major attributes were established. Since the early 1990s, the quantitative analysis of seismic attributes has become widely used and applied through calibration with well bore measurements (Doyen, 1988, Schultz et al.1994, Taner et al.. 1994, Trappe and Hellmich, 1998).

In reservoir geophysics, rock physics play a role of a bridge establishing physical relationships between seismic attributes and reservoir properties. Many examples are found in literature related to seismic attributes and their application to reservoir

characterization;(Taner et al. 1979; Lawrence 1998; Brown 1999 and 2001; Skiruis 1999; Hampson et al. 2001).

3.4 Classification of Seismic Attributes

Chan and Sidney (1997) divided seismic attributes into two categories

Horizon based attributes

The average properties of the seismic trace are computed between two geologic boundaries generally defined by picked horizons.

Sample based attributes

The input seismic traces are transformed in such a way as to produce a new output trace with the same number of samples as the input (e.g., transformation of seismic amplitude sample based volume to acoustic impedance sample based volume).

Post stack attributes can, therefore, be extracted along one horizon or over a specific window (window attributes).

Taner et al. (1994) divided the attributes into two general categories

3.4.1 Geometrical attributes (reflection configuration)

They describe the spatial and temporal relationship of all other attributes. Lateral continuity measured by semblance is a good indicator of bedding similarity as well as discontinuity. Bedding dips and curvatures give depositional information. Geometrical attributes are generally found useful in structural interpretation (e.g., faults) and in seismic stratigraphic interpretation of 3D data volumes. Their objective is to enhance the

visibility of the geometrical characteristics of seismic events for the interpreter (Taner et al. 1994, 2000).

3.4.2 Physical attributes (reflection characteristics).

They are related to physical qualities and quantities. The magnitude of the trace envelope is proportional to the acoustic impedance contrast, frequencies are related to the bed thickness, wave scattering and absorption. Instantaneous and average velocities are directly related to rock properties. These attributes are mainly applicable for lithological and reservoir characterization (Taner et al., 2000). They can be divided into two sets

- Attribute computed from seismic data planes (2-D planes): these attributes, computed from analytical traces, are the most widely used ones. They include the trace envelope and its first and second derivatives, instantaneous phase and instantaneous frequency, instantaneous acceleration, apparent polarity, bandwidth, instantaneous Q factor (attenuation), and their statistic computed along reflectors over a time window.
- Attributes computed from the pre-stack data: which reflect variation of various attributes with offset, such as amplitude (AVO) and instantaneous frequency, ect. (Taner et al., 1994).

3.4.3 Pre-stack Attributes: Seismic data are CDP or image gather traces.

They will have directional (azimuth) and offset related information. Computations generate huge amounts of data; hence they are not practical for initial studies (Taner, 2000).

3.4.4 Post stack Attributes: Stacking is an averaging process, losing offset and azimuth information. Seismic data could be CDP stacked or migrated.

Based on the information content, attributes are divided into two groups (Taner, 2000).

3.4.5 **Instantaneous Attributes:**

Instantaneous attributes computed sample by sample, representing instantaneous variations of different parameters. Instantaneous values of attributes such as trace envelope, its derivatives, frequency and phase may be determined from the complex trace.

3.4.6 Wavelet Attributes: Instantaneous attributes computed at the peak of the trace envelope have a direct relation to the Fourier transform of the wavelet in the vicinity of the envelope peak. For example, the instantaneous frequency at the peak of the envelope is equal to the mean frequency of the wavelet amplitude spectrum.

Therefore, attributes can be divided into two sets based on their origin.

3.4.7 Reflection Attributes: They correspond to the characteristics of interfaces. All instantaneous and wavelet attributes can be included under this category. Pre-stack attributes such as AVO are also reflective attributes, since AVO analysis measures the angle versus reflection response of an interface.

3.4.8 Transmissive Attributes: they are related to the characteristics of a bed between interfaces. Q, absorption, dispersion, interval-, RMS- and average velocities come under this category

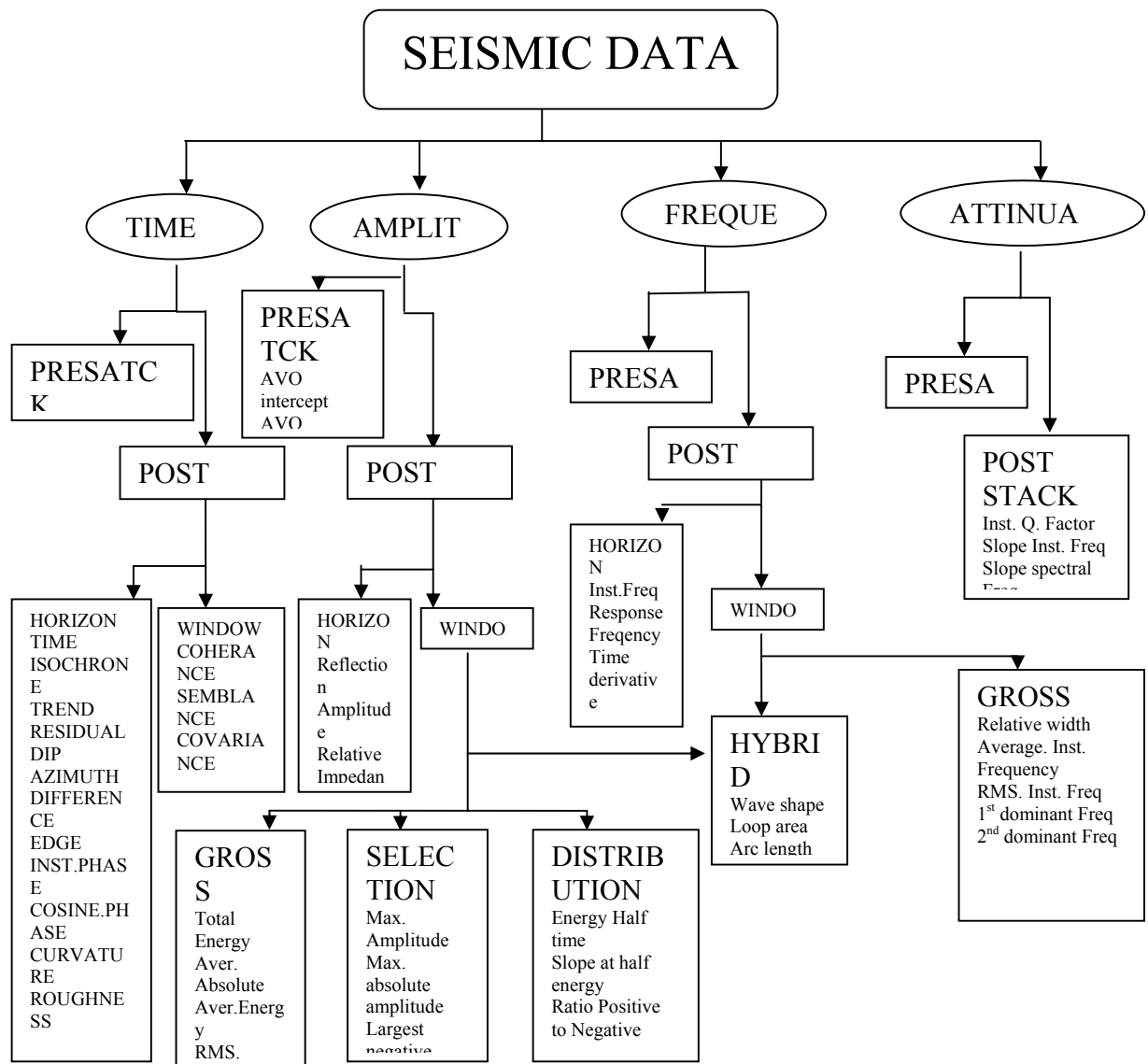


Fig 3.1 Seismic Attributes Classification (After Brown,2001)

3.5 Hilbert Transform

Hilbert transform and analytical signal are useful for several applications in the field of telecommunication and electronics. Hilbert transform has many seismic applications such as:

- Introducing a phase shift.
- Measure of trace envelope.
- Measure of Instantaneous phase.
- Measure of Instantaneous frequency.

In seismic, these concepts are used to provide the local characteristics of a trace.

3.5.1 Definition of the Hilbert Transform

The Hilbert Transform of a function $s(t)$ is given by:

$$\hat{s}(t) = \text{HT} [s(t)] \quad (3.1)$$

In the frequency domain HT defined by:

$$S_q(f) = \text{FT} [\hat{s}(t)] = -i \text{sign}(f) \cdot S(f) \quad (3.2)$$

In the time domain the transform is :

$$\hat{s}(t) = s(t) * \frac{1}{\pi} Pp \frac{1}{t} = \frac{1}{\pi} Pv \int_{-\infty}^{+\infty} \frac{s(\tau)}{t - \tau} d\tau \quad (3.3)$$

Where Pv means Cauchy's principal value. Principal value integration is the limit of the sum of two integrals from $-\infty$ to $-\epsilon$ and from ϵ to $+\infty$ as ϵ tends to zero.

PP: Principal part. The integration of the convolution is done as a principal value.

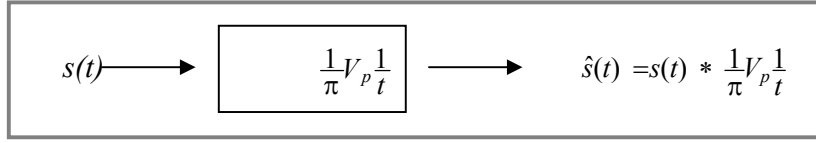


Figure 3.2 Hilbert Filter

3.5.2 Properties of Hilbert Transform

BEDROSIAN Theorem

Let $s_1(t)$ and $s_2(t)$, two signals, the HT of their product is

$$\text{HT} [s_1(t) \cdot s_2(t)] = \frac{1}{\pi} V_p \frac{1}{t} * [s_1(t) \cdot s_2(t)]$$

$$\text{HT} [s_1(t) \cdot s_2(t)] = \left(\frac{1}{\pi} V_p \frac{1}{t} * s_1(t) \right) s_2(t) \quad (3.4)$$

which enable us to write the following equality

$$\text{HT} [s_1(t) \cdot s_2(t)] = s_1(t) \cdot \text{HT} [s_2(t)] = \text{HT} [s_1(t)] \cdot s_2(t) \quad (3.5)$$

Orthogonality

The scalar product $\langle s(t), \text{HT} [s(t)] \rangle$ is zero

Therefore,

$$\langle s(t), \hat{s}(t) \rangle = \int_{-\infty}^{\infty} s(t) \hat{s}(t) dt = \int_{-\infty}^{\infty} \overline{S(f)} \hat{S}(f) df \quad (3.6)$$

with

$$\text{FT} \left[\frac{1}{t} \right] = -j\pi \text{sgn}(f)$$

So

$$\hat{S}(f) = -j \operatorname{sgn}(f) \cdot S(f)$$

The final result will be

$$\langle \hat{s}, s \rangle = -j \int_{-\infty}^{\infty} |S(f)|^2 \operatorname{sgn}(f) df = 0 \quad (3.7)$$

Convolution

The HT of a convolution product is equal to the convolution product of one of the

signals with the HT of the other. If $s_1(t) * s_2(t) \leftrightarrow S_1(f) \cdot S_2(f)$

$$\begin{aligned} \text{HT} [S_1(f) \cdot S_2(f)] &= j \operatorname{sgn}(-f) \cdot [S_1(f) \cdot S_2(f)] \\ &= [j \operatorname{sgn}(-f) \cdot S_1(f)] \cdot S_2(f) \\ &= \text{HT} [S_1(f)] \cdot S_2(f) \end{aligned}$$

So

$$\text{HT} [s_1(t) * s_2(t)] = \text{HT} [s_1(t)] * s_2(t) = s_1(t) * \text{HT} [s_2(t)] \quad (3.8)$$

3.5.3 Discrete Hilbert Transform

The introduction of the discrete Hilbert transform makes possible the calculation of analytical signal from sampled data, knowing that the majority of the data gathered for processing, particularly in seismic, are in numerical form.

Given, the discrete sequence of complex numbers $S(n)$, whose real part is indicated by $s_r(n)$, imaginary part by $s_i(n)$:

$$s_r(n) = \operatorname{Re} [s(n)]$$

$$s_i(n) = \text{Im} [s(n)]$$

in the frequency domain the Fourier Transform is:

$$S(f) = S_r(f) + jS_i(f) \quad (3.9)$$

Fourier Transform causality is defined by:

$$S(f) = \begin{cases} S(f) & 0 \leq f \leq \frac{1}{2} \\ 0 & -\frac{1}{2} \leq f < 0 \end{cases} \quad (3.10)$$

The conjugate of $S(f)$ is given by:

$$\overline{S(-f)} = S_r(-f) - jS_i(-f)$$

$s_r(n)$ is real so: $S_r(-f) = S_r(f)$

from equations (3.9) and (3.10) we get:

$$S_r(f) = \frac{1}{2} [S(f) + \overline{S(-f)}] \quad (3.11)$$

And

$$S_i(f) = \frac{1}{2j} [S(f) - \overline{S(-f)}] \quad (3.12)$$

Following the property of causality of Fourier transform, a relation between the real and imaginary parts can be established.

$$2S_r(f) = \begin{cases} S(f) & 0 \leq f \leq \frac{1}{2} \\ \overline{S(-f)} & -\frac{1}{2} \leq f < 0 \end{cases} \quad (3.13)$$

$$2jS_i(f) = \begin{cases} S(f) & 0 \leq f \leq \frac{1}{2} \\ -\overline{S(-f)} & -\frac{1}{2} \leq f < 0 \end{cases} \quad (3.14)$$

By comparing these two last expressions, the relation established is

$$S_i(f) = \begin{cases} -jS_r(f) & 0 \leq f \leq \frac{1}{2} \\ jS_r(f) & \frac{1}{2} \leq f < 0 \end{cases} \quad (3.15)$$

Or

$$S_r(f) = G(f) \cdot S_i(f) \quad (3.16)$$

with

$$G(f) = \begin{cases} -j & 0 \leq f \leq \frac{1}{2} \\ j & -\frac{1}{2} \leq f < 0 \end{cases}$$

$G(f)$ can be written in another form: $G(f) = -j \operatorname{sgn}(f)$ with $f \leq \frac{1}{2}$

$$\begin{aligned} g(n) = \text{FT}^{-1} [G(f)] &= \int_{-\infty}^{+\infty} G(f) e^{j2\pi fn} df \\ &= j \int_{-\frac{1}{2}}^0 e^{j2\pi fn} df - j \int_0^{\frac{1}{2}} e^{j2\pi fn} df \\ &= \frac{1}{\pi n} (1 - \cos \pi n) \\ &= \frac{2}{\pi n} \sin^2 \left(\frac{\pi n}{2} \right) \end{aligned}$$

Finally, the impulse response of Hilbert filter is given by

$$g(n) = \begin{cases} \frac{2 \sin^2(\pi n/2)}{\pi n} & \text{if } n \neq 0 \\ 0 & \text{if } n = 0 \end{cases}$$

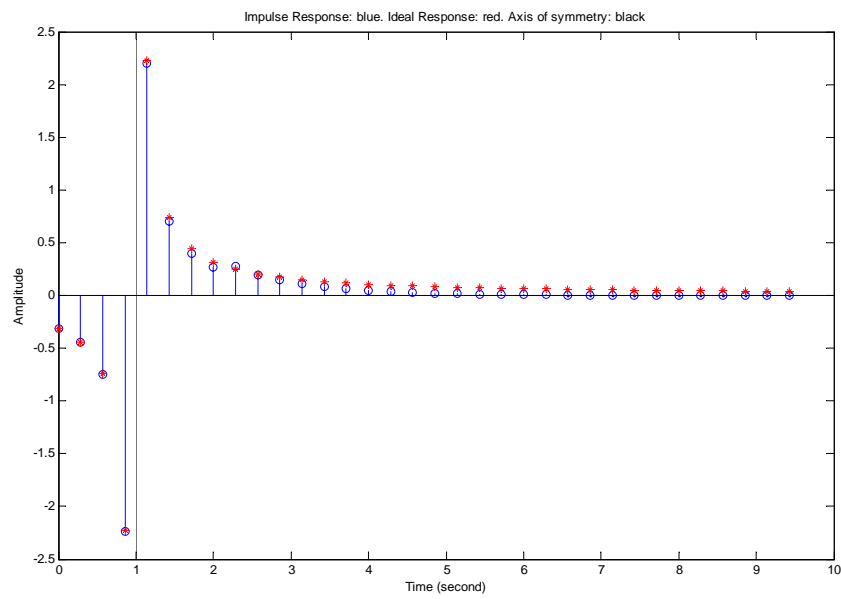


Figure 3.3 Impulse Response of Hilbert Transform

3.6 Computation of Seismic Attributes

In this section several methods of analytic trace computation will be reviewed.

Frequency Domain Computation

The real and imaginary part of the analytical trace are Hilbert Transform pairs, then their Fourier Transforms have to be causal, their amplitude spectra have to be the same and their phase spectra have to be 90 degrees out of phase.

The analytical trace can be formed by the following steps:

- Transfer the seismic trace to a complex array and place it into the real part, leaving the imaginary part equal to zero.
- Compute Fourier Transform by FFT.
- Zero out negative frequency, double the positive side, but leave zero and folding frequencies as they are. This will create the causal Fourier Transform.
- The inverse Fourier Transform will give an input trace that is unaltered in the real part and the imaginary part will contain the Hilbert Transform of the input trace.

Discrete Time Domain Computation

The discrete Hilbert Transform in the time domain is an infinitely long filter with zero weights at the center and at all even-numbered samples. Its odd numbered coefficients are $1/n$ (Clearbout, 1976). In practice we use a limited-length filter which causes the spectrum of the computed imaginary part to differ from that of the real part. The main problem comes from phase discontinuities at zero samples. In order to overcome this, we use a more convenient band-pass filter (Butterworth).

Gabor-Morlet Decomposition

A major problem associated with the Hilbert Transform is that it is only valid for narrow-band signals. For example, the spike has the widest possible bandwidth among all signals

and its Hilbert Transform is the time domain response of the transform. In the Gabor-Morlet decomposition we divide the signal bandwidth into smaller Gabor-Morlet bands.

$$G(\omega, t) = \exp(\alpha t^2) \cdot \exp(-i\omega t) \quad (3.17)$$

The decomposition process is done by convolving the data by a series of Gabor-Morlet wavelets. Since the wavelets are complex valued, their output will also be complex valued and analytic.

3.6.1 Formulation of Seismic Attributes

Taner et al. (1979) gave the initial formulation of seismic attributes as applied to seismic interpretation. His work covered five main attributes: envelope amplitude, instantaneous phase, instantaneous frequency, weighted mean frequency and apparent polarity. Their application was discussed by Robertson and Nogami (1984) for thin bed analysis, and Robertson and Fisher (1988) for general interpretation.

In this section we will discuss the attributes computed directly from individual traces. We will give the mathematical formulation of each attribute and indicate their direct or possible relation to the physical properties of the subsurface.

(Amplitude/Trace) Envelope:

Let the analytical trace be given by

$$F(t) = s(t) + ih(t) \quad (3.18)$$

where

$s(t)$: the real part corresponding to the seismic data.

$h(t)$: the imaginary part corresponding to the Hilbert Transform of $s(t)$.

The envelope is the modulus of the complex function $F(t)$

$$E(t) = \sqrt{s^2(t) + h^2(t)} \quad (3.19)$$

it represents the total energy, varies between 0 and the maximum amplitude of the trace.

The trace envelope is a physical attribute and it can be used as an indicator of the following characteristics:

- Represents mainly the acoustic impedance contrast, hence reflectivity,
- Bright spots,
- Possible gas accumulation,
- Sequence boundaries,
- Unconformities,
- Major change in lithology,
- Major change in depositional environment,
- Lateral change indicating faulting,
- It has spatial correlation to porosity

Rate of Change of the Envelope

It shows the variation of the energy of the reflected events, it indicates the absorption effects. A slower rise indicates larger absorption. The mathematical expression is given by:

$$d[E(t)]/dt = E(t) * diff(t) \quad (3.20)$$

where

*: denotes convolution operation

diff: the differentiation operation.

This attribute has a concrete physical meaning and it can be used to detect possible fracturing and absorption effects.

Instantaneous Phase

The argument of the complex analytic signal is the instantaneous phase

$$Ph(t) = \arctan\left[\frac{h(t)}{s(t)}\right] \quad (3.21)$$

The phase information is independent of trace amplitude and it relates to the propagation phase of the seismic wave front. The instantaneous phase is also a physically meaningful attribute and can be used for:

- To indicate lateral continuity,
- To compute the phase velocity,
- Has no amplitude information, hence all events are represented, even the weak ones
- Shows discontinuity, but may not be the best for this purpose
- Indicate sequence boundaries,
- Gives detailed visualization of bedding configurations,
- It is used to compute instantaneous frequency and acceleration

Instantaneous frequency

Represent the time rate of change of phase

$$Freq(x, t) = \frac{\partial[Ph(x, t)]}{\partial t} \quad (3.22)$$

Instantaneous frequency is a physical attribute; it can be used as effective discriminator in case of lateral changes:

- Seismic character correlator in lateral direction,
- Indicates the edges of low impedance thin beds,
- Hydrocarbon indicator by low frequency anomaly,
- Fracture zone indicator, fractures may appear as lower frequency zones.
- Bed thickness indicator, high frequencies indicate sharp interface of thin shale bedding, lower frequencies indicate sand-rich bedding.
- Sand /Shale ratio indicator in a clastic environment

Thin Bed Indicator

Information that can be extracted is the locations where instantaneous frequencies jump or go in the reverse direction. These jumps are indicative of closely arriving reflected wavelets. The thin-bed indicator is computed as the difference between the instantaneous- and the time-averaged frequencies

$$thin.bed(t) = \omega(t) - \overline{\omega(t)} \quad (3.23)$$

This attribute is a physical attribute, it can be used for

- As an indicator of overlapping events,
- To indicate thin beds, when laterally continuous,
- To indicate non-reflecting zones, when they appear laterally random.
- Shows the fine details of bedding patterns.

Instantaneous Dominant Frequency

Similar to instantaneous frequency, it can be used as a reflection correlation tool.

Instantaneous Band Width

Related to overall absorption effects, considered as a high resolution seismic character correlator tool.

Instantaneous Q Factor

It is a good indicator of absorption effects, fractures, gas zone and a possible permeability indicator.

Normalized Amplitude

Useful for correlation , it is an event tracking tool and event termination indicator.

Dip of Maximum Coherency (a coherency attribute)

It is a good indicator for parallel, divergent or convergent bedding.

Apparent polarity

May differentiate between various types of bright spots, a section polarity indicator

Arc length

It measures reflection heterogeneity, and may be used to quantify lateral changes in reflection patterns. It is calculated using the following formula:

$$Z = \frac{\sum_{j=i}^{n-1} \sqrt{(Amp(j) - Amp(j+1))^2 + (t)^2}}{(n-1) \times sample \ rate} \quad (3.24),$$

where Z is in milliseconds in time domain, or in feet or meters in depth domain.

Arc length is a stratigraphic sequence indicator.

Average energy

This is the squared RMS (Root Mean Square) Amplitude. This attribute is a measure of reflectivity within a time or depth window and may be used to map direct hydrocarbon indicators in a zone.

Average energy is computed using the following formula:

$$\frac{\sum_{i=1}^k \left(\text{Amp}(i) - \frac{\sum_{j=1}^k \text{Amp}(j)}{k} \right)^2}{k} \quad (3.25)$$

assuming all samples are live samples.

Half energy

This operation computes the time or depth required for the cumulative energy within a window to reach one-half of the total energy within the entire window. Half Energy is computed by finding $k_{1/2}$ from the following equation:

$$\frac{\sum_{i=1}^k \left(\text{Amp}(i) - \frac{\sum_{j=1}^k \text{Amp}(j)}{k} \right)^2}{2} = \sum_{i=1}^{k_{1/2}} \left(\text{Amp}(i) - \frac{\sum_{j=1}^k \text{Amp}(j)}{k} \right)^2 \quad (3.26)$$

Half energy may indicate asymmetric changes in lithology or porosity within a specified zone.

RMS Amplitude

RMS Amplitude is the square root of the sum of all squared amplitudes, divided by the number of live samples as shown in the following formula:

$$\left[\frac{\sum_{i=1}^n \left(\text{Amp} (i) - \left(\frac{\sum_{j=1}^k \text{Amp} (j)}{k} \right) \right)^2}{k} \right]^{1/2} \quad (3.27)$$

Where n is number of all amplitudes, k is the number of live samples.

RMS may map directly to hydrocarbon indicators and other geologic features which emerge from the background by their amplitude response. Additional discussion on attribute categories and their relationships to reservoir properties are found in much geophysical literature such as: Chen and Sidney (1997); Taner et al. (1979 & 2000) and Brown (2001).

CHAPTER FOUR

Artificial Neural Networks

4.1 Definition

The Artificial Neural Network (ANN) is a processing paradigm imitating the way biological nervous systems (eg: brain), process information, in other words, is an emulation of a biological neural system. It is composed of a large number of interconnected elements (neurons) working in parallel to solve specific problems. A given ANN is configured for the specific application, such as pattern recognition or data classification, through a learning process. Learning in biological systems involves adjustments to the synaptic connections that exist between the neurons. This is true of ANNs as well.

4.2 Historical background of Neural Networks

The history of neural networks can be divided into several periods:

4.2.1 First Period (Initial attempts)

In 1943, McCulloch and Pitts developed models of neural networks based on their expertise in neurology. These models involved several assumptions about how neurons worked. The networks were based on simple neurons which were considered to be binary devices with fixed thresholds. The outputs of the models were simple logic functions such as "A or B" and "A and B". An other attempt was made by using computer simulations. In 1954, Farley and Clark (IBM researchers) maintained closed contact with

neuroscientists at McGill University. So whenever their models did not work, they consulted the neuroscientists. This interaction established a multidisciplinary trend which has continued to the present day.

4.2.3 Second Period (Promising & Emerging Technology)

Not only was neuroscience influential in the development of neural networks, but psychologists and engineers also contributed to the progress of neural network simulations. Rosenblatt (1958) stirred considerable interest and activity in the field when he designed and developed the Perceptron. The Perceptron had three layers with the middle layer known as the association layer. This system could learn to connect or associate a given input to a random output unit. In 1960, Rosenblatt demonstrated the Mark I Perceptron. The Mark I was the first machine that could “learn” to identify optical patterns.

Another system was the ADALINE (Adaptive Linear Element) which was developed in 1960 by Widrow and Hoff (of Stanford University). The ADALINE was an analogue electronic device made from simple components. The method used for learning was different to that of the Perceptron, it employed the Least-Mean-Squares (LMS) learning rule.

4.2.4 Third Period (Frustration & Disrepute)

In 1969, Minsky and Papert wrote a book in which they generalized the limitations of single layer Perceptrons to multilayered systems. In the book they said: "...our intuitive judgment that the extension (to multilayer systems) is sterile". The result of their book

was to eliminate funding for research with neural network simulations. As a result, considerable prejudice against this field was created.

4.2.5 Fourth Period (Innovation)

Although public interest and available funding were minimal, several researchers continued working to develop neuromorphically based computational methods for problems such as pattern recognition. During this period several paradigms were generated which modern work continues to enhance. Grossberg's (Steve Grossberg and Gail Carpenter in 1988) influence founded a school of thought which explores resonating algorithms. They developed the ART (Adaptive Resonance Theory) networks based on biologically plausible models. Anderson and Kohonen developed associative techniques, independently of each other. Klopff in 1972, developed a basis for learning in artificial neurons based on a biological principle for neuronal learning called it heterostasis.

Werbos (1974) developed and used the back-propagation learning method, however several years passed before this approach was popularized. Back-propagation nets are probably the most well known and most widely applied of the neural networks today. In essence, the back-propagation net is a Perceptron with multiple layers, a different threshold function in the artificial neuron, and a more robust and capable learning rule.

Amari (A. Shun-Ichi, 1967) was involved with theoretical developments, he published a paper which established a mathematical theory for a learning basis (error-correction method) dealing with adaptive pattern classification. Fukushima (F. Kuniyiko) developed a step-wise trained multilayered neural network for interpretation of handwritten characters. The original network was published in 1975 and was called the Cognitron.

4.2.6 Fifth Period (Re-Emergence)

Progress during the late 1970's and early 1980's was important for the re-emergence of interest in neural networks. Several factors influenced this movement. For example, comprehensive books and conferences provided a forum for people in diverse fields with specialized technical languages, and the response to conferences and publications was quite positive. The news media picked up on the increased activity and tutorials helped disseminate the technology. Academic programs appeared and courses were introduced at most major Universities (in US and Europe). In Europe, Japan and the US funding had become available, and several new applications in industry and financial institutions emerged.

4.2.7 Today

Significant progress has been made in the field of neural networks. Improvement beyond current commercial applications appears to be possible, and research is advancing the field on many fronts. Clearly, today is a period of transition for neural network technology.

Why use neural networks

Neural networks, with their ability to derive meaning from complicated or imprecise data, can be used to extract patterns and detect trends that are too complex to be noticed by either humans or other computer techniques. A trained neural network can be thought of as an "expert" in the category of information it has been trained to analyze. This expert system can then be used to provide projections for new situations of interest and answer "what if" questions.

Other advantages include:

a) Adaptive learning

An ability to learn how to do tasks based on the data given for training or initial experience.

b) Self-Organization

An ANN can create its own organization or representation of the information it receives during the learning time.

c) Real Time Operation

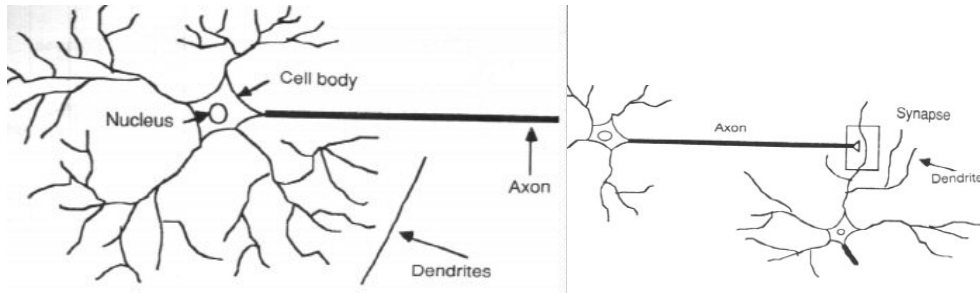
ANN computations may be carried out in parallel, and special hardware devices are being designed and manufactured which take advantage of this capability.

d) Fault Tolerance via Redundant Information Coding

Partial destruction of a network leads to the corresponding degradation of performance. However, some network capabilities may be retained even with major network damage.

4.2 Comparison between Artificial neurons and Human neurons

Little information is available about how the human brain trains itself to process data. To construct an artificial neural network, researchers imitated the individual cells that make up of the brain rather than the whole brain which is enormously complicated. A neuron cell, as seen in Figure (4.1) is the basic building block of the human brain. A typical neuron collects signals from other neurons through a net of fine structures called *dendrites*.



Components of neurons

the synapse

Figure.4.1 Comparison between Artificial neurons and Human neurons

(*Practical Neural Networks Recipes in C++*)

4.3.1 a simple neuron

An artificial neuron is a device which has many inputs and one output (figure 4.2). The neuron has two modes of operation: The training mode and the using mode.

In the training mode, the neuron can be trained to fire (or not), for particular input patterns. In the using mode, when an already encountered ("taught") input pattern is detected at the input, its associated output becomes the current output. If the input pattern does not belong to the taught list of input patterns, the "firing rule" is used to determine whether to fire or not.

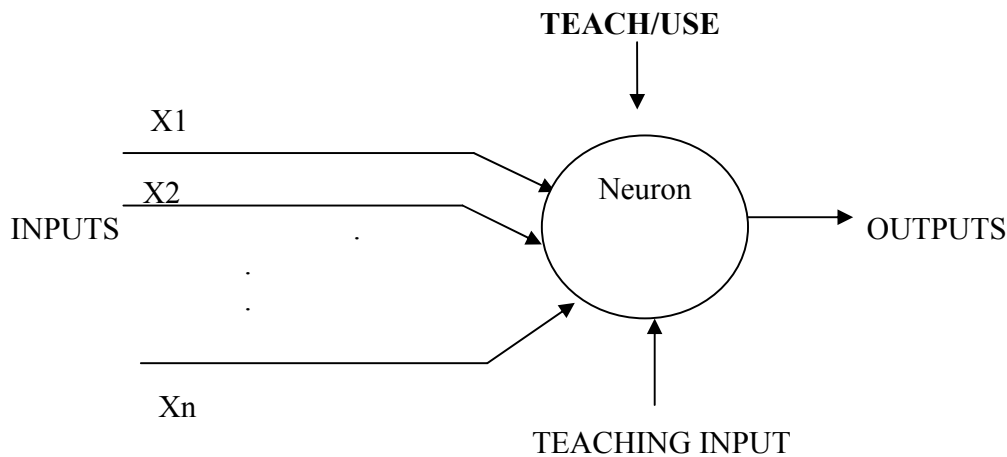


Figure 4.2 a simple neuron

4.3.2 Firing rules

The firing rule is an important concept in neural networks. It determines how one calculates whether a neuron should fire for a given input pattern. It relates to all possible input patterns, not only to the ones on which the node was trained.

A simple firing rule can be implemented by using the Hamming distance technique. The rule goes as follows:

- ☒ Take a collection of training patterns, some of which cause it to fire (the set of patterns taught as "1") and others which prevent it from doing so (the set taught as "0").
- ☒ The patterns not in the collection cause the node to fire as follows: if on comparison, they have more input elements in common with the 'nearest' pattern in the "1" set than with the 'nearest' pattern in the "0" set. If there is a tie, then the pattern remains in the undefined state.

Example:

A 3-input neuron is taught to produce output 1 when the input (X1, X2 and X3) is 111 or 101 and to output 0 when the input is 000 or 001. Then, before applying the firing rule, the truth table is:

Table 2: The truth table

X1	0	0	0	0	1	1	1	1
X2	0	0	1	1	0	0	1	1
X3	0	1	0	1	0	1	0	1
output	0	0	0/1	0/1	0/1	1	0/1	1

4.3.3 How the firing rule works**Example 1:**

Take the pattern 010. It differs:

- ☒ from 000 in 1 element
- ☒ from 001 in 2 elements
- ☒ from 101 in 3 elements
- ☒ from 111 in 2 elements.

Therefore, **the 'nearest'** pattern is 000 which belongs in the 0-taught set. Thus the firing rule requires that the neuron should not fire when the input is 001.

Example 2:

The pattern 011 is equally distant from two taught patterns that have different outputs and thus the output stays undefined (0/1).

By applying the firing rule, the truth table becomes

X1	0	0	0	0	1	1	1	1
X2	0	0	1	1	0	0	1	1
X3	0	1	0	1	0	1	0	1
output	0	0	0	0/1	0/1	1	1	1

Note : the difference between the two tables is called" **the generalization of the neuron**".

4.4 Neural network structure

An artificial Neural Network is composed of several elements:

A - Input layer: the role of the input units is to receive the raw information that is fed into the network.

B- Hidden layers: it is the processing unit for the network. Its activity is determined by the activities of the input units and the weights of the connections between the input and the first row of the hidden units, or between nodes of adjacent hidden layers.

C- Output layer: The behavior of the output units depends on the activity of the last row of the hidden units and the weights between the nodes in this row and the output units.

D- Neuron: it is the basic elements of the neural network. It is a communication conduit that accepts inputs and produces outputs. In the case when a neuron produces output, it becomes active, or "fires". A neuron will be active when the sum of its inputs satisfies the neuron's activation function.

4.4.1 Feed-forward networks

Feed-forward ANNs (figure 4.3) allow signals to travel one way only; from input to output. There is no feedback (loops) i.e. the output of any layer does not affect that same layer or a previous layer. Feed-forward ANNs tend to be straight-forward networks that associate inputs with outputs. They are extensively used in pattern recognition.

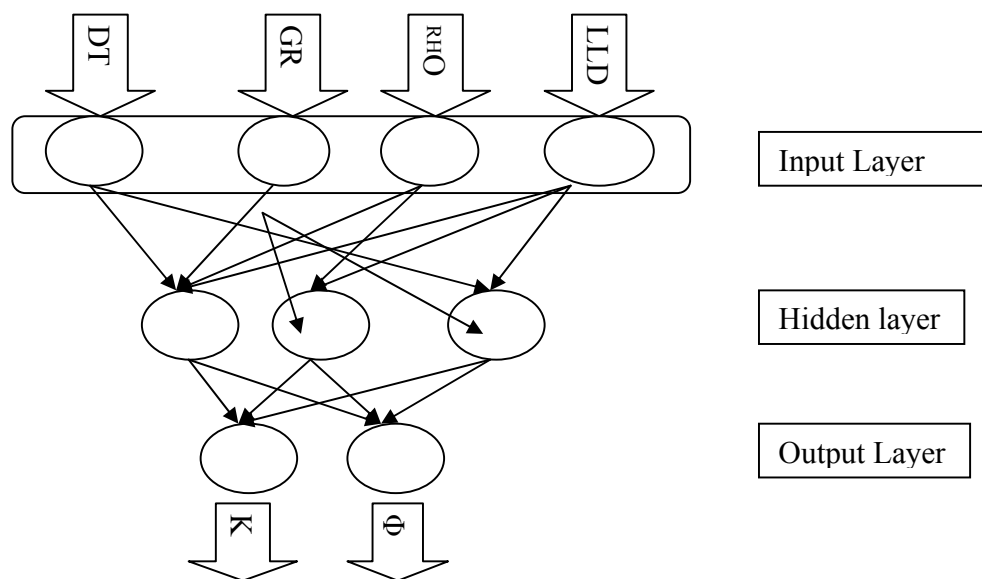


Figure 4.3 Feed Forward Neural Networks Structure

The Learning Process

Memorization of patterns and subsequent response of the network can be categorized into:

Associative mapping

In which the network learns to produce a particular pattern on the set of input units whenever another particular pattern is applied on the set of input units. In associative mapping the network stores the relationships among patterns. It can generally be broken down into two mechanisms:

Auto association and hetero-association.

Regularity detection

In which the network learns to respond to particular properties of the input patterns. In regularity detection the response of each unit has a particular 'meaning'. This type of learning mechanism is essential for feature discovery and knowledge representation.

Notice that information is stored in the weight matrix of the neural network.

Following the way as the network learns we can distinguish between two types of neural networks:

A- Fixed networks

In which the weights can not be changed ($dW/dt=0$). In such networks, the weights are fixed *a priori* according to the problem to solve.

B- Adaptive networks

These are able to change their weights ($dW/dt \neq 0$).

4.4.2 Adaptive networks

Adaptive means that the system parameters (Weights) are changed during operations.

This is called done during the training step. After the training phase the Artificial Neural

Network parameters are fixed and the system is deployed to solve the problem at hand (the testing phase). Learning methods used in adaptive neural networks can be categorized into two groups:

☒ **Supervised learning** (Figure 4.4)

Which incorporates an external teacher, the network is trained by providing it with input and matching output patterns. During the learning process global information may be required. Paradigms of supervised learning include error-correction learning, reinforcement learning and stochastic learning. An important issue concerning supervised learning is the problem of error convergence, the minimization of error between the desired and computed unit values. The aim is to determine a set of weights which minimizes the error. In one well-known method, which is commonly used for many learning paradigms, the system converges to a set of weights providing the least mean square (LMS) error.

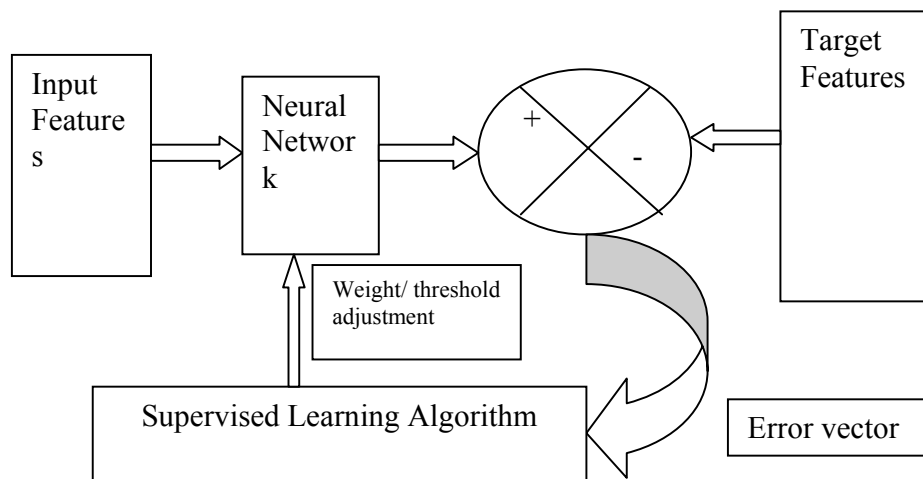


Figure 4.4 Supervised Learning Scheme

☒ Unsupervised learning

It is based upon only local information (no external teacher), it is also called Self Organization, in the sense that it self-organizes the data presented to the network and detects their emergent collective properties. In this paradigm the system is supposed to discover statistically salient features of the input data. Unlike the supervised learning process, there is no a priori set of categories into which the patterns are to be classified; rather the system must develop its own representation of the input stimuli.

4.5 The Mathematical Model (figure 4.5)

When we model a biological neuron, there are three important components:

- 1- The synapses of the neuron are modeled as weights. The strength of the connection between an input and a neuron is given by the value of the weight.

- 2- An adder sums up all the inputs multiplied by their respective weights. This activity is referred to as linear combination.
- 3- An activation function controls the amplitude of the output of the neuron. An acceptable range of output is usually between 0 and 1, or -1 and 1.

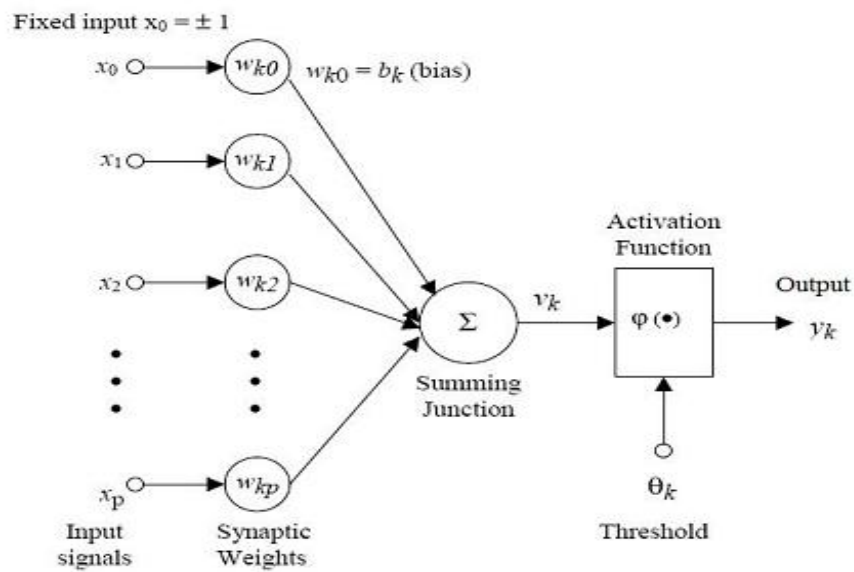


Figure 4.5 Mathematical model of ANNs

(Artificial Intelligence Technologies Tutorial 2002)

Mathematically the function of the neuron k can be expressed by equation 4.1:

$$y_k = \varphi (u_k + b_k) \quad (4.1)$$

Where

$$u_k = \sum_{j=1}^m w_{kj} x_j \quad (4.2)$$

And where

x_j is the input signal from an m dimensional input.

w_{kj} is the synaptic weights of neuron k .

u_k is the linear combiner output due to the input signals.

b_k is the bias, $\varphi(\cdot)$ is the activation function.

y_k is the output signal of the neuron.

The relation between the linear combiner output u_k and the activation potential v_k is

$$v_k = u_k + b_k \quad (4.3)$$

The activation function $\varphi(v)$ defines the output of a neuron in terms of the induced local field v .

Activation Function

The behavior of an ANN (Artificial Neural Network) depends on the weights and the input-output function (transfer function) that is specified for the units. This function typically falls into one of three categories:

- ☒ Linear: the output activity is proportional to the total weighted output. The mathematic expression is $y = ax$, its graph is given in figure (4.6).

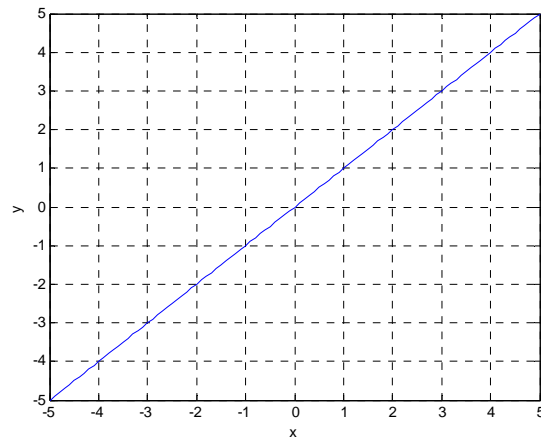


Figure 4.6 Purelinear function

☒ Threshold Function (figure 4.7)

The output is set at one of two levels, depending on whether the total input is greater than or less than some threshold value. The mathematical expression is given by:

$$\phi(v) = \begin{cases} 1 & \text{if } v \geq 0 \\ 0 & \text{if } v < 0 \end{cases}$$

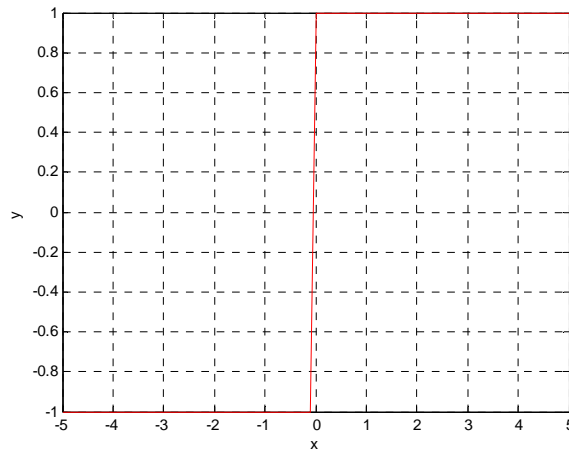


Figure 4.7 Threshold function

☒ Sigmoid: the output varies continuously but not linearly as the input changes.

Notice that sigmoid units bear a greater resemblance to real neurons than do linear or threshold units, but all three must be considered rough approximations. The mathematical expression is given by

$$\phi(v) = \frac{1}{1 + e^{-av}}$$

where a is the slope parameter of the sigmoid function. By varying the parameter a , we can obtain sigmoid functions of different slopes.

A sigmoid graph is given in figure 4.8. For $a = 1$.

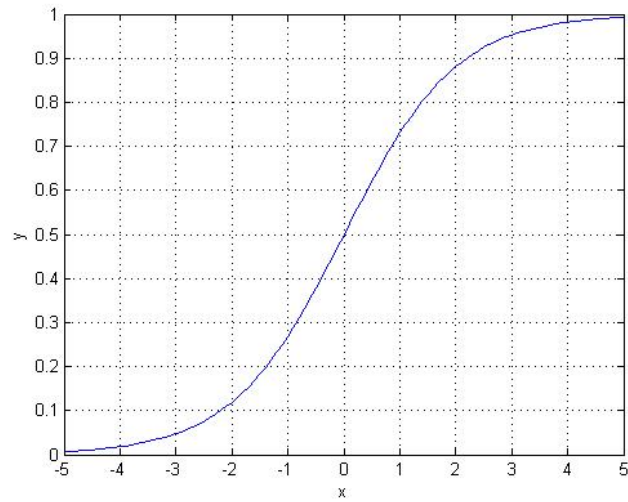


Figure 4.8 Sigmoid Function

Tangent Hyperbolic Function

This transfer (activation) function is sometimes used in place of the sigmoid function and is described by the following mathematical form

$$\phi(v) = \tanh(v) = \frac{e^{av} - e^{-av}}{e^{av} + e^{-av}}$$

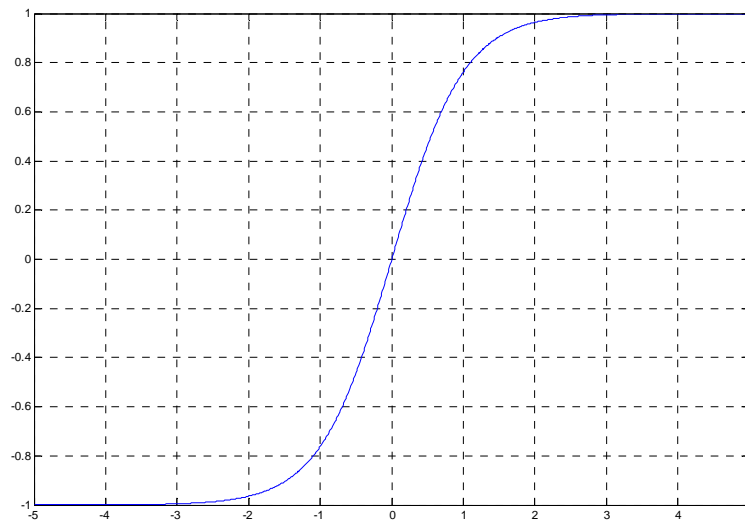


Figure 4.9 *Tangent Hyperbolic Function* for $a=1$.

4.6 Multilayer Perceptron Neural Network (MLP)

Feed-forward neural networks are the type most used in both correlation- and prediction problems. In Feed-forward neural networks, the neurons are organized in different layers, and each of the neurons in one layer can receive only one input from units in the previous layers. Figure 4.10 gives a simple example of a four-layer neural network that contains an input layer, two hidden layers, and an output layer, interconnected by modifiable weights, represented by links between layers.

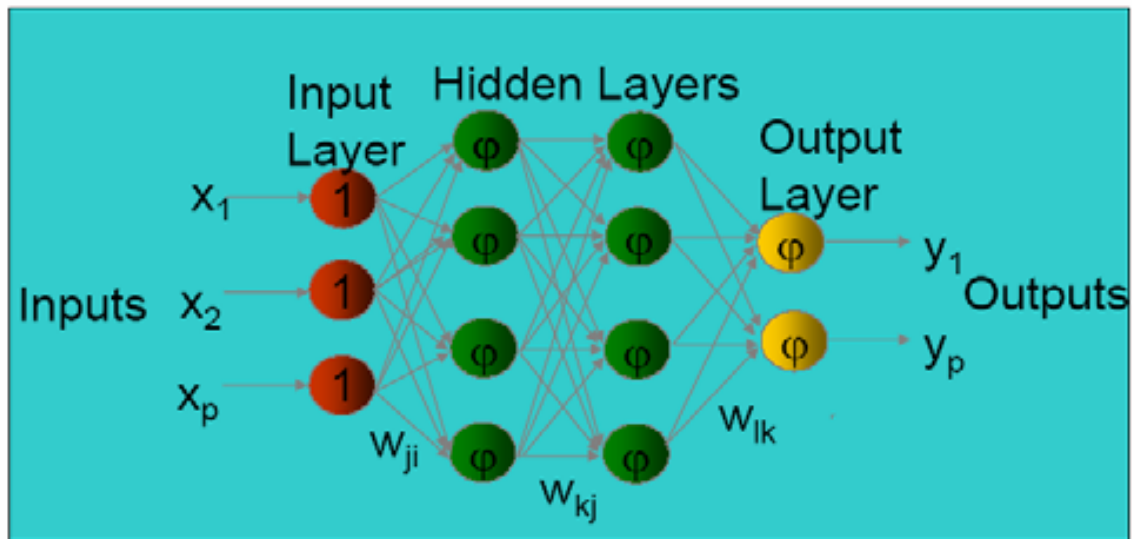


Figure 4.10: Multilayer Perceptron with two hidden layers (Artificial Intelligence Technologies Tutorial 2002)

The presence of one or more hidden layers, whose neurons are correspondingly called hidden neurons, enables the network to extract higher order statistics. Thus the network acquires a global perspective, despite its local connectivity, by virtue of the extra set of synaptic connections and the extra dimension of neural interaction. Such a network is called a “multilayer feed-forward network”.

Learning Process of MLP

In the learning procedures one provides the network with a training set of patterns having inputs and outputs. Real valued m -dimensional input feature vectors

(x_1, x_2, \dots, x_n) are presented to each of the first hidden layer units through the weight vector

w . Hidden layer unit k receives input j through the synaptic weight w_{kj} $\begin{cases} k = 1, 2, \dots, n \\ j = 1, 2, \dots, m \end{cases}$.

Unit k computes a function of the input signal x and the weights w_{kj} and then it passes its output forward to all of the units in the next successive layer. Like the first hidden layer, the units of the second hidden layer are fully connected to the previous layer through the synaptic weights. These units also compute a function of their inputs and their synaptic weight and they pass their output on to the next layer. The output of one layer becomes the input to the following layer. Then, at the output, the unit error is calculated between the target value and the computed value of the pattern. This process is repeated until the final computation is produced by the output unit. The learning algorithm for this type of network is called the back propagation (BP) algorithm, and it was published in the mid-1980s for multilayer perceptrons. This architecture of the network is the basic unit in the present study. Hornik et al. (1989) suggested that, if a sufficient number of hidden units are available, then an MLP with one hidden layer and a sigmoid transfer function in the hidden layer and a linear transfer function in the output layer can approximate any function to any degree of accuracy.

Back-propagation is a reliable method for training multilayer neural networks due to its strong mathematical foundation. Despite its limitations, back-propagation has dramatically expanded the range of problems we can solve by ANN's. Many successful implementations demonstrate its power. The steps to implement the back-propagation algorithm are as follows: The error signal at the output of neuron j at iteration n (i.e. presentation of the n th training pattern) is defined by

$$E_j(n) = d_j(n) - y_j(n) \quad (4.4)$$

where
 $d_j(n)$ is the desired response for neuron j

$y_j(n)$ is the function signal appearing at the output of neuron j

$E_j(n)$ refers to the error signal at the output of neuron j .

- ✚ The instantaneous value of the sum of squared errors is obtained by summing the sum of squared errors over all neurons in the output layer; as

$$\xi = \frac{1}{2} \sum_{j \in c} e_j^2(n) \quad (4.5)$$

- ✚ The net internal activity level $v_j(n)$ produced at the of neuron j is therefore written as

$$v_j = \sum_{i=0}^p w_{ji}(n) y_i(n) \quad (4.6)$$

where p is the total number of inputs applied to neuron j and $w_{ji}(n)$ denote the synaptic weight connecting the output of neuron i to the input of neuron j at iteration n . Hence the output of neuron j at iteration n is given as

$$Y_j(n) = \phi_j(v_j(n)) \quad (4.7)$$

- ✚ The instantaneous gradient which is proportional to the weight correction term is given as

$$\frac{\partial \xi(n)}{\partial w_{ji}(n)} = \frac{\partial \xi(n) \partial e_j(n) \partial y_j(n) \partial v_j(n)}{\partial e_j(n) \partial y_j(n) \partial v_j(n) \partial w_{ji}(n)}$$

$$\frac{\partial \xi(n)}{\partial w_{ji}(n)} = -e_j(n) \phi'_j(v_j(n)) y_j(n) \quad (4.8)$$

- ✚ The correction $\Delta w_{ji}(n)$ applied to $w_{ji}(n)$ is defined by the delta rule as

$$\begin{aligned}
\Delta w_{ji}(n) &= \eta \frac{\partial \xi(n)}{\partial w_{ji}(n)} \\
\Delta w_{ji}(n) &= \eta \delta_j(n) y_i(n) \\
\delta_j(n) &= e_j(n) \phi'_j(v_j(n))
\end{aligned} \tag{4.9}$$

η is a small constant called Learning rate, it determines to what extent the newly acquired information will override the old ones.

When neuron j is located in a hidden layer of the network, the local gradient is redefined as

$$\begin{aligned}
\delta_j(n) &= \frac{\partial \xi(n)}{\partial y_j(n)} \phi'_j(v_j(n)) \\
\delta_j(n) &= \phi'_j(v_j(n)) \sum_k \delta_k w_{kj}(n)
\end{aligned} \tag{4.10}$$

where computation of δ_k requires the knowledge of the error signals e_k for all those neurons that lie in the layer to the immediate right of hidden neuron j . The $w_{kj}(n)$ consists of the synaptic weights associated with these connections. We are now ready to carry out the weight correction update for the back-propagation algorithm, which is defined by the delta rule

$$\Delta w_{ji}(n) = \eta \delta_j y_j \tag{4.11}$$

Note: the weight correction term depends on whether neuron j is an output node or a hidden node:

- ✚ if neuron j is an output node, equation 4.10 is used for the computation of the local gradient.

✚ if neuron j is a hidden node, equation 3.11 is used for the computation of the local gradients.

4.6.1 The Network Performance

The network performance is checked by monitoring the mean square error. The mean squared error is obtained by summing $\xi(n)$ over all n and then normalizing with respect to N (number of training patterns)

$$\xi_{Av} = \frac{1}{N} \sum_{n=1}^N \xi(n) \quad (4.12)$$

The process is repeated several times for each pattern in the training set, until the total output squared error converges to a minimum, or until some preset limit is reached in the number of training iterations.

One of the major problems with the back propagation algorithm is the long training times due to the steepest descent method of optimization (minimization), which is algorithmically simple but slow. The learning rate is sensitive to the weight changes. The smaller the learning rate, the smaller will be the changes to the synaptic weights from one iteration to the next, and the smoother will be the trajectory in the weight space.

However, if the learning rate is chosen too large in order to speed up the learning process, the resulting large changes in the synaptic weights make the network unstable. The solution for this problem is to add a momentum term to the weight update in the back propagation algorithm.

Momentum term is simple to implement, and it significantly increases the speed of convergence. The inclusion of the momentum term may also have the benefit of

preventing the learning process from terminating in shallow local minima on the error surface.

An other method of accelerating the back propagation algorithm is achieved by using the Levenberg - Marquardt algorithm (Hagan et al., 1996). It is based on Newton's optimization method (Hagan et al., 1996) and differs from the usual back propagation algorithm in the manner in which the resulting derivatives are used to update the weights. The main drawback of the LMBP (Levenberg - Marquardt Back Propagation) algorithm is the need for large memory and storage space of the free parameters in the computers. If the network has more than a few thousand parameters, the algorithm becomes impractical on current machines.

4.6.2 Testing (Generalizing)

A network is said to generalize well when the input-output mapping computed by the network is correct for test data which is unknown to the network. A well designed neural network will produce a correct output mapping, even when the input is slightly different from the data used for training. However, when a neural network has too many neurons in the hidden layers, the network may end up memorizing the training data. It even find some irrelevant feature that is present in the training data (noise) but not a real property of the underlying function that is to be modeled. This phenomenon is referred to as overfitting. Overfitting is the result of more hidden neurons than actually necessary, with the result that undesired contributions in the input space due to noise, spurious periodicities, etc. are stored in the synaptic weights.

On the other hand if the number of hidden neurons is less than the optimum number, then the network is unable to learn the correct input-output mapping. Therefore, it is important to determine the optimum number of hidden neurons for a given problem.

Testing is influenced by three factors (Haykin, 1999)

- ✚ the size of the training set.
- ✚ the architecture of the neural network.
- ✚ the complexity of the problem.

4.6.3 Advantages and disadvantages of MLP

An MLP network generates a nonlinear relationship between inputs and outputs by interconnecting nonlinear neurons. The nonlinearity is distributed throughout the network. It does not require any assumption about the underlying data distribution for designing the networks. The network exhibits a great degree of robustness or fault tolerance because of its built-in redundancy. Damage to a few nodes or links thus need not impair overall performance significantly. It can form in any unbounded decision region in the space spanned by the inputs. Such regions include convex polygons and unbounded convex regions. The network has a strong capability for function approximation. The abilities to learn and generalize are additional qualities. Previous knowledge of the relationship between input and output is not necessary, unlike for statistical methods. The MLP has a built-in capability to adapt its synaptic weights to changes in the surrounding environment by adjusting the weights to minimize the error. Experience with neural networks has revealed a number of drawbacks for the technique. For an MLP network, the, i.e. the number of hidden layers and neurons, the size of the

training dataset, and the type of transfer function(s) for neurons in the various layers are all important for the solution of a given problem,. With no analytical guidance on the choice of the design parameters (initial weights, learning rate, and momentum), the developer has to follow an *ad hoc*, trial-and-error approach of manual exploration. Although acceptable results may be obtained with some effort, it is obvious that potentially superior models might be easily overlooked. The considerable amount of user intervention not only slows down model development, but also works against the principle of ‘letting the data speak’, i.e. objectivity. Over-fitting or poor network generalization with new data during actual use is another problem. The commonly used back-propagation training algorithm, with a gradient descent approach to minimize the error during training, suffers from the local minima problem, which may prevent to arrive at the optimum model.

Another problem is the black-box nature of neural network models. The lack of explanation capabilities is a handicap in many decision support applications such as medical diagnostics, where the user would naturally like to know how the model has come to a certain conclusion. Model parameters are buried in large weight matrices, making it difficult to gain insight into the modeled phenomenon or compare the model with available empirical or theoretical models. Information on the relative importance of the various inputs to the model is not readily available, which hampers efforts for model reduction by discarding less significant inputs. Additional processing, using techniques such as the principal component analysis, may be required for this purpose.

4.7 General Regression Neural Networks

In 1990, Donald F. Specht formulated the weighted-neighbor method in the form of a neural network. He called this a Probabilistic Neural Network. Here is a diagram of a GRNN network

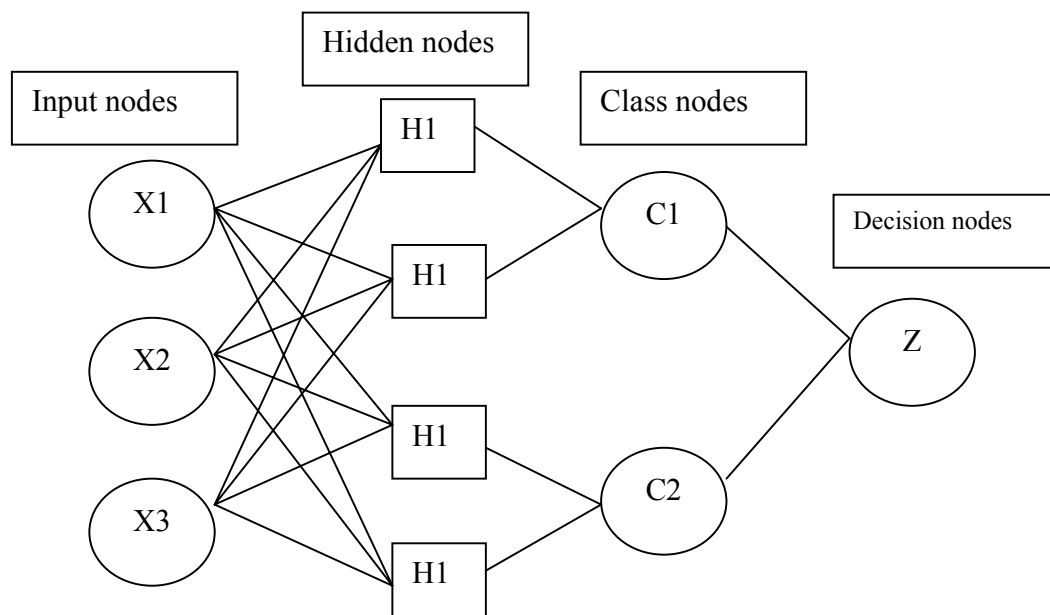


Figure.4.11 Typical GRNN architecture

All GRNN networks have four layers:

🚦 Input layer (Input nodes)

There is one neuron in the input layer for each predictor variable. The input neurons (or pre-processing before the input layer) standardize the range of the values by subtracting the median and dividing by the interquartile range. The input neurons then feed the values to each of the neurons in the hidden layer.

🚧 Hidden layer (Hidden nodes)

This layer has one neuron for each case in the training data set. The neuron stores the values of the predictor variables for the case along with the target value. When presented with the \mathbf{x} vector of input values from the input layer, a hidden neuron computes the Euclidean distance of the test case from the neuron's center point and then applies the RBF (Radial Basis Function) kernel function using the sigma value(s). The resulting value is passed to the neurons in the pattern layer.

🚧 Pattern layer (Class nodes)

This layer has one neuron for each case in the training data set. The neuron stores the values of the predictor variables for the case along with the target value. When presented with the \mathbf{x} vector of input values from the input layer, a pattern neuron computes the Euclidean distance of the test case from the neuron's center point, and a radial basis function (RBF) (also called a "kernel function") is applied to the distance to compute the weight (influence) for each point,

$$Weight = RBF(distance) \text{ (equation 4.13).}$$

The calculations performed in each pattern neuron of GRNN are $\exp(-D^2/2\sigma^2)$ with the normal distribution centered at each training sample. The radial basis function is so named because the radial distance is the argument to the function. The further some other point is from the new point, the less influence it has. Different types of radial basis functions can be used, but the most common is the Gaussian function (figures 4.12 & 4.13). The peak of the radial basis function is always centered on the point it is weighting. The function's sigma value (σ) determines the spread of the RBF function; that is, how quickly the function declines as the distance increases from the point. With

larger sigma values and more spread, distant points have a greater influence. Then the resulting value is passed to the neurons in the summation layer.

Summation layer

There are only two neurons in the summation layer. One is the denominator summation unit, the other numerator summation unit. The denominator summation unit adds up the weight values coming from each of the hidden neurons. The numerator summation unit adds up the weight values multiplied by the actual target value for each hidden neuron.

Decision layer (Decision nodes)

The decision layer divides the value accumulated in the numerator summation unit by the value in the denominator summation unit, and it uses the result as the predicted target value.

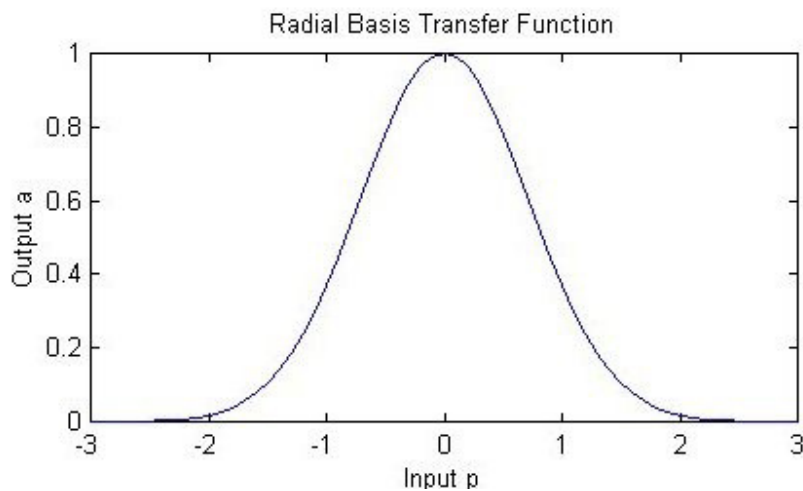


Figure.4.12 Radial Basis Transfer Function for one input

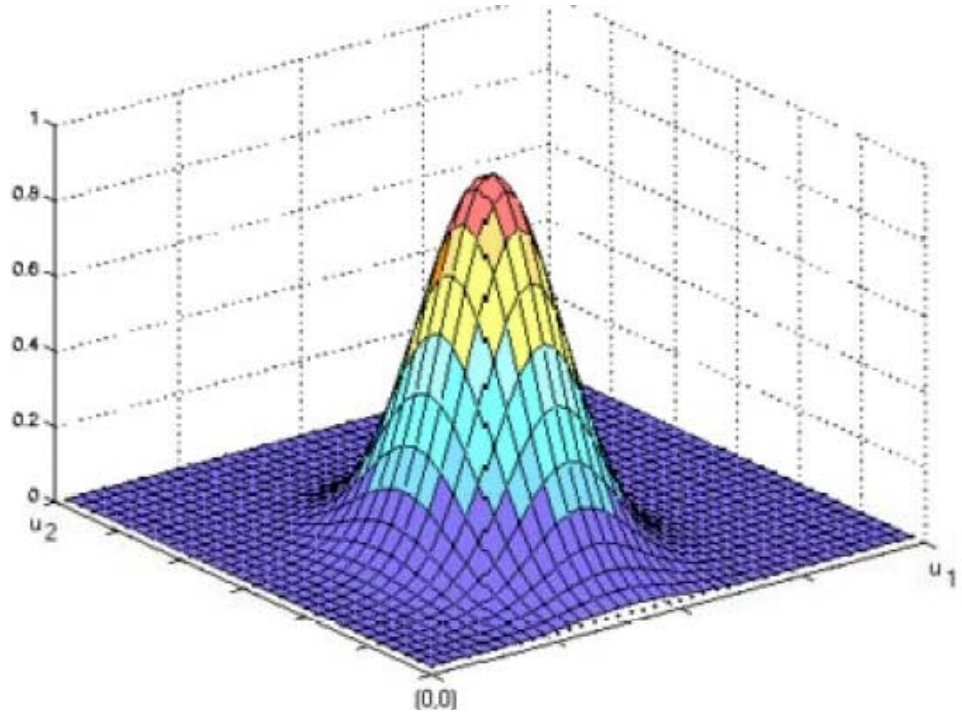


Figure.4.13 Radial Basis Transfer Function for multi inputs

The main consideration when training a GRNN network is the proper selection of the optimal sigma values to control the spread of the RBF functions.

$$Y(x) = \frac{\sum_{i=1}^n y_i \exp(-D_i^2 / 2\sigma^2)}{\sum_{i=1}^n \exp(-D_i^2 / 2\sigma^2)} \quad (4.13)$$

$$D_i^2 = (x - x_i)^T (x - x_i)$$

4.7.1 Advantages and disadvantages of GRNN

GRNN networks have advantages and disadvantages compared to multilayer perceptron networks:

- ✚ It is usually much faster to train a GRNN network than an MLP network.
- ✚ GRNN networks are often more accurate than MLP networks.
- ✚ GRNN networks are relatively insensitive to outliers
- ✚ GRNN networks are slower than MLP networks at classifying new cases.
- ✚ GRNN networks require more memory space.

CHAPTER FIVE

PERFORMANCE ANALYSIS AND COMPARATIVE STUDIES

5.1 Overview

The main contribution of this Thesis is to investigate and develop neural network models for porosity, permeability and lithofacies estimation using Multilayer Perception Neural Network and General Regression Neural Network.

In the first part of this chapter, I present the implementation process for estimation of porosity, permeability and lithofacies from well logs based on the framework discussed in Chapter 4. The results to be presented have been obtained from the implementation of Multilayer Perception Neural Network (MLP) and General Regression Neural Networks (GRNN).

In the second part, I present the estimation of reservoir properties (porosity, permeability and lithofacies) from Seismic Attributes. Only those results will be presented which were obtained using General Regression Neural Network (GRNN).

In the third part, integration of well logs and seismic attributes will be used to predict porosity, permeability and lithofacies as a function of depth.

In the last part of the Thesis, I present the spatial prediction of these properties. The Neural Network Model used for this purpose was built using the professional software “Petrel” of Schlumberger.

5.2 DATA ANALYSIS

In this study I used a data set from a Reservoir in South Algeria. The data consist of well logs, core porosity values, core permeability values and data of a 3-D seismic survey. The study area has seven wells from which 3 wells have core data. In this work we used two wells named Well-1 , Well-2 with a total of 145 data samples. I investigated these data sets, and performed statistical analysis to determine the hidden patterns and deterministic relationship between the actual outputs and the provided input features. This helps to get more knowledge about the data. The two wells were combined together and divided randomly into two sets, namely the training and testing sets of 70% and 30% respectively. The training set was then used to build the model while the testing set was used to evaluate the predictive power of the model. In order to study the prediction of porosity and permeability six well logs namely; Sonic log (DT), Neutron log (NPHI), Density log (RHOB), Gamma Ray (GR), Deep Resistivity (LLD), and Shale Volume (Vsh) were used as inputs to both networks.

To determine the performance and accuracy of the models, I made use of some of the statistical quality measures, namely: correlation coefficient, and root mean squared error. A good model should have a high correlation coefficient (CC) and a low root mean square error (RMSE).

Table 5.1: Statistics of the combined wells 1 and 2 (Training set)

Well Logs	Min	Max	Mean	STDEV
DT(Sonic) <i>foot / μs</i>	52.94	72.54	65.61	3.96
GR(Gamma Ray) <i>API</i>	43.12	132.80	84.36	22.23
RHOB(Bulk Density) <i>g / cm³</i>	2.40	2.77	2.62	0.08
NPHI (Porosity Log) %	3.31	18.41	8.91	3.67
LLD(deep resistivity) <i>Ωm</i>	2.93	16.79	7.55	2.97
Vsh(Shale volume) %	12.30	99.80	58.19	28.21

Table 5.2: Statistics of the combined wells 1 and 2 (Testing set)

Well Logs	Min	Max	Mean	STDEV
DT(Sonic) <i>foot / μs</i>	52.94	72.54	64.91	3.84
GR(Gamma Ray) <i>API</i>	43.12	132.80	87.99	41.44
RHOB(Bulk Density) <i>g / cm³</i>	2.41	2.77	2.53	0.08
NPHI (Porosity Log) %	3.31	18.41	5.56	1.18
LLD(deep resistivity) <i>Ωm</i>	2.93	16.79	6.98	4.76
Vsh(Shale volume) %	12.30	99.8	23.21	12.24

5.3 Experimental Results Using Mutilayer Perception and General Regression Neural Networks

An MLP model was developed to estimate porosity and permeability along the vertical axis using well log data. Different models were tried before selecting the best one. The best model had one input layer with six neurons, two hidden layers with twenty neurons (ten for each) and one output layer. Purely linear and sigmoidal functions were used as activation functions for this model.

5.3.1 Porosity Estimation Results From Well Logs

✚ The MLP model is able to predict porosity, with a correlation coefficient $CC=0.91$ and $MSE=0.10$ for the training set, but $CC = 0.66$ and $MSE= 0.40$ for the testing set. The results for the estimation are shown in Table 4.3, while Figures 4.1a and 4.1b show the performance plot for the best selected model.

✚ The GRNN model was built to predict porosity, using the following parameters: The appropriate sigma (0.01-50) for each variable and the Gaussian as kernel function. The results provided by GRNN were for the training process $CC=0.97$ and $MSE =0.07$, while for the testing process $CC=0.81$ and $MSE=0.37$. Figures 4.2a and 4.2b show the performance plot for the best selected model.

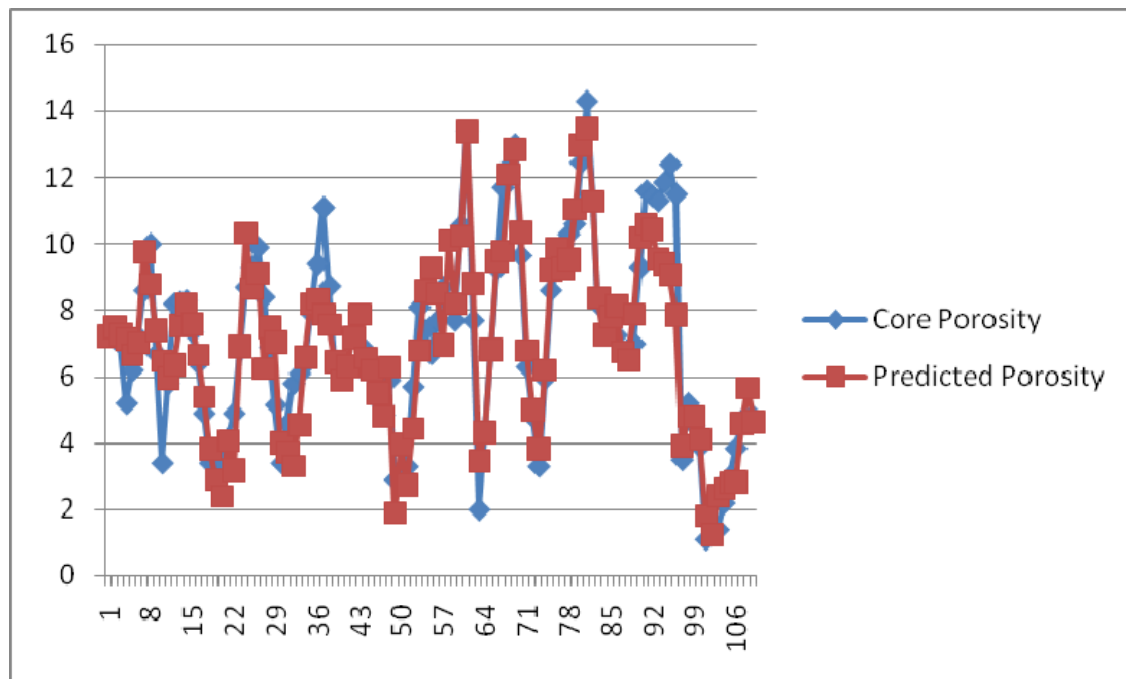
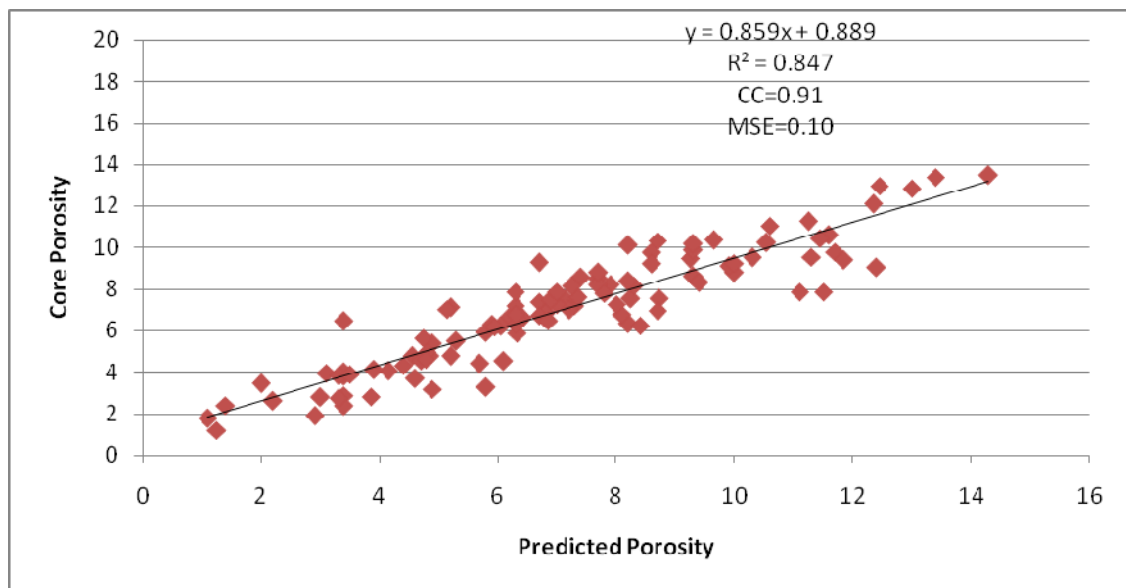


Figure 5.1a Training core porosity vs predicted porosity using MLP

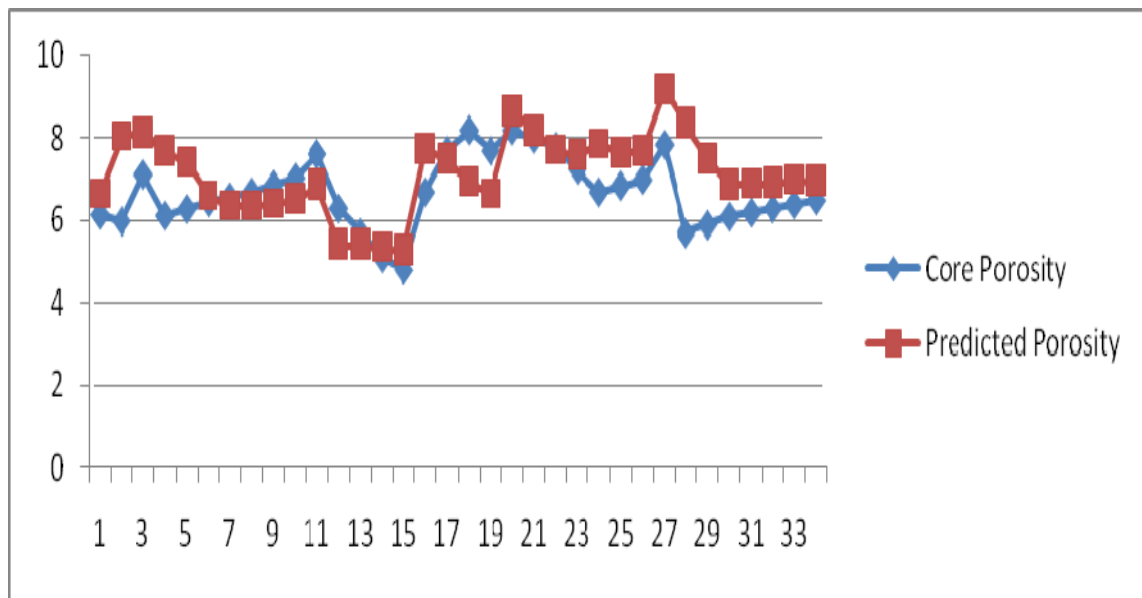
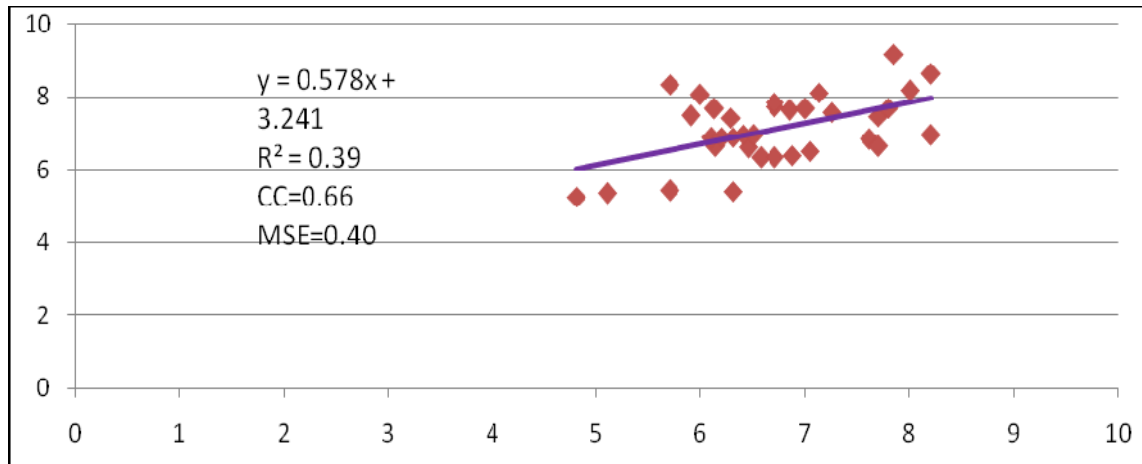


Figure 5.1b Testing core porosity vs predicted porosity using MLP

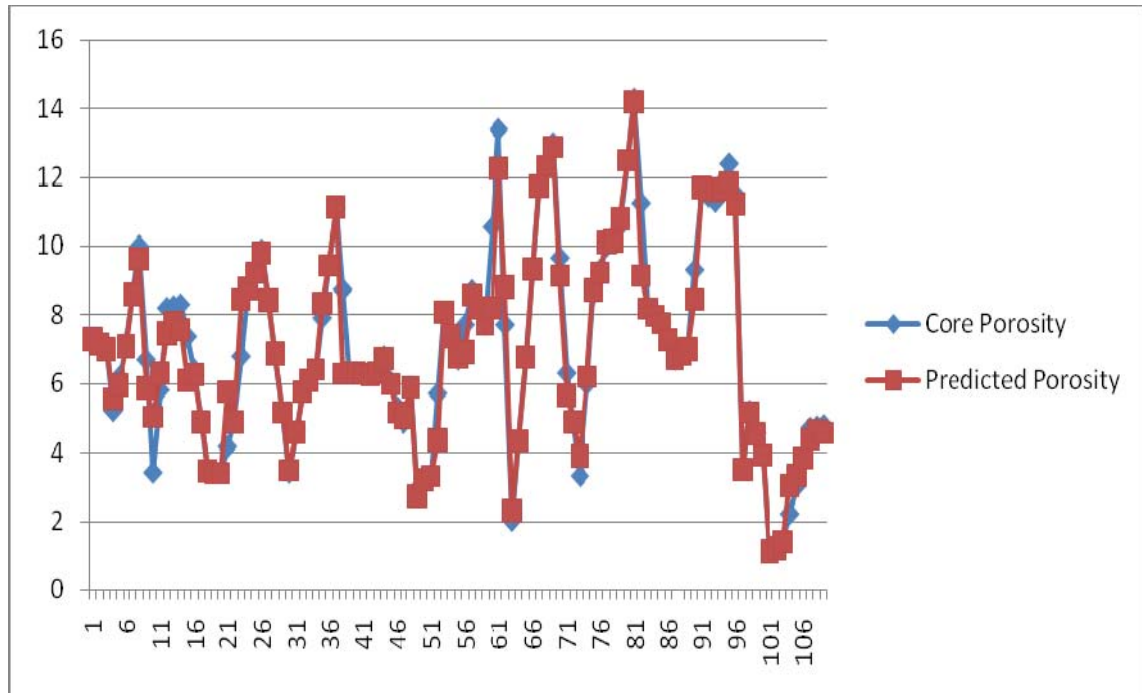
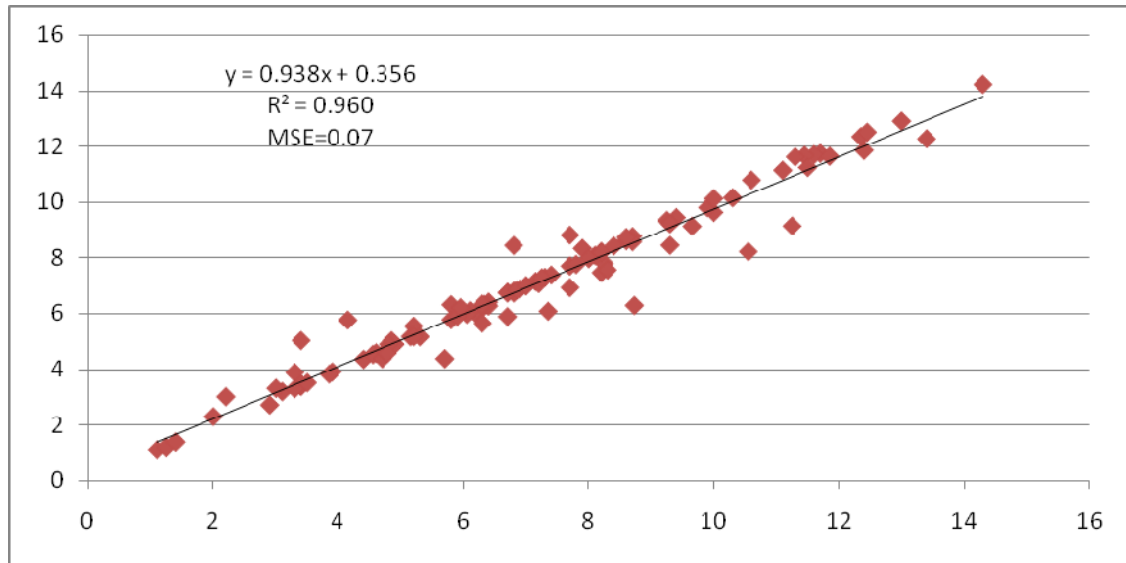


Figure 5.2a Training core porosity vs predicted porosity using GRNN

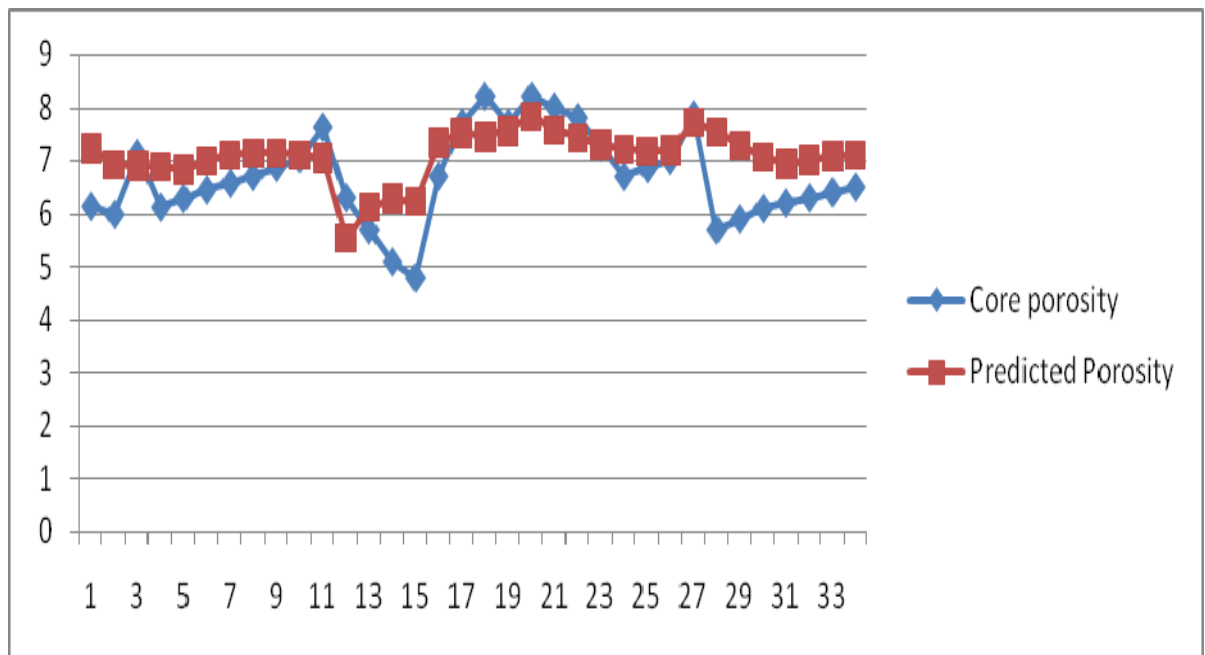
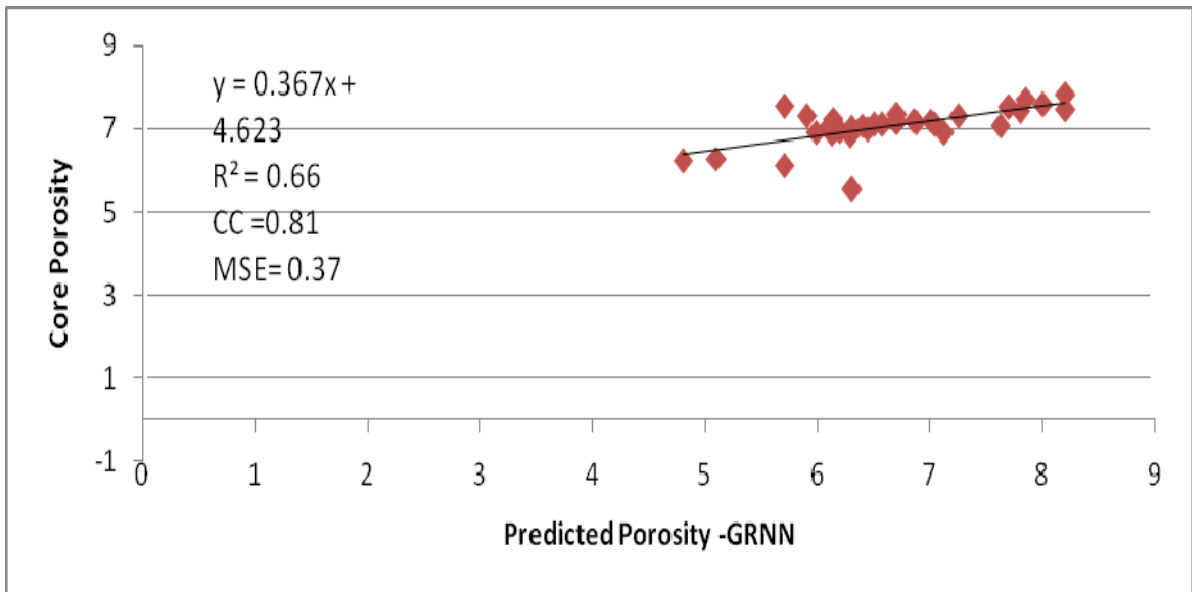
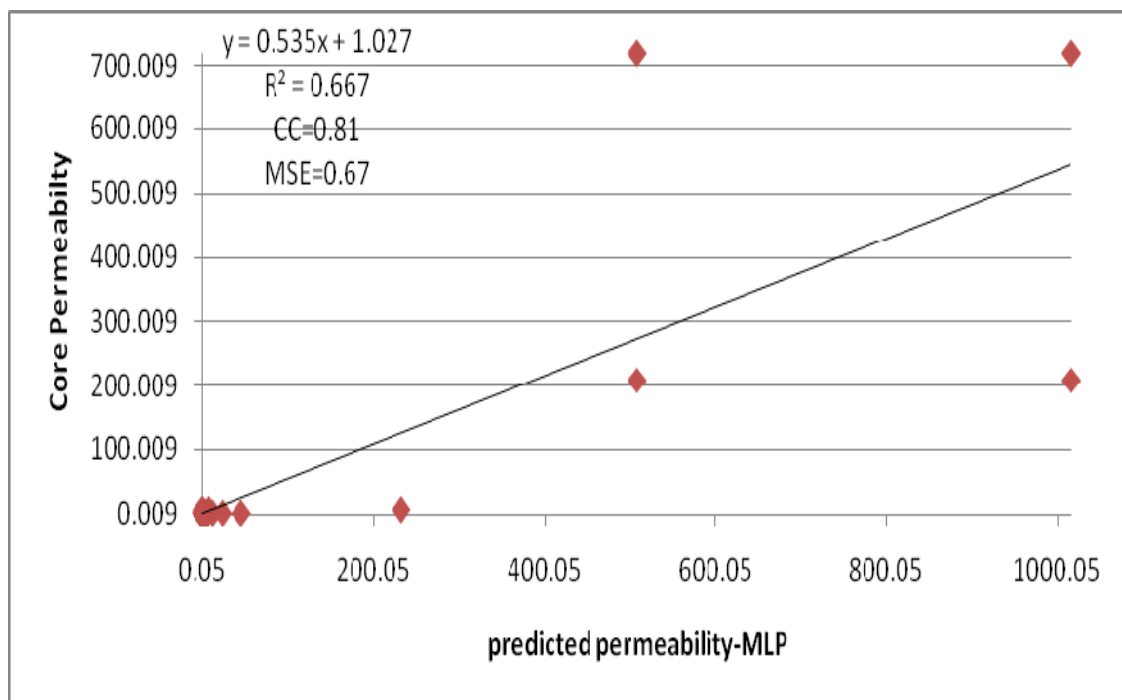


Figure 5.2b Testing core porosity vs predicted porosity using GRNN

5.3.2 Permeability Estimation Results From Well Logs

✚ An MLP model was built to predict permeability from well log data. The results gave a correlation coefficient $CC=0.81$ and $MSE=0.67$ for the training set, but $CC = 0.72$ and $MSE= 0.37$ for the testing set. Figures 4.3a and 4.3b show the performance plot for the permeability prediction using MLP model.

✚ Another model for permeability estimation was developed using GRNN paradigm. The results were much better with $CC=0.99$ and $MSE=0.23$ for training data and $CC=0.96$ and $MSE =0.24$ for the testing data. Figures 4.4a and 4.4b show the performance of the model.



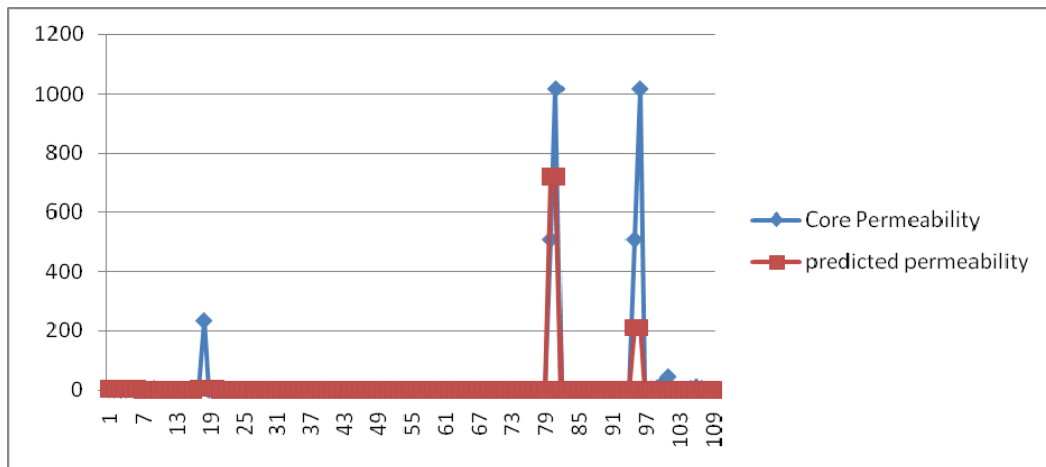
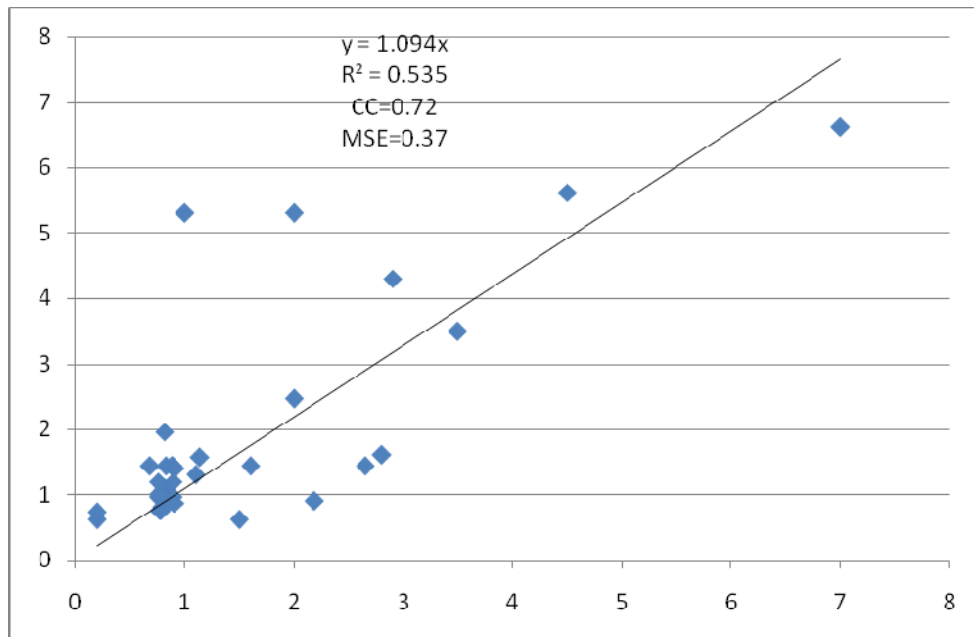


Figure 5.3a Training core permeability vs predicted permeability using MLP



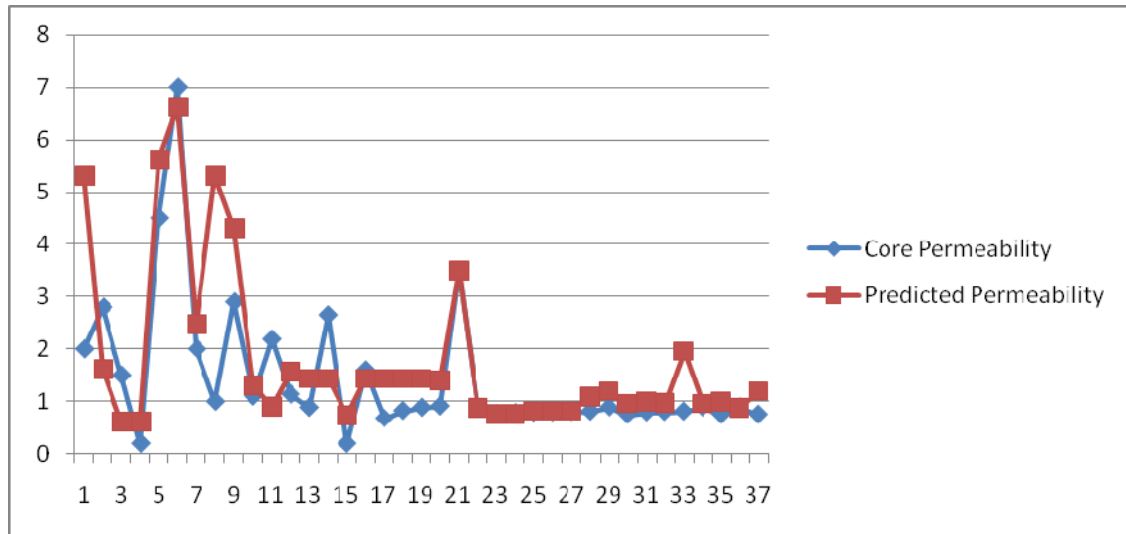
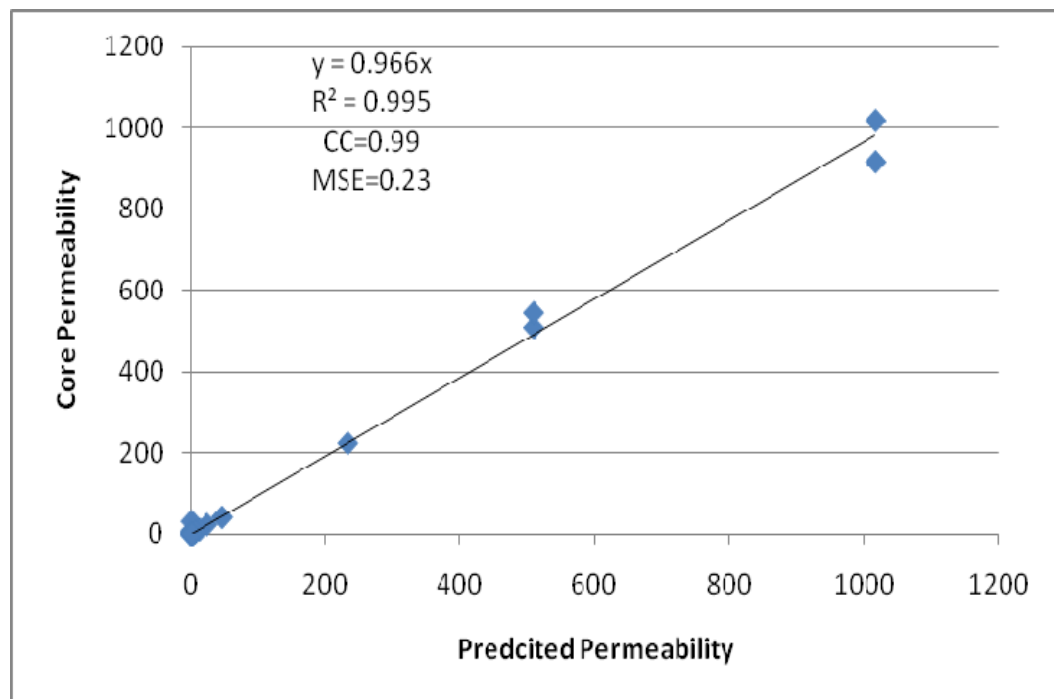


Figure 5.3b Testing core permeability vs predicted permeability using MLP



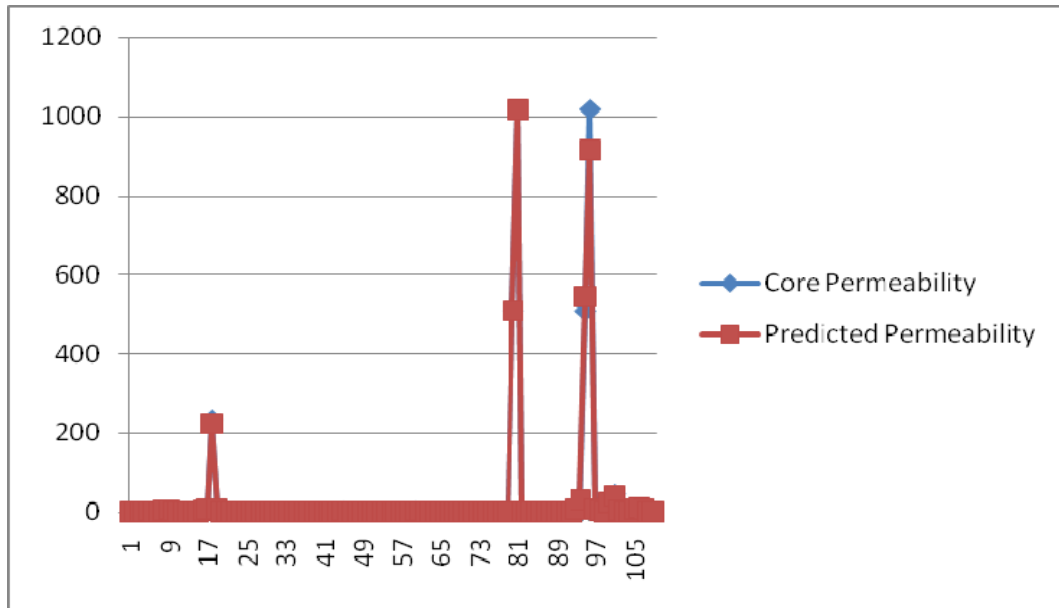
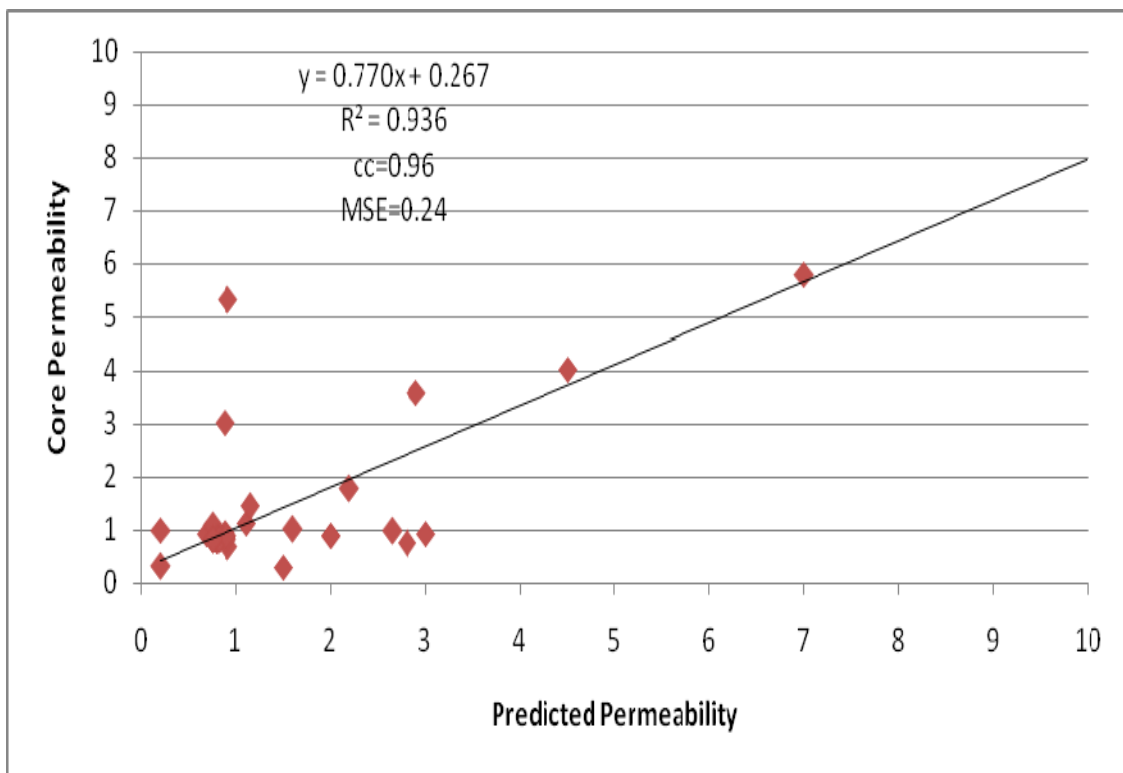


Figure 5.4a Training core permeability vs predicted permeability using GRNN



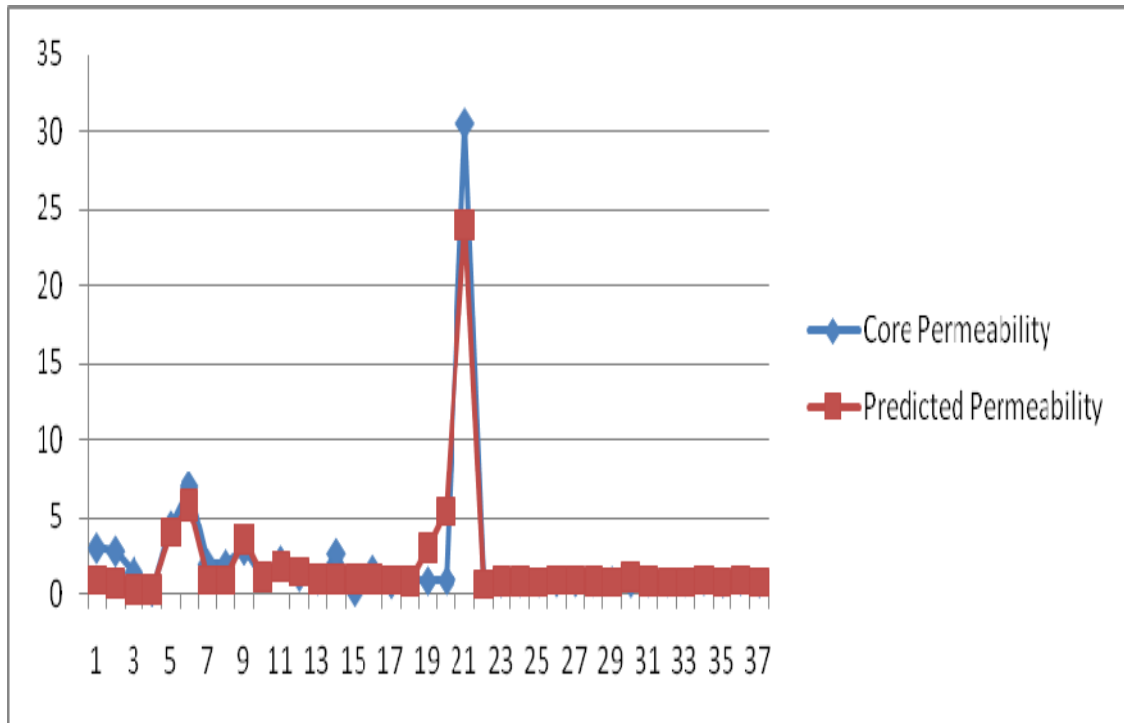


Figure 5.4b Testing core permeability vs predicted permeability using GRNN

Table 5.3 Results Summary for MLP and GRNN models

Type of Paradigm	Porosity	Permeability
Multilayer Perceptron Neural Network	Training (CC=0.91& MSE=0.10)	Training (CC=0.81 & MSE=0.67)
	Testing (CC=0.66 & MSE=0.40)	Testing (CC=0.72 & MSE=0.37)
General Regression Neural Network	Training (CC=0.97 & MSE=0.67)	Training (CC=0.99 & MSE=0.23)
	Testing (CC=0.81& MSE=0.37)	Testing (CC=0.96 & MSE=0.24)

5.3.3 Porosity Estimation Results From Seismic Attributes

In this study five attributes were selected for reservoir properties prediction:

Instantaneous Frequency, Instantaneous Phase, Arc length, Half Energy, RMS amplitude.

These attributes were described in Chapter Three (Seismic Attributes).

Table 4.4 and 4.5 summarize the statistical properties of the selected attributes

Table 5.4 Statistical Properties of the Seismic Attributes (Training set)

Seismic Attributes	Min	Max	Mean	STDEV
Instantaneous Frequency	26.31	98.82	39.47	17.12
Instantaneous Phase	-28.02	29	-3.83	12.29
Arc length	60.1	5741.5	480.04	705.94
Half energy	4	26	13.28	5.80
RMS amplitude	1888.24	210696	10364.64	25688.18

Table 5.5 Statistical Properties of the Seismic Attributes (Testing set)

Seismic Attributes	Min	Max	Mean	STDEV
Instantaneous Frequency	25.92	40.92	32.65	3.60
Instantaneous Phase	-43.47	-0.52	-21.23	12.18
Arc length	228.80	5741.50	424.90	115.52
Half energy	10	26	18.5	4.98
RMS amplitude	1091.18	7861.8	5834.81	2198.29

Note: For GRNN and MLP models using Seismic Attributes I used the two wells, and extracted the seismic attributes at the well location ("Well Seismic"). I took as a reference the top of the reservoir and calculated the attributes at every two millisecond (sample rate =2 ms) for the total depth of 80ms (TWT) in each well.

Figures 4.5 and 4.6 show the base map and the 3-D seismic volume for the study site in which it indicates the location of the main wells drilled in this area. Figure 4.7 illustrate the top of the reservoir T1.

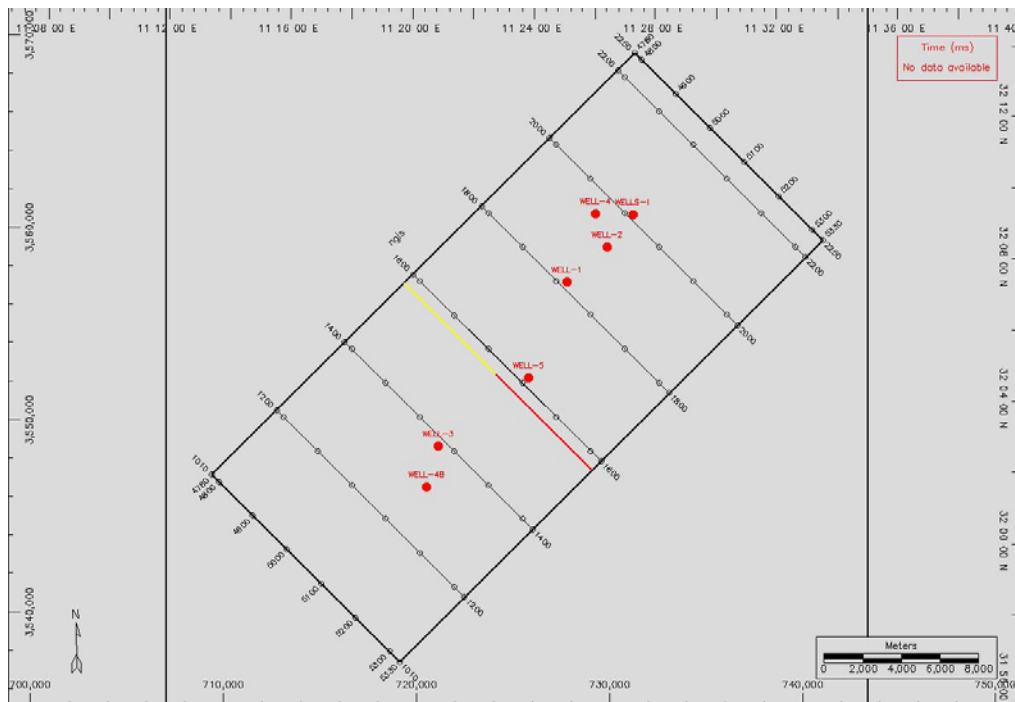


Figure 5.5 Base map of the study area

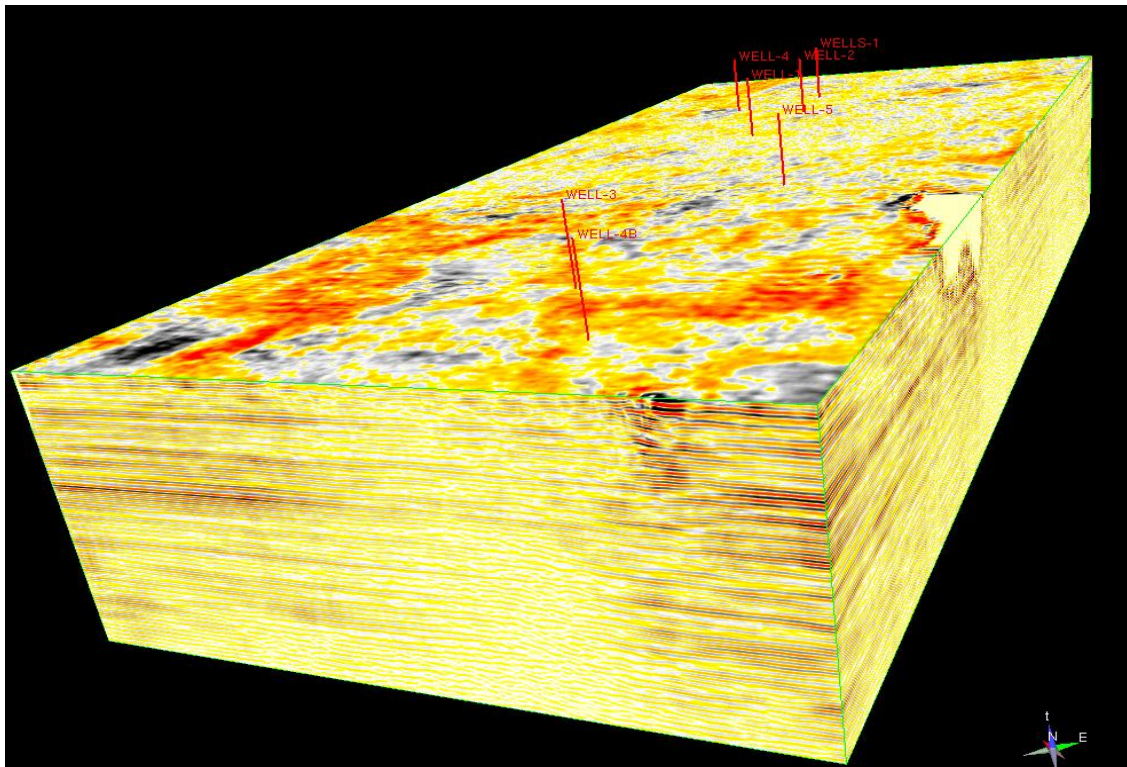


Figure 5.6 3D Seismic Volume of the study site

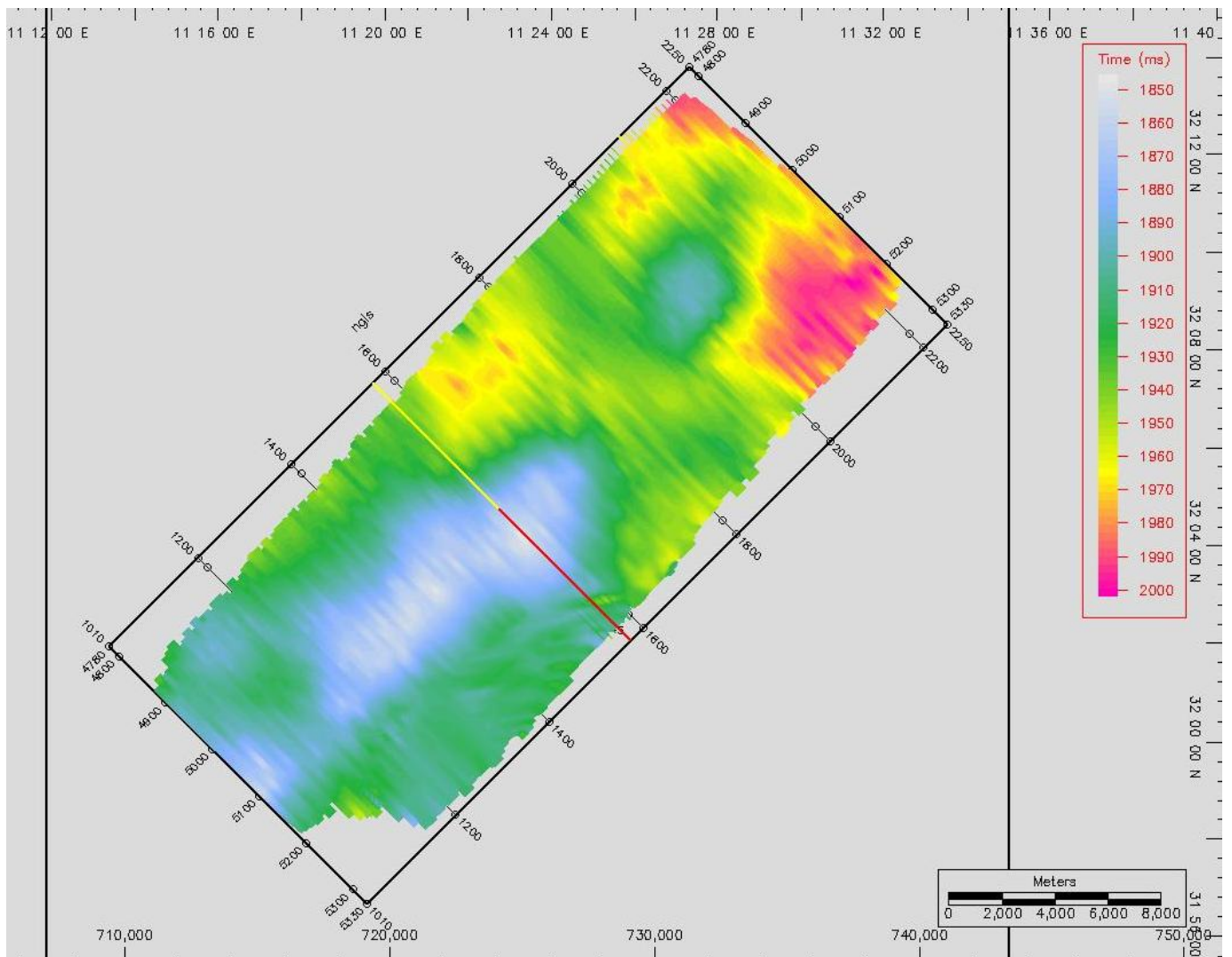


Figure 5.7 Top of T1 on base map

As it was mentioned in Chapter Three, the seismic attributes can be extracted as a total volume or as a surface or horizon. Figures 4.8 and 4.8b illustrate the total volume of the instantaneous frequency and RMS amplitude attributes.

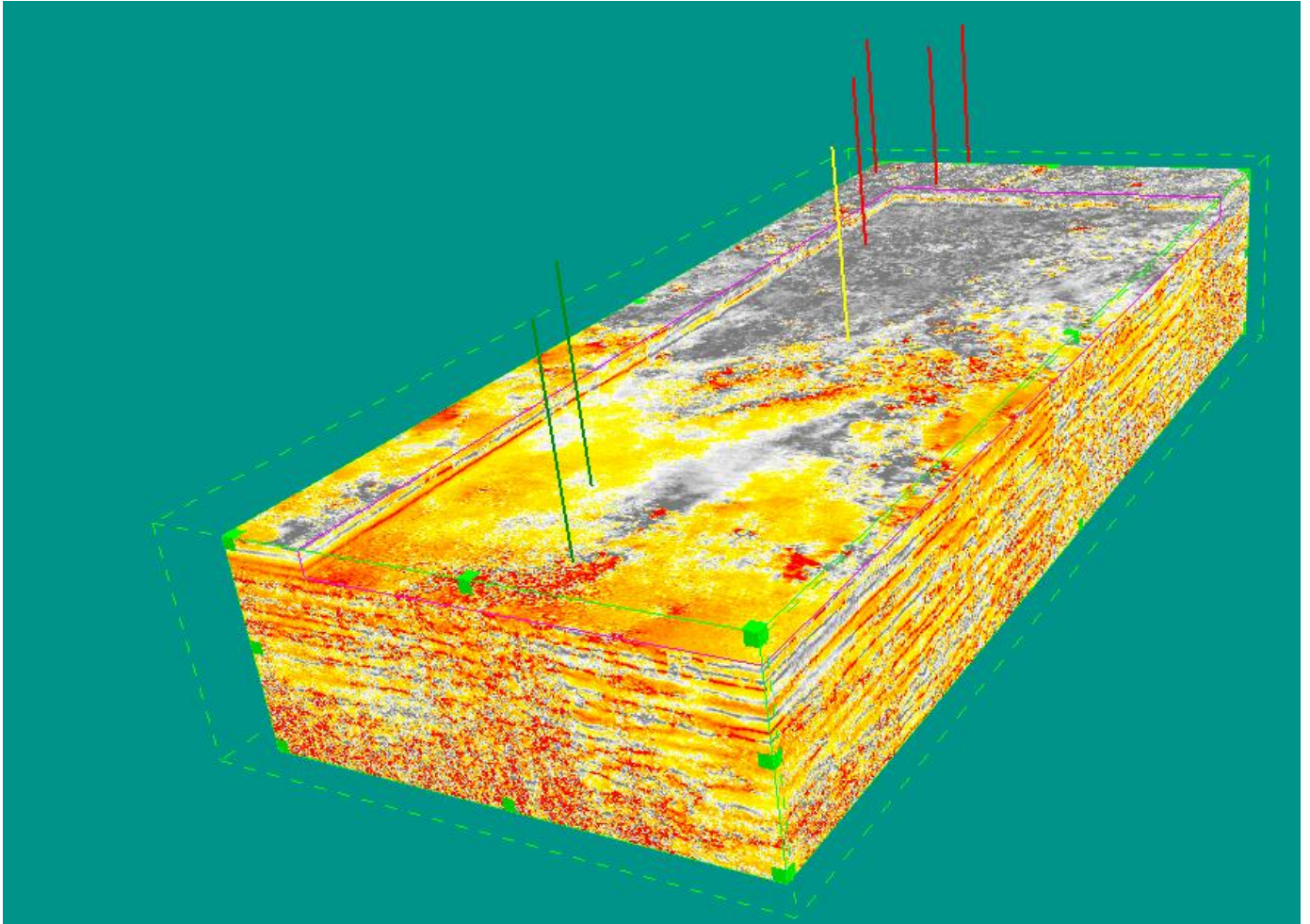


Figure 5.8a 3D Volume of Instantaneous Frequency

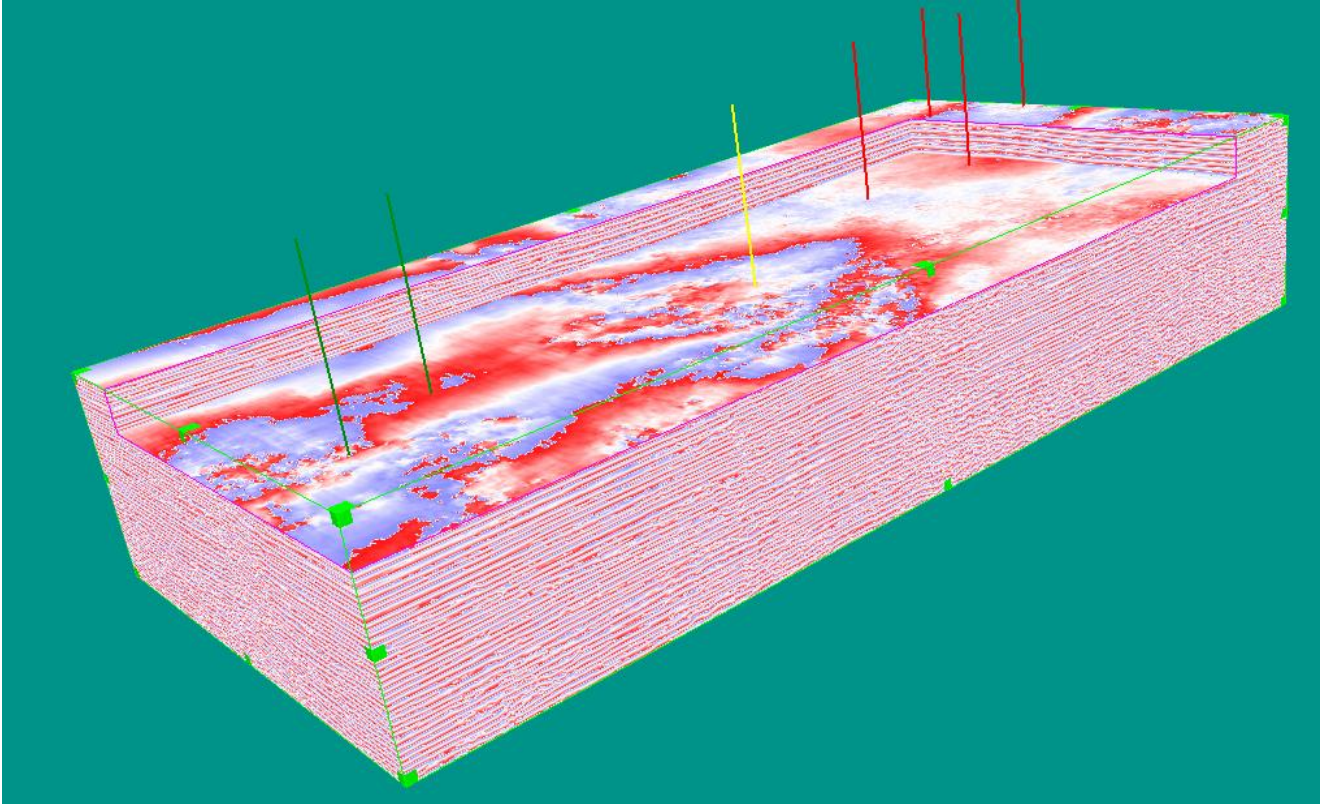


Figure 5.8b 3D Volume of RMS amplitude

From these volumes surface or horizon attributes can be extracted. Figures 4.9a, 4.9b, 4.9c, 4.9d show the time-slice attributes (Instantaneous Frequency) at different levels (2ms,8ms,12ms,20ms), while figures 4.10a, 4.10b, 4.10c, 4.10d show the time slice of (Instantaneous Phase) at (2ms,6ms,10ms,12ms).

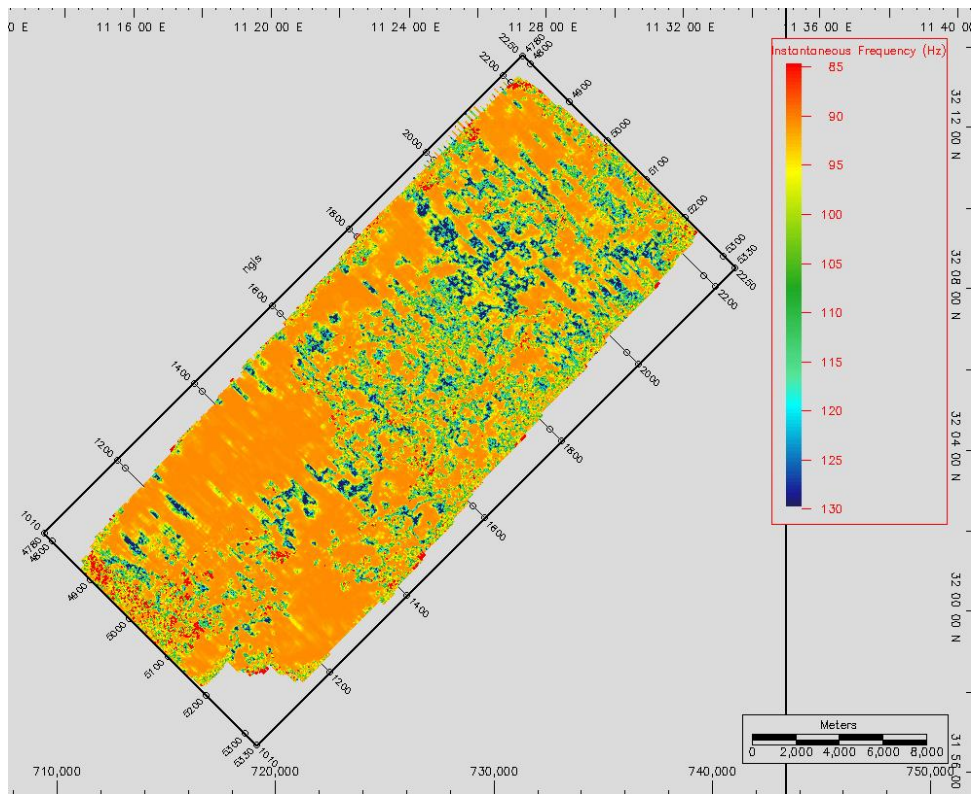


Figure 5.9a Time slice of the Instantaneous Frequency at 2ms

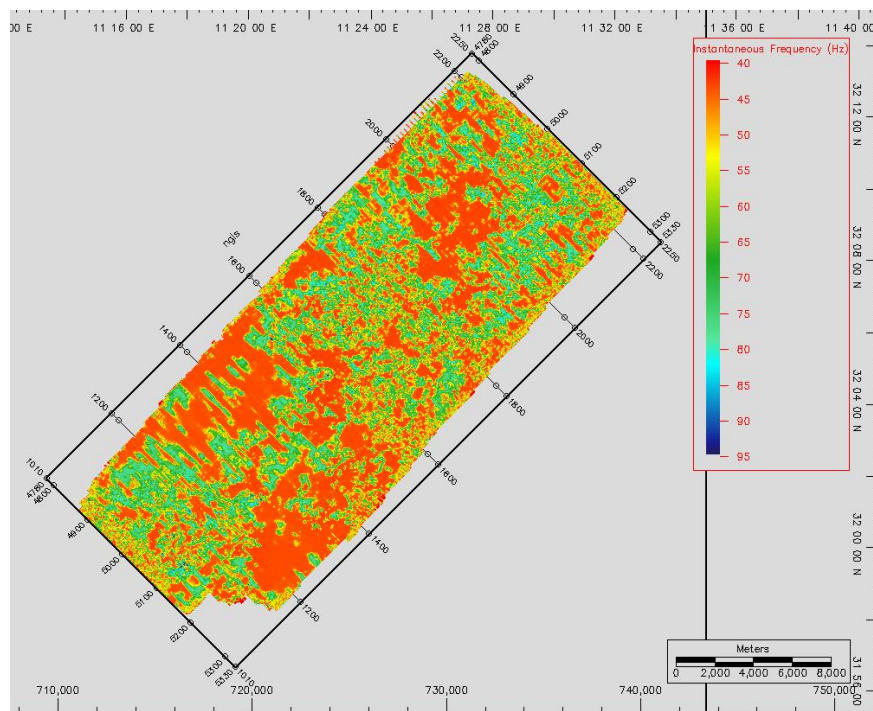


Figure 5.9b Time slice of the Instantaneous Frequency at 8ms

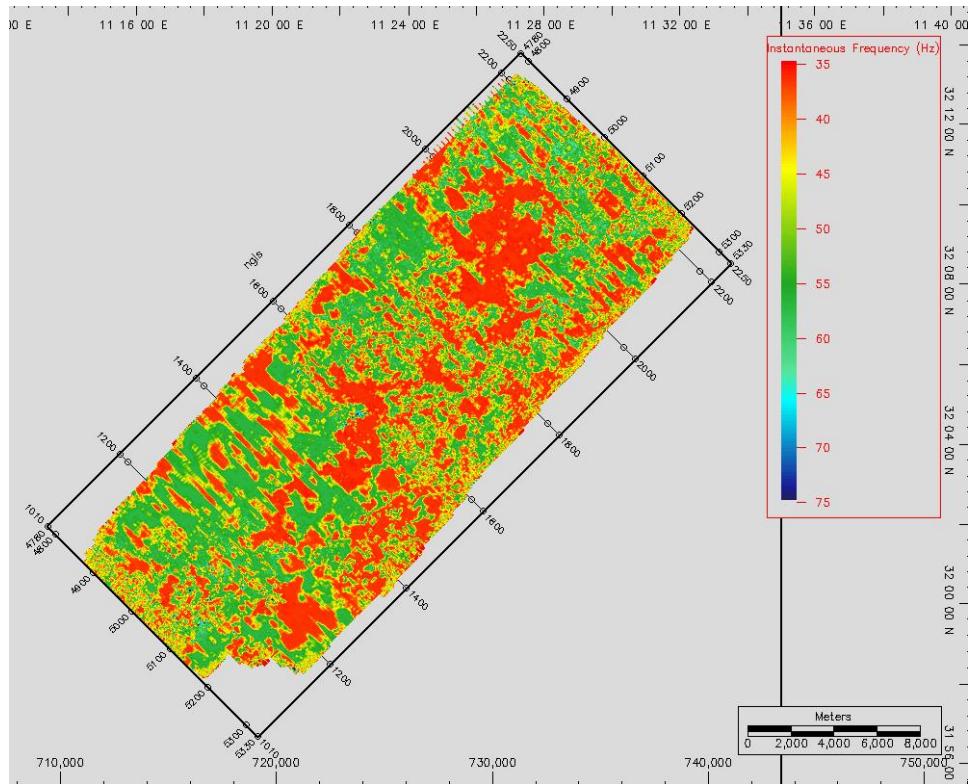


Figure 5.9c Time slice of the Instantaneous Frequency at 12ms

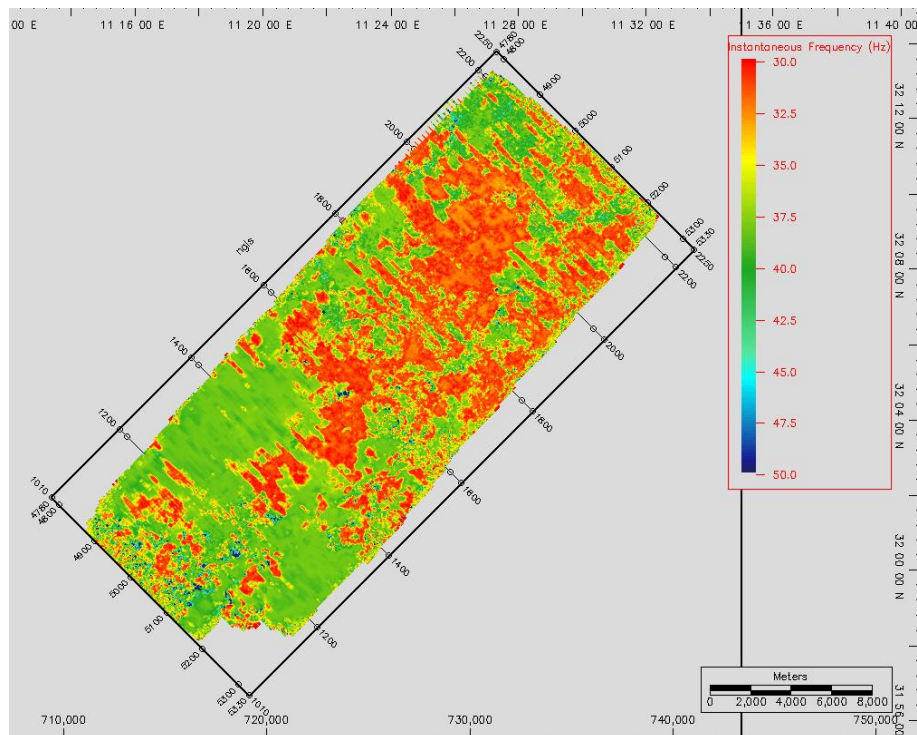


Figure 5.9d Time slice of the Instantaneous Frequency at 20ms

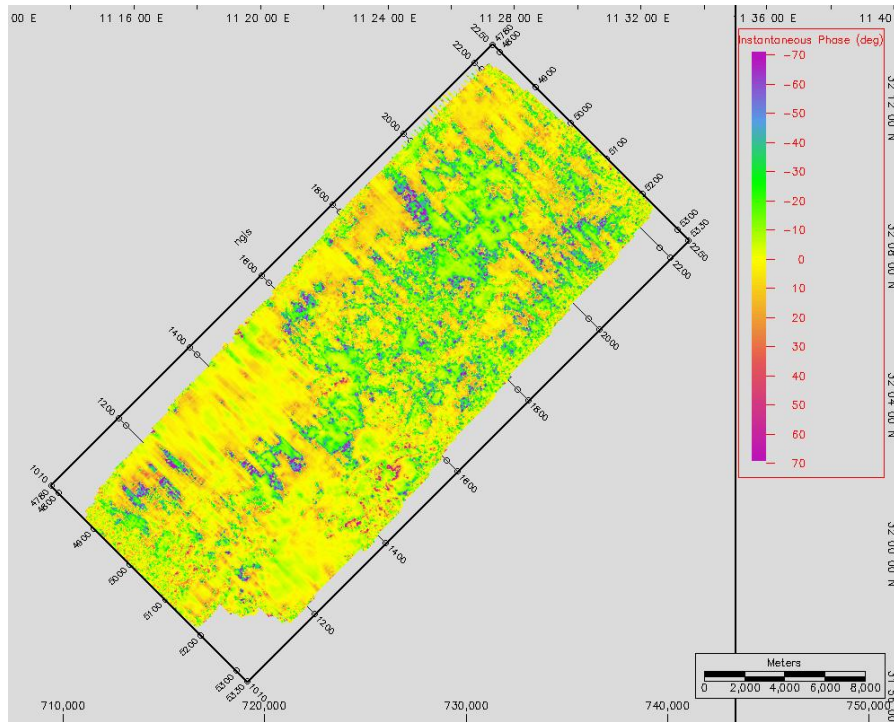


Figure 5.10a Time slice of the Instantaneous Phase at 2ms

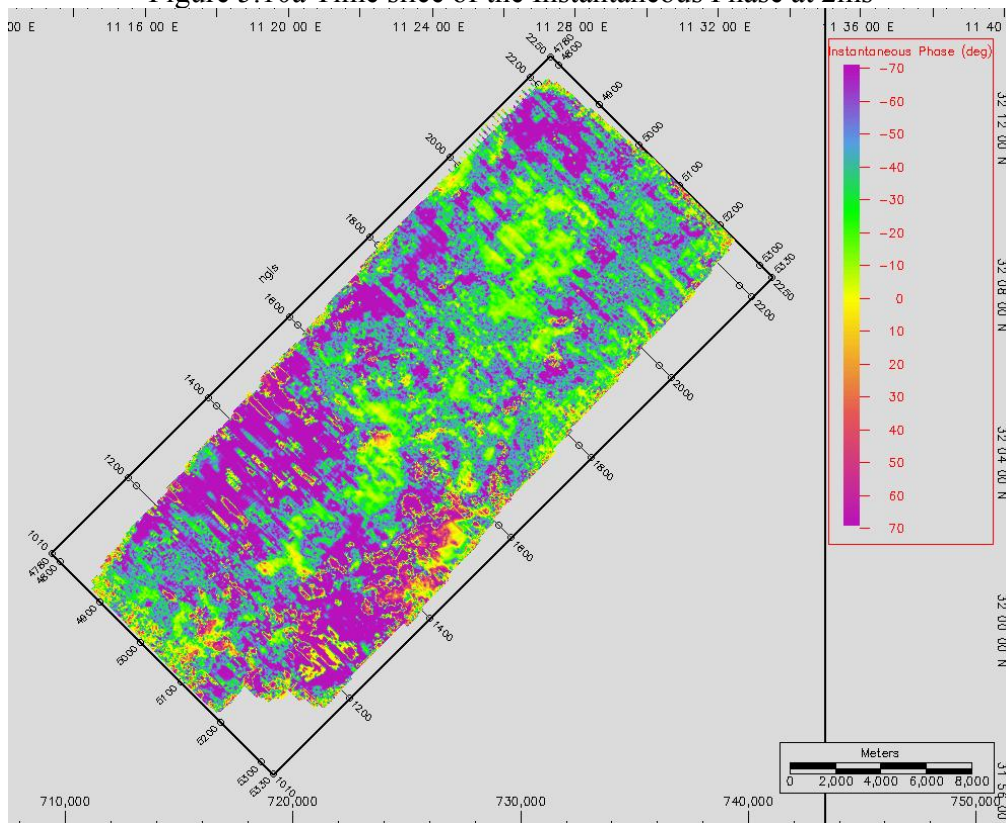


Figure 5.10b Time slice of the Instantaneous Phase at 6ms

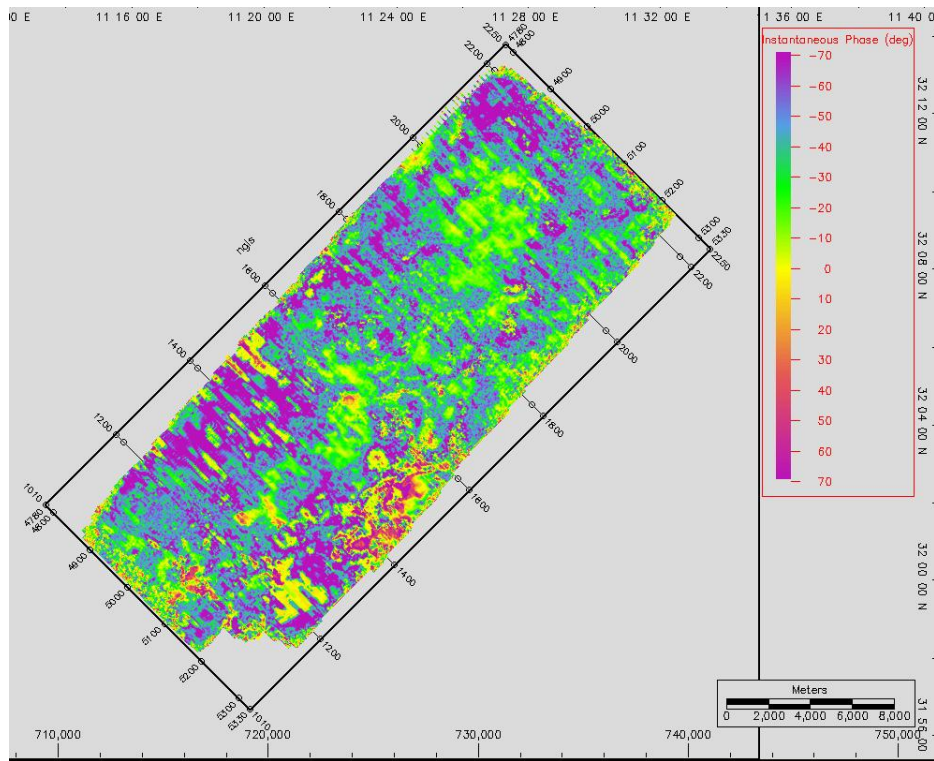


Figure 5.10c Time slice of the Instantaneous Phase at 10ms

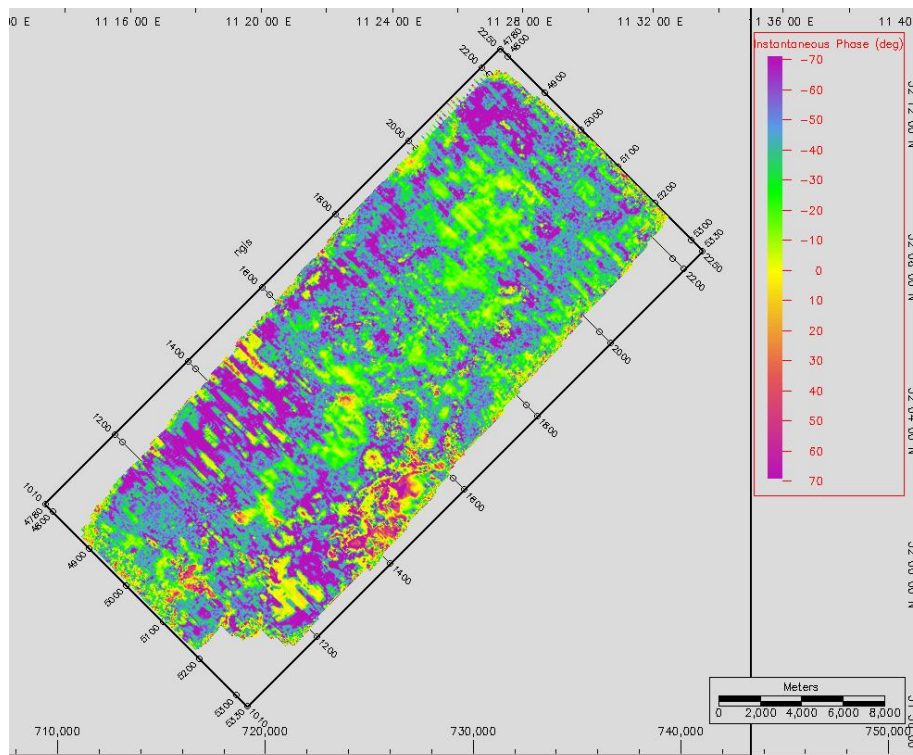


Figure 5.10d Time slice of the Instantaneous Phase at 12ms

5.3.4 GRNN MODEL FOR POROSITY

General Regression Neural Network was used to predict porosity along the vertical axis. Note that the core porosities used in the training process were averaged and scaled to be at the same scale as the seismic attributes. The results were acceptable with CC= 0.76 and MSE= 1.05 in the training stage, while the testing process gave CC=0.66 and MSE=0.66. Figures 4.11a and 4.11b show the model results

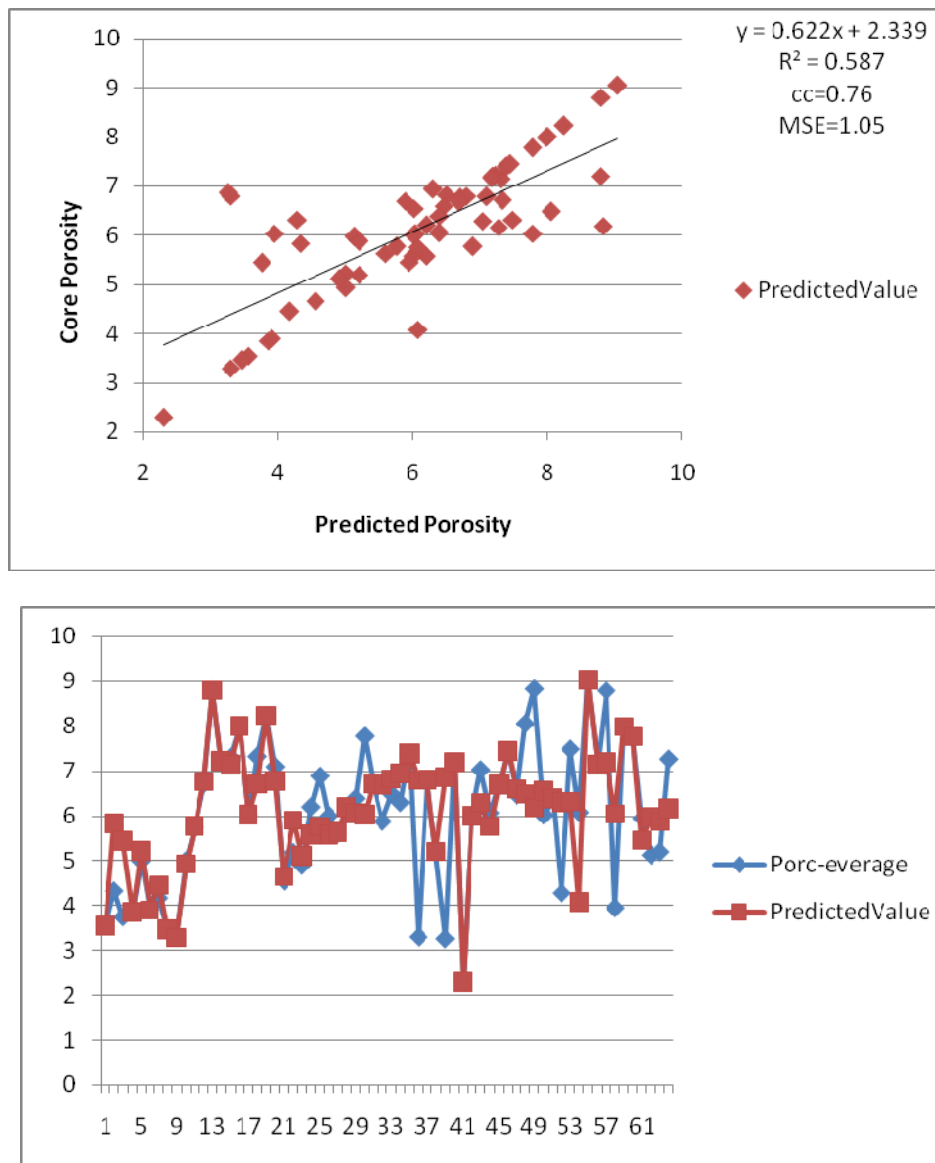


Figure 5.11a Training core porosity vs predicted porosity using GRNN

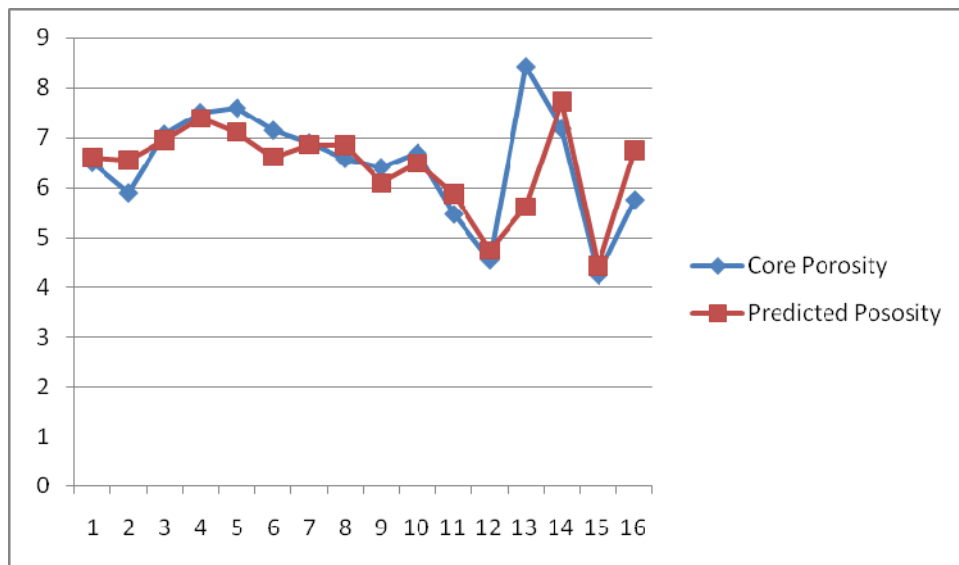
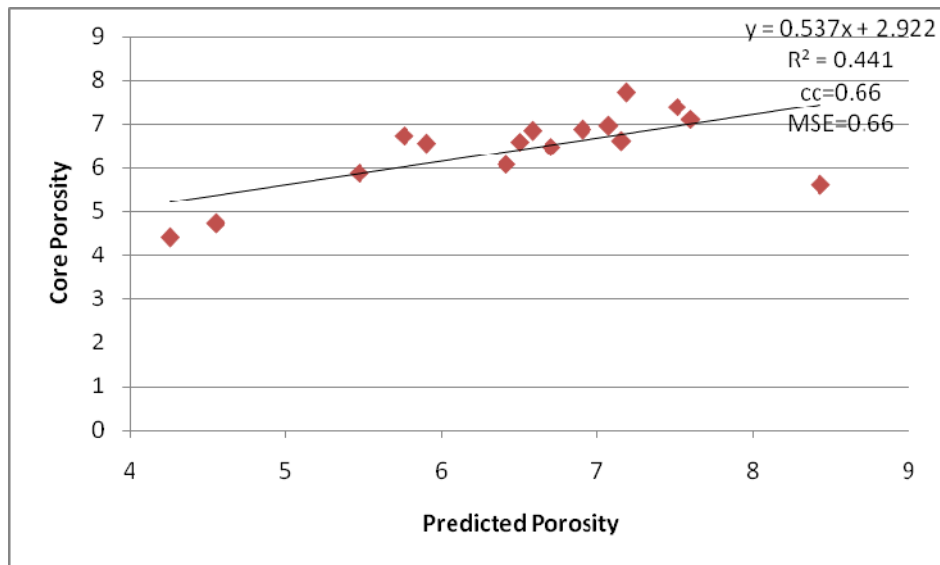


Figure 5.11b Testing core porosity vs predicted porosity using GRNN

5.3.5 GRNN MODEL FOR PERMEABILITY

The same what I did for porosity prediction was also repeated with the permeability model. The results gave CC= 0.83 and MSE = 2.21 in the training process but CC= 0.73 and 0.77 in the testing stage. Figures 4.12a and 4.12b illustrate the model performance.

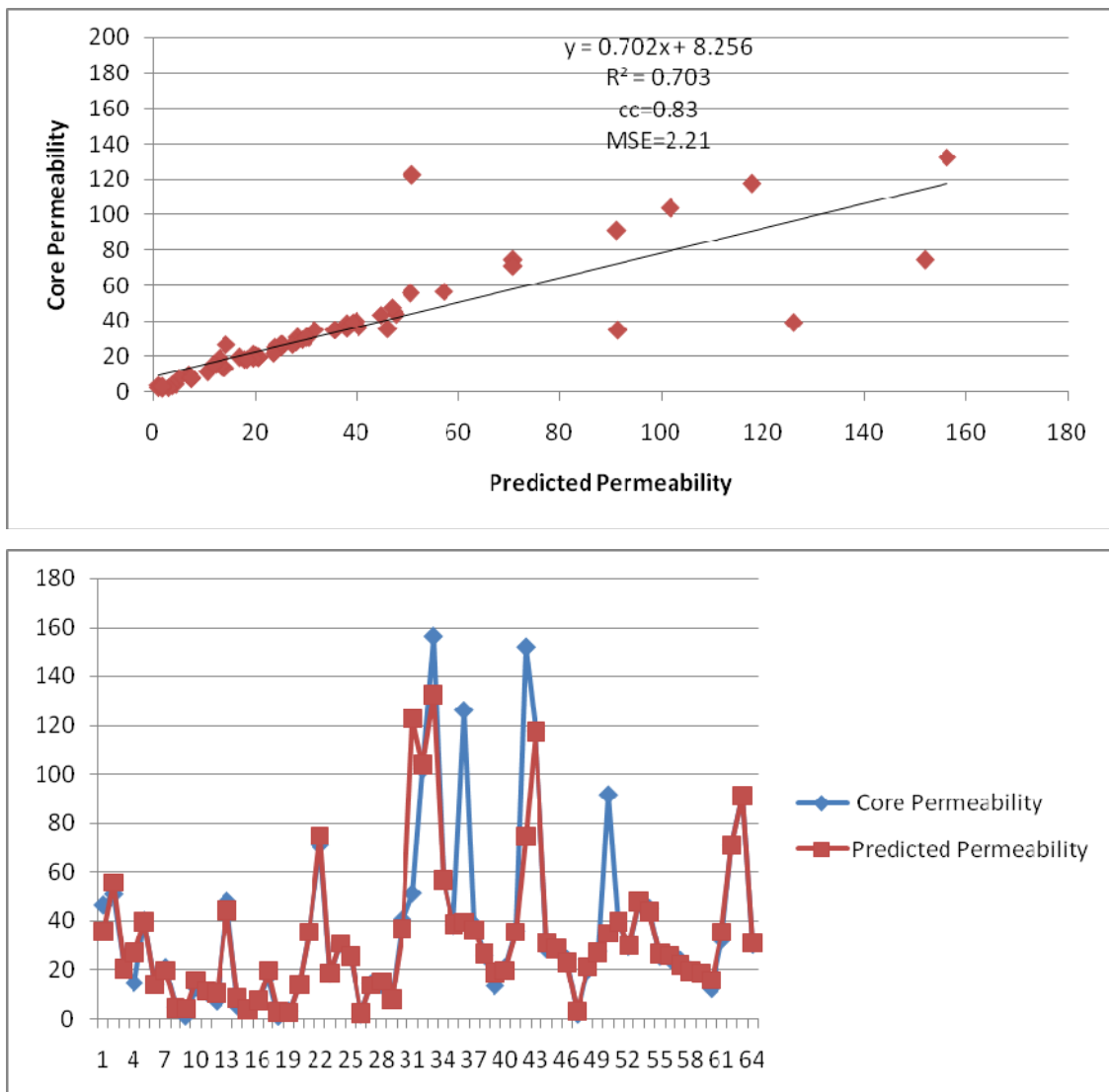


Figure 5.12a Training core permeability vs predicted permeability using GRNN

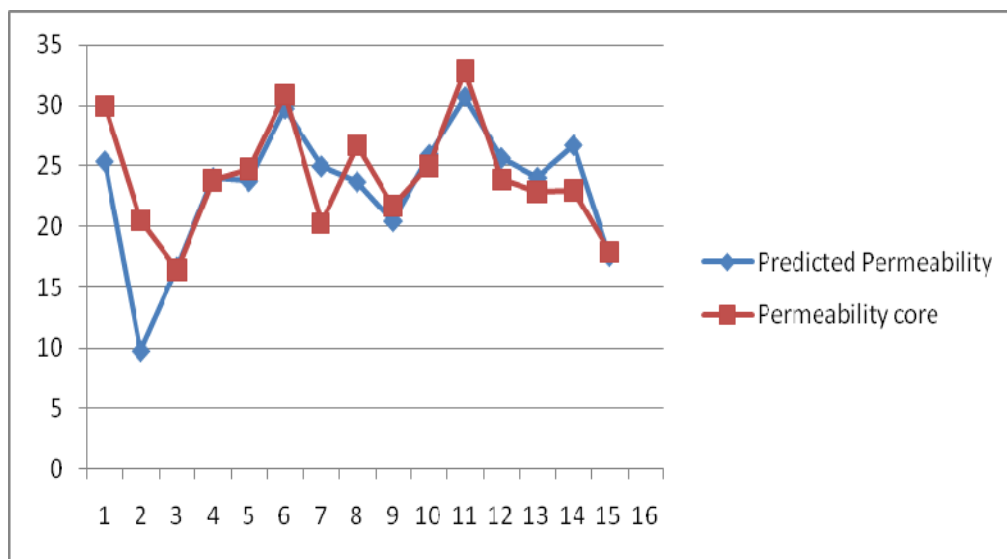
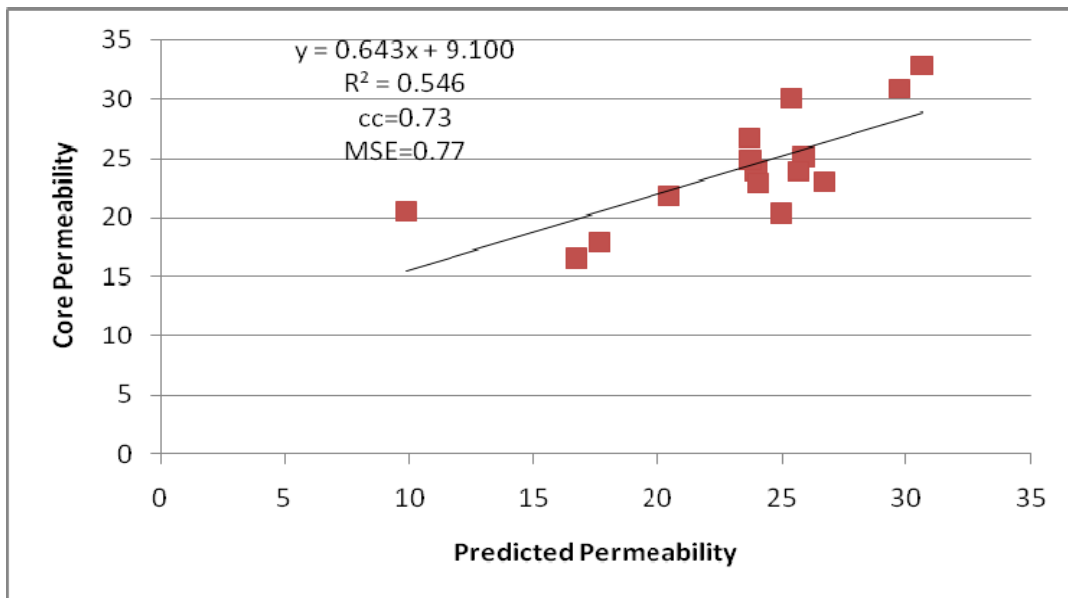


Figure 5.12b Testing core permeability vs predicted permeability using GRNN

5.4 Predicting Porosity and Permeability using Well logs and Seismic Attributes

The main objective of this Thesis has been the integration of well log data and seismic attributes to improve the results provided by each of them.

As I did in the previous section when I averaged the core data, in this section the logs were also averaged. Tables 4.6 and 4.7 summarize the statistical analysis of both seismic attributes and well logs after averaging.

Table 5.6 Statistical Analysis for Seismic Attributes and Logs (Training data)

Seismic Attributes	Min	Max	Mean	STDEV
Instantaneous Frequency	26.31	98.82	39.48	17.12
Instantaneous Phase	-28.02	29	-3.83	12.29
Arc length	60.10	5741.50	480.04	705.94
Half energy	4	26	13.28	5.80
RMS amplitude	1888.24	210696	10364.64	25688.18
DT(Sonic) <i>foot / μs</i>	58.06	77.88	66.07	4.24
GR(Gamma Ray) <i>API</i>	26.66	168.32	69.88	37.66
RHOB(Bulk Density) <i>g / cm³</i>	2.29	2.72	2.56	0.08
NPHI (Porosity Log) %	0.82	16.52	7.25	3.49
LLD(deep resistivity) Ωm	2.32	87.72	10.76	18.59
Vsh(Shale volume) %	3.74	99.80	35.43	26.38

Table 5.7 Statistical Analysis for Seismic and Logs (Testing data)

Seismic Attributes and well logs	Min	Max	Mean	STDEV
Instantaneous Frequency	25.92	40.92	32.65	3.60
Instantaneous Phase	-43.47	-0.52	-21.23	12.18
Arc length	228.8	5741.5	424.9	115.52
Half energy	10	26	18.5	4.98
RMS amplitude	1091.18	7861.8	5834.81	2198.29
DT(Sonic) <i>foot / μs</i>	68.44	55.93	62.41	3.74
GR(Gamma Ray) <i>API</i>	102.24	36.73	65.18	20.25
RHOB(Bulk Density) <i>g / cm³</i>	2.69	2.20	2.45	0.14
NPHI (Porosity Log) %	27.86	5.17	11.90	5.94
LLD(deep resistivity) Ωm	102.52	4.47	34.07	35.58
Vsh(Shale volume) %	70.94	4.35	28.42	21.25

5.4.1 GRNN MODEL FOR POROSITY

A GRNN model was built to estimate porosity using both seismic attributes and well log data. The results show CC = 0.93 and MSE =0.29 in the training stage, while testing produced results with CC= 0.90 and MSE= 0.16. Figures 4.13a and 4.13b show the model performance

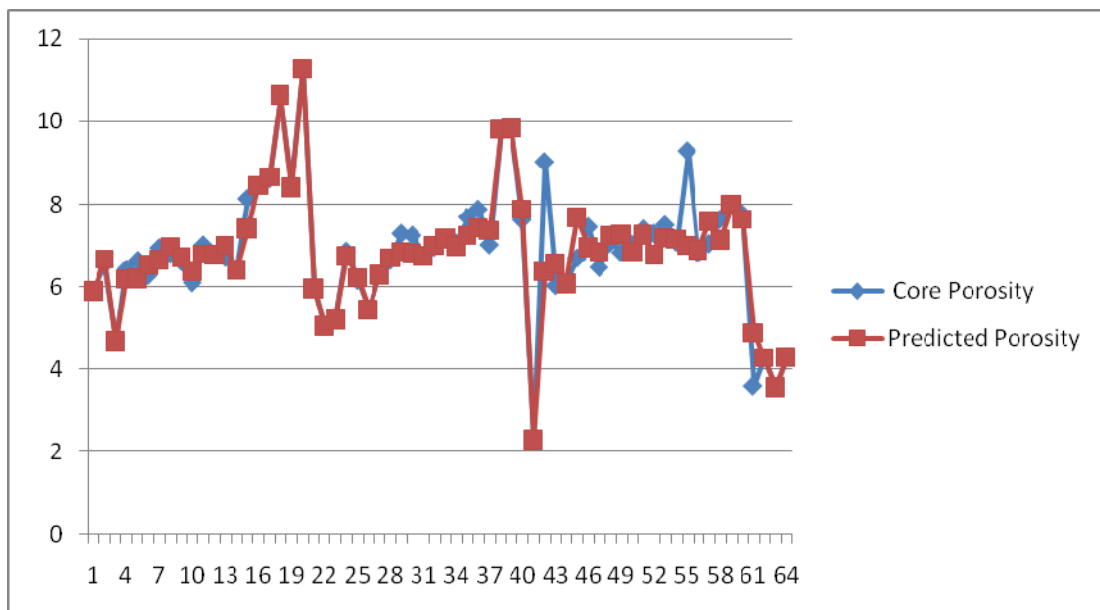
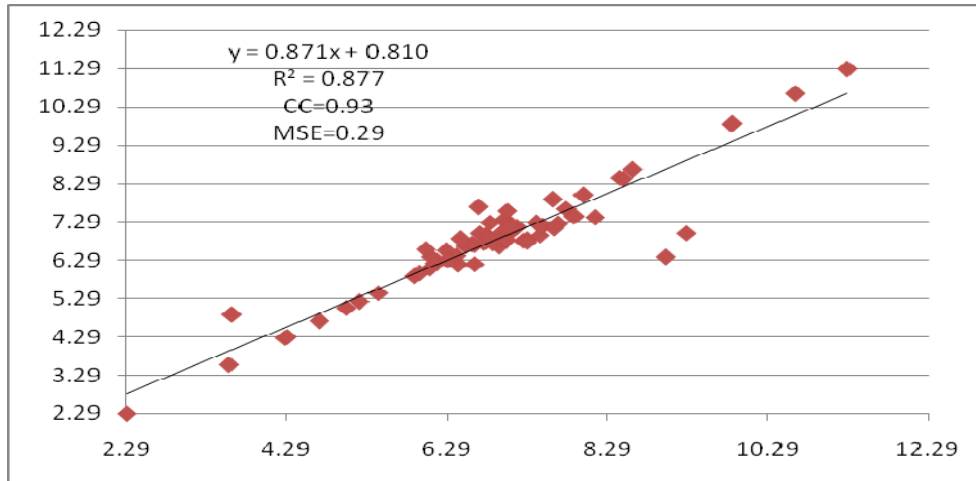


Figure 5.13a Training core porosity vs predicted porosity using GRNN (Logs + Attributes)

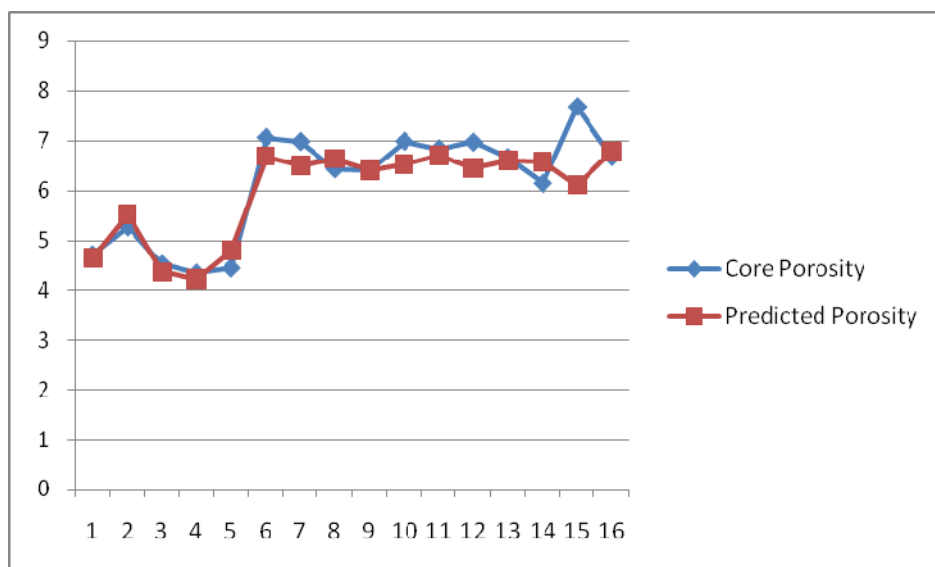
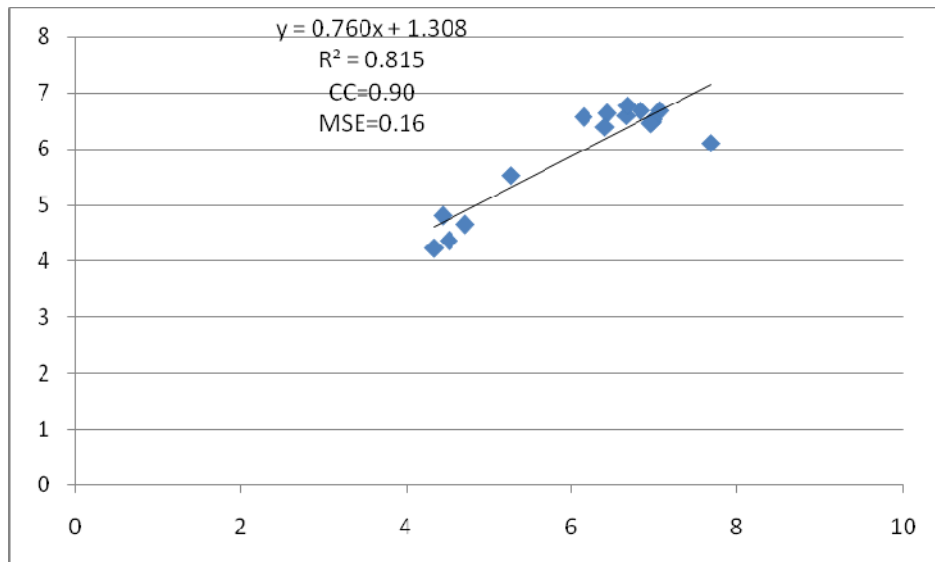


Figure 5.13b Testing core porosity vs predicted porosity using GRNN (Logs + Attributes)

5.4.2 GRNN MODEL FOR PERMEABILITY

A model was built using GRNN to estimate permeability using both seismic attributes and well log data. The results show $CC = 0.99$ and $MSE = 0.32$ in training stage, while testing produced results with $CC = 0.96$ and $MSE = 1.29$. Figures 4.14a and 4.14b show the model performance for permeability prediction.

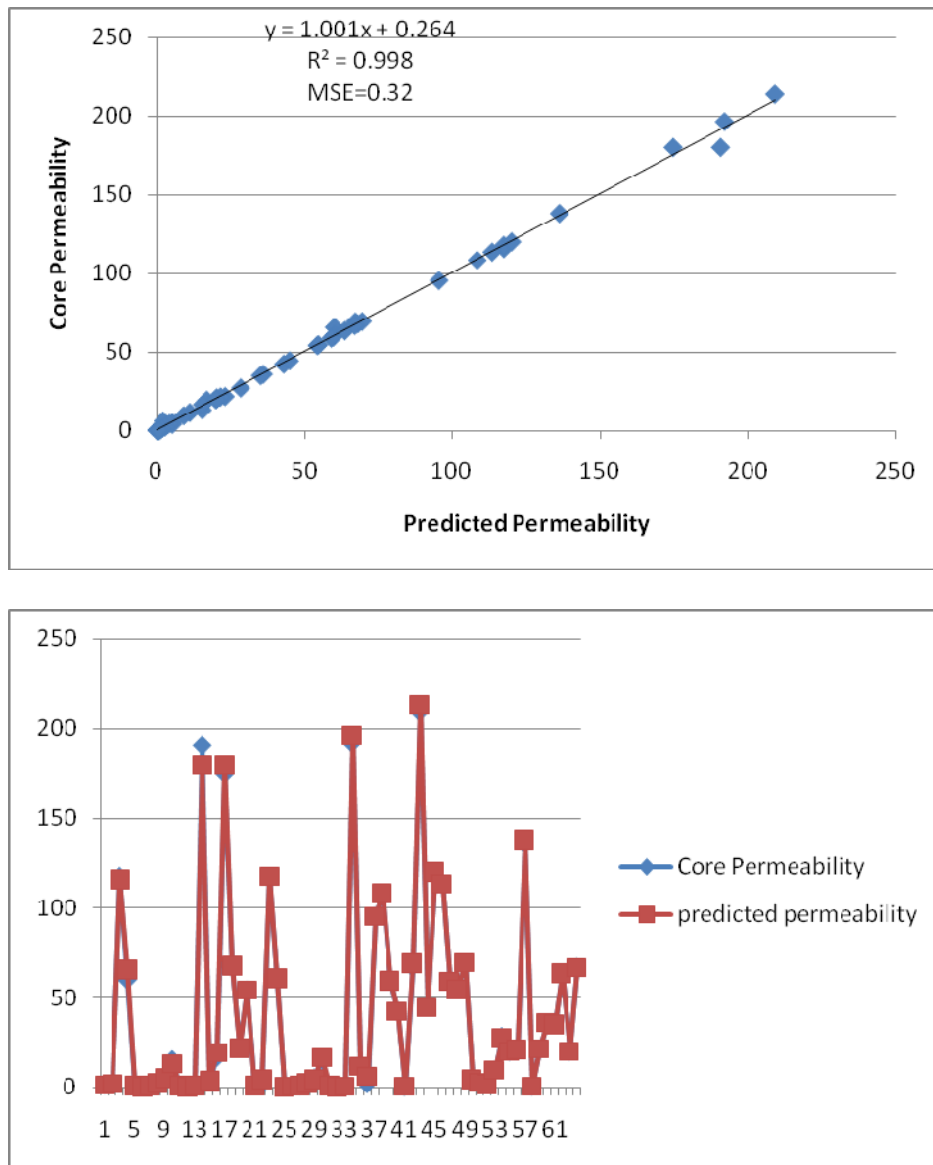


Figure 5.13c Training core permeability vs predicted permeability using GRNN (Logs + Attributes)

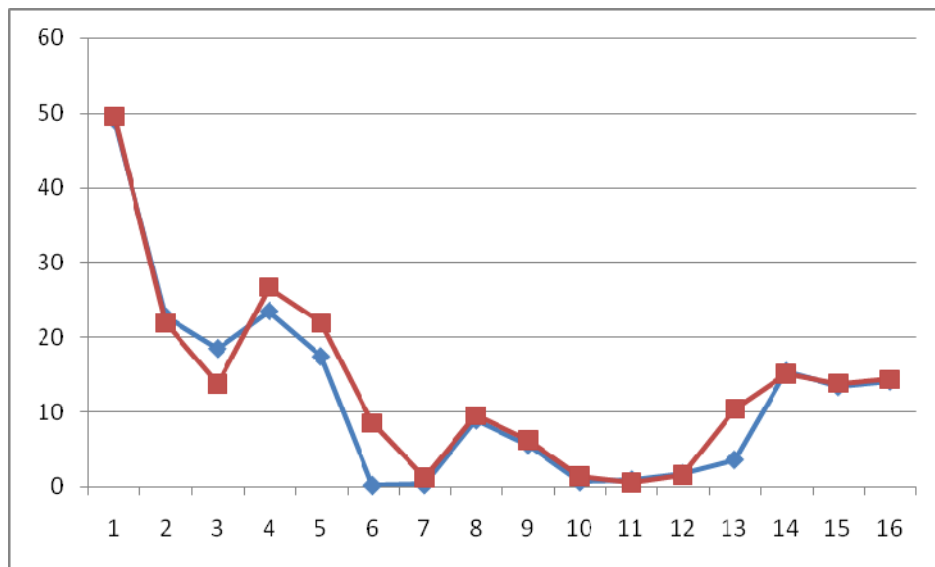
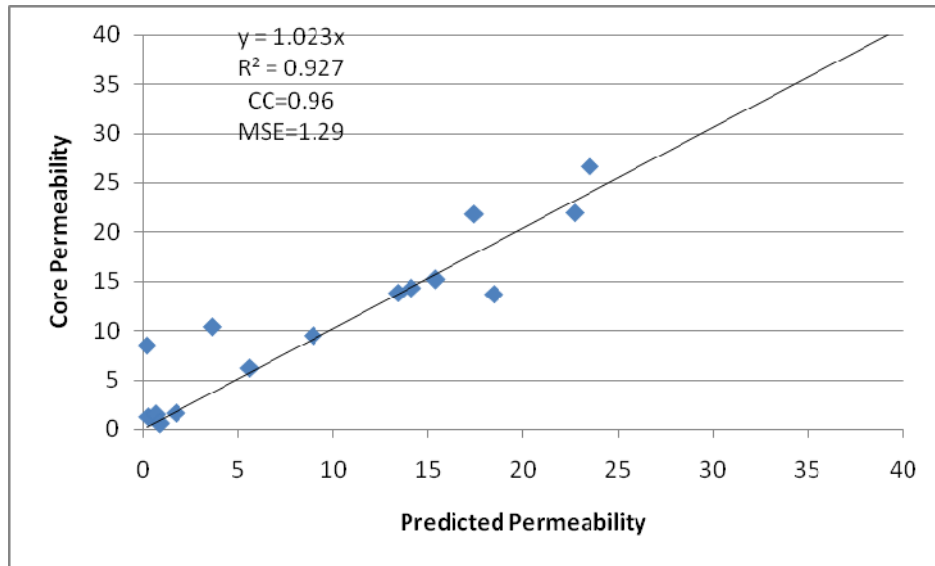


Figure 5.13d Testing core permeability vs predicted permeability using GRNN (Logs + Attributes)

5.5 Prediction of Lithofacies Using ANNs

The last properties which were predicted in this work are the rock types or lithofacies. In this part we used only the log data to estimate lithofacies at the bore hole locations. The same two wells were selected for this purpose. The results are given in Figure 4.14b show a good match between rock types interpreted by geologists and those given by ANNs. Figure 4.14a shows the facies descriptions from well log data.

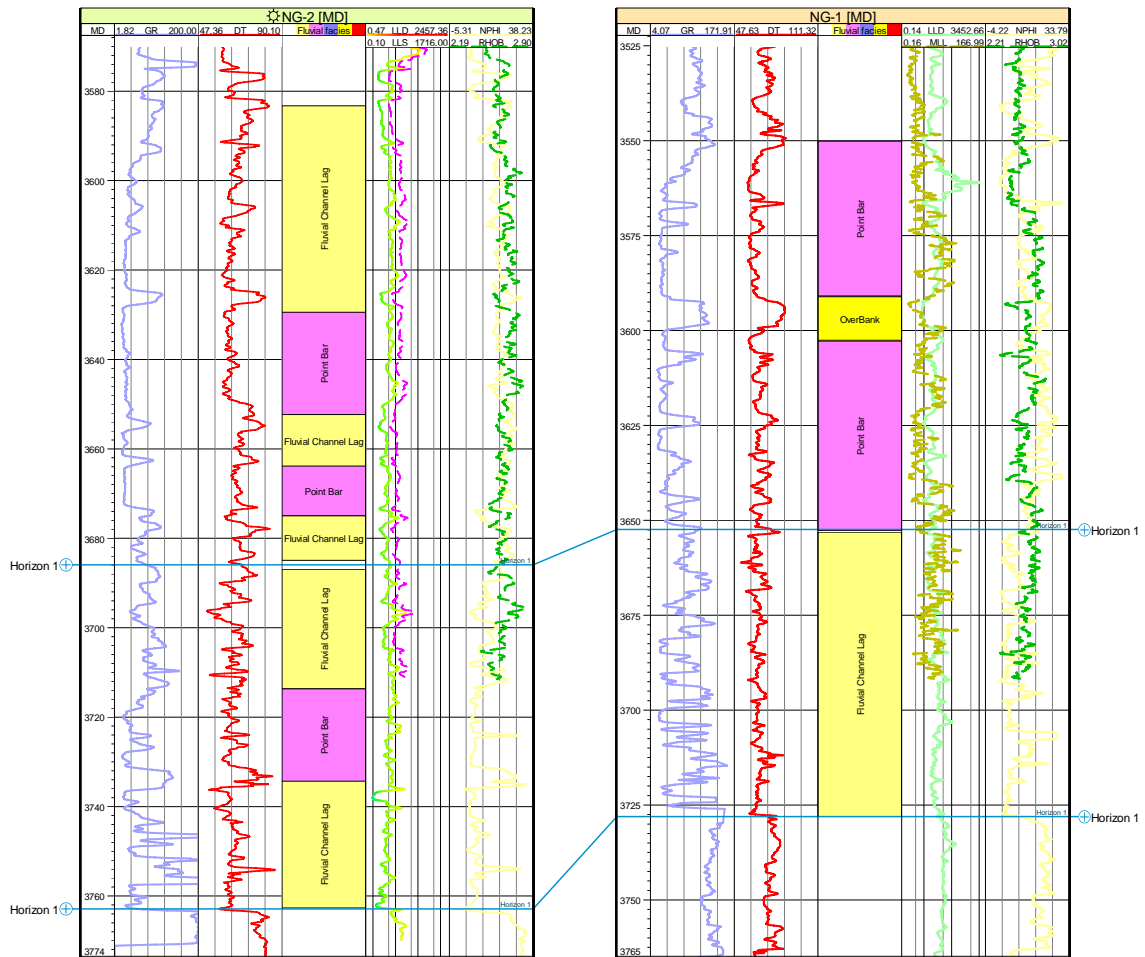


Figure 5.14a Facies Description of well-1 and well-2

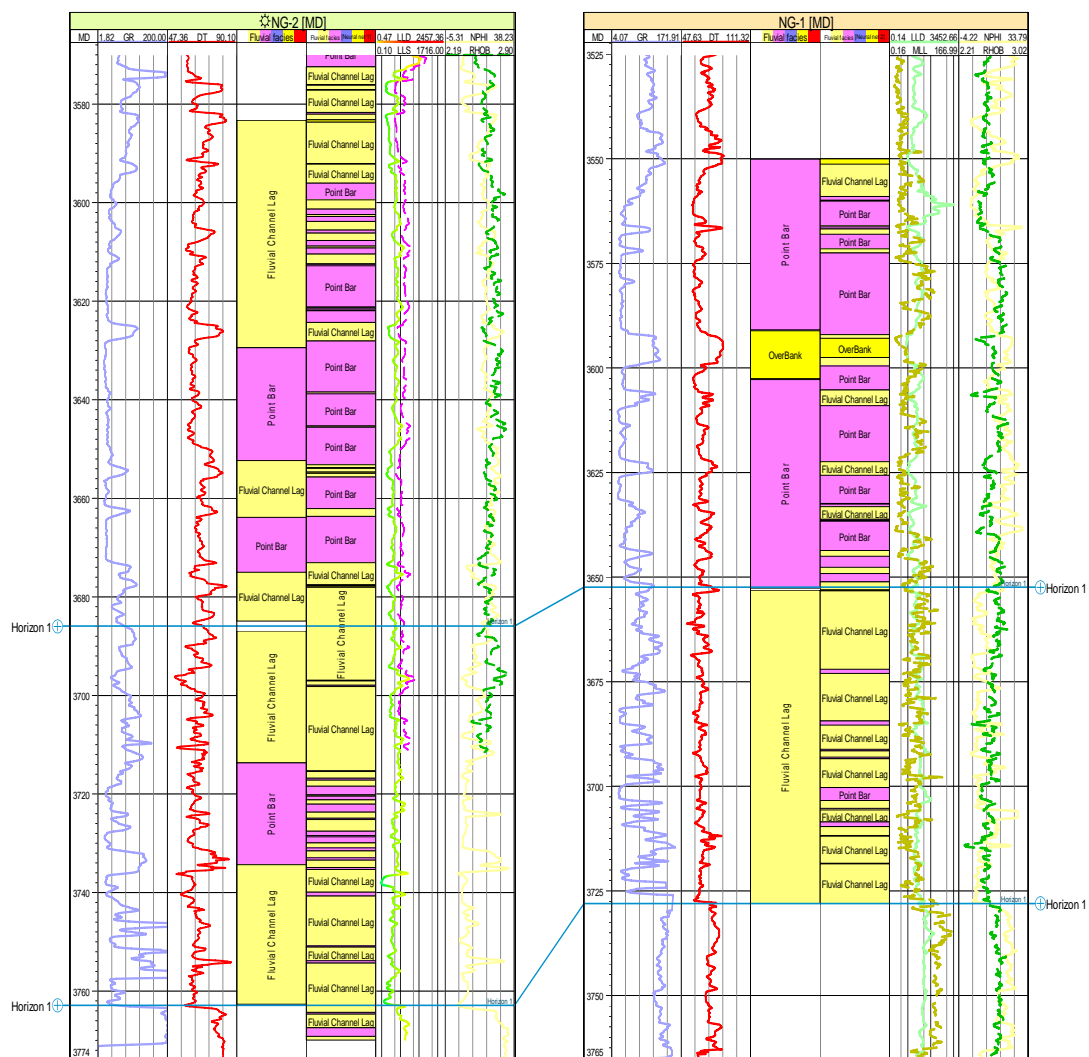


Figure 5.14b Facies Predictions using ANNs

5.6 Predicting the Spatial Distribution of Porosity, Permeability and Lithofaces

The last part of this study is to build a 3D model for porosity, permeability and rock type for a given reservoir. Petrel software from Schlumberger was used to build the 3D grid from the interpreted seismic surfaces. The model was built using the top and the bottom of the reservoir. Figure 4.15 shows the seismic interpretation of the three main reservoirs existing in the study area.

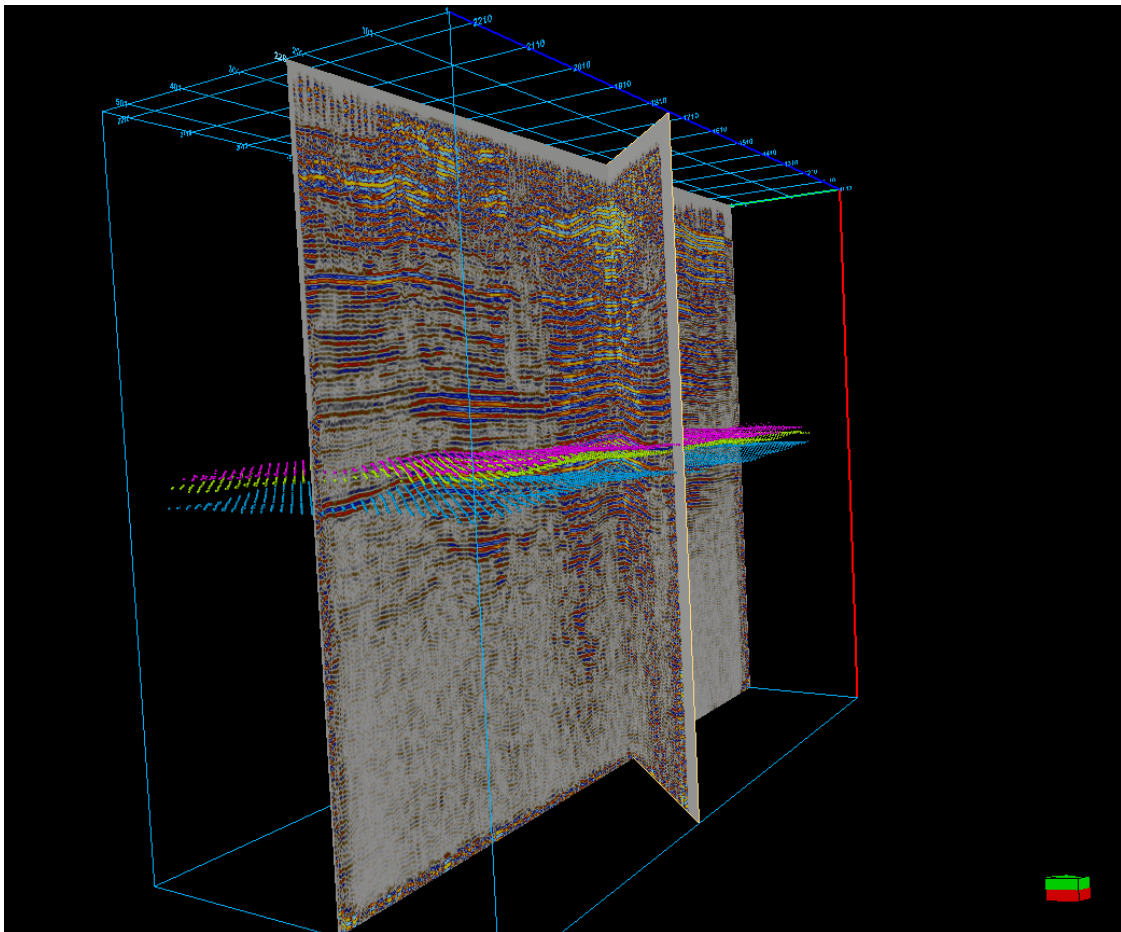


Figure 5.15 Seismic Interpretation of T1, SI and Dev reservoirs in the study area

5.6.1 Porosity Models

Figure 4.16 shows the histogram of porosity distribution. Figure 4.16a shows the porosity model for the given reservoir, while Figures 4.16b and 4.16c present the porosity distribution from 10% to 30 % and from 0% to 9.9% separately.

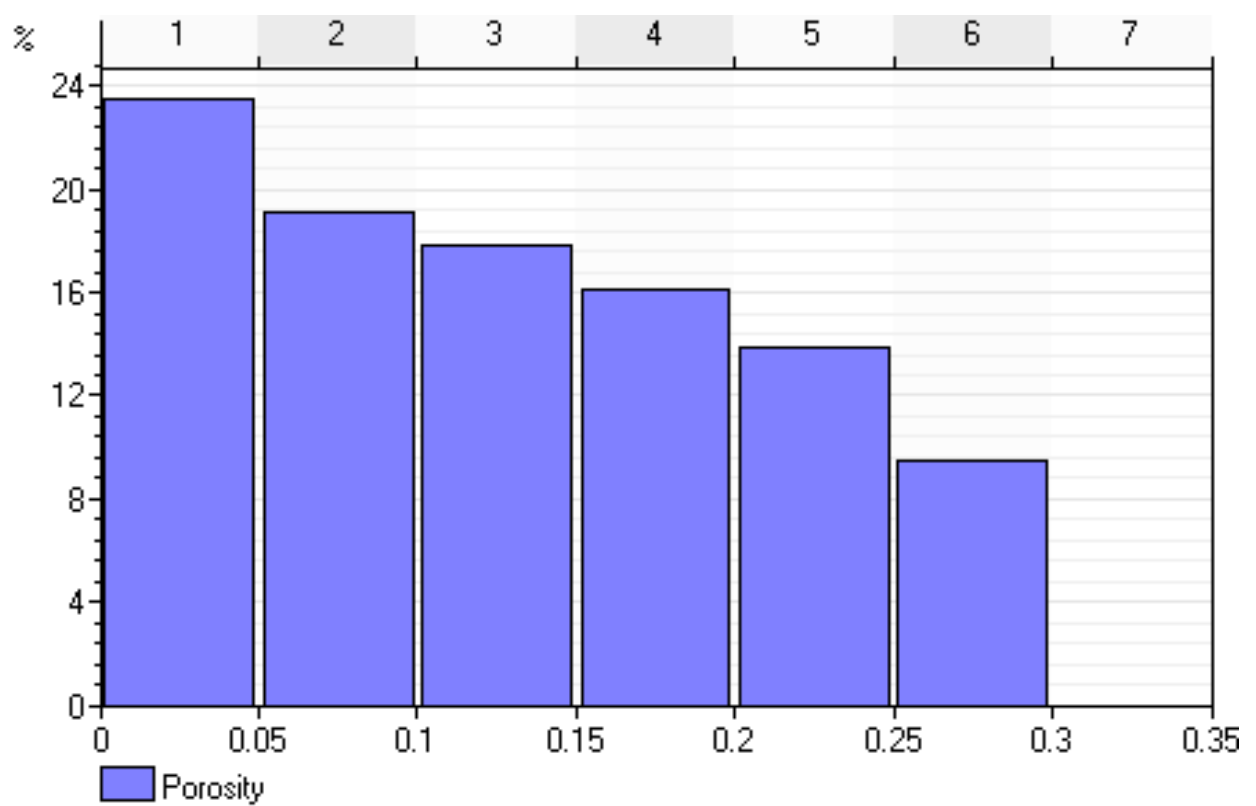


Figure 5.16a Histogram of the porosity distribution

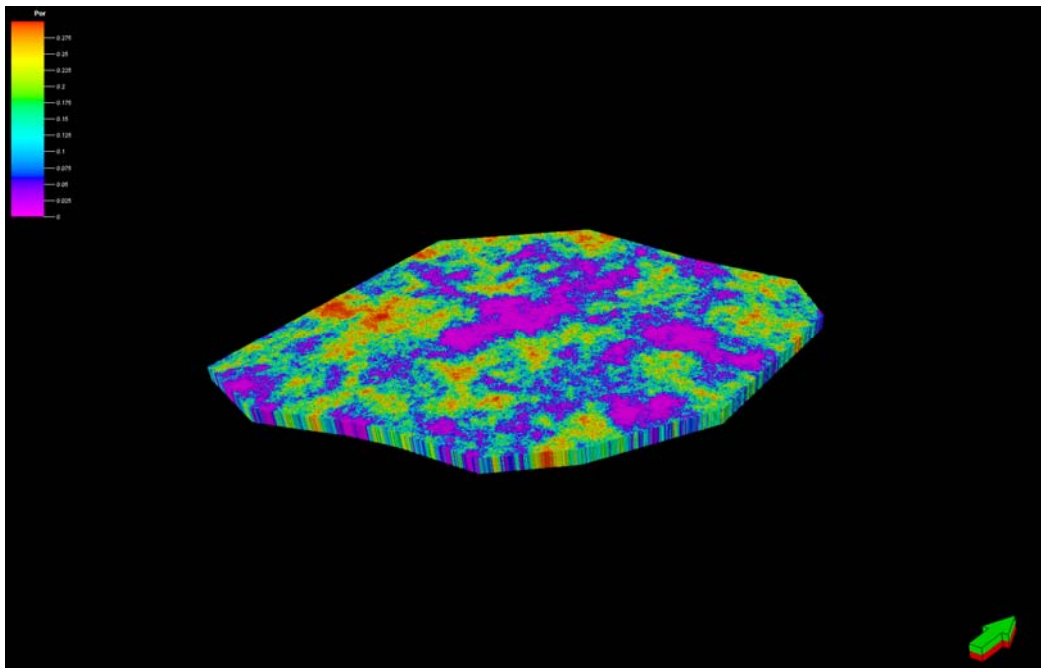


Figure 5.16b Porosity distributions in the 3D model for SI Reservoir, pink color indicates low porosity, red color indicates high porosity

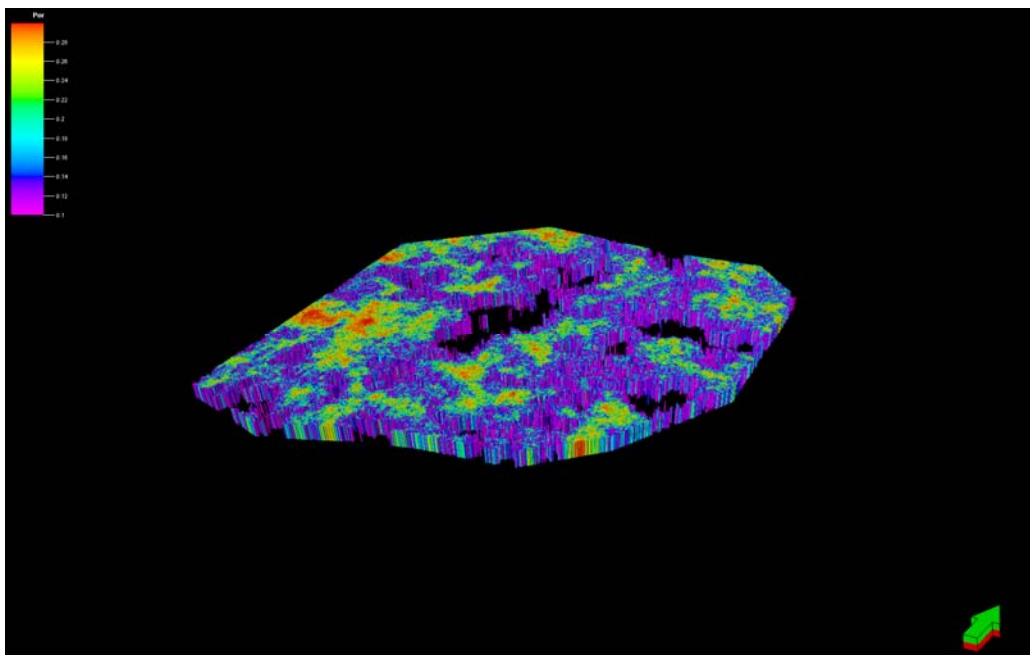


Figure.5.16c Porosity (10% - 30 %) distribution in the 3D model for SI Reservoir, pink color indicates low porosity, red color indicates high porosity

5.6.2 Permeability Models

Figure 4.17 shows the histogram of permeability distribution. Figure 4.17a illustrates permeability model obtained using ANNs, while Figure 4.17b shows permeability distribution from 10 mD to 300mD.

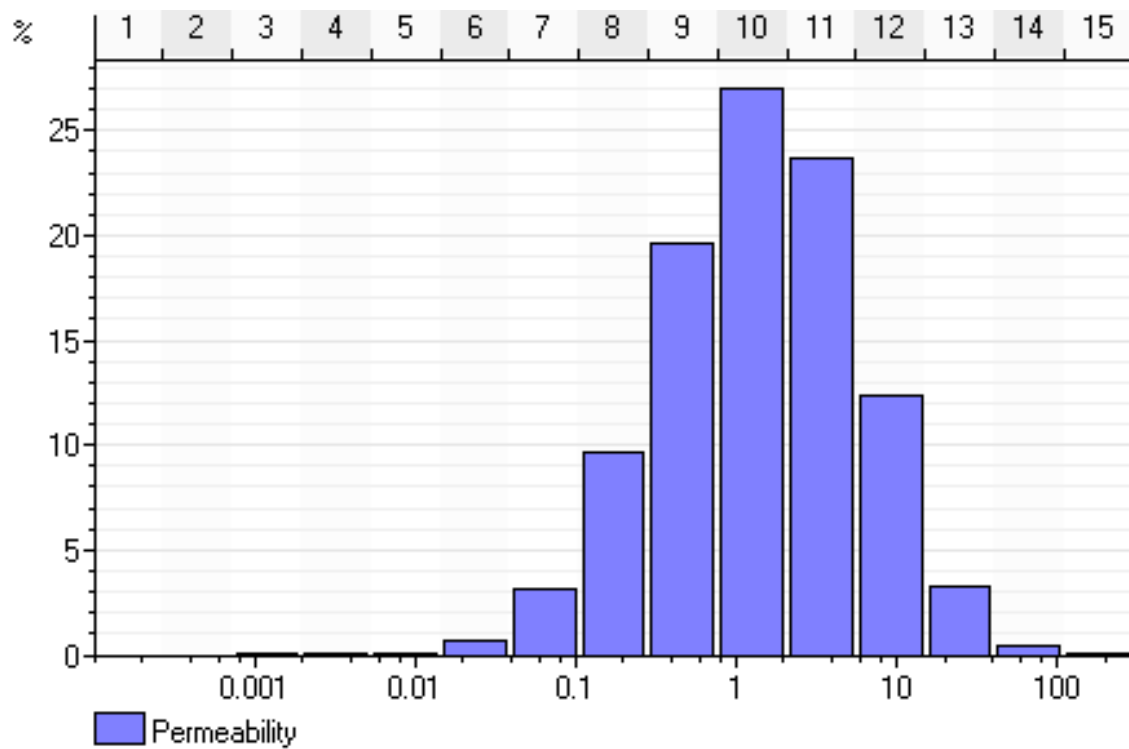


Figure 5.17 Histogram of permeability distribution

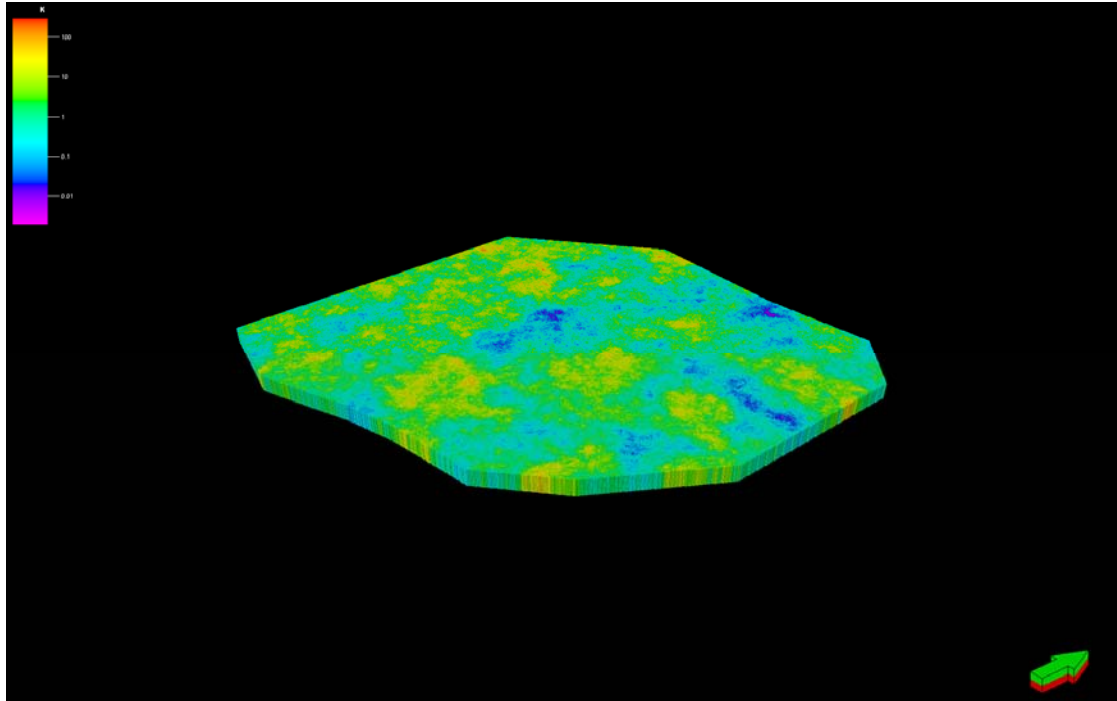


Figure 5.17 a. Permeability Distribution in 3D model for SI Reservoir, pink color indicates low permeability, red color indicates high permeability

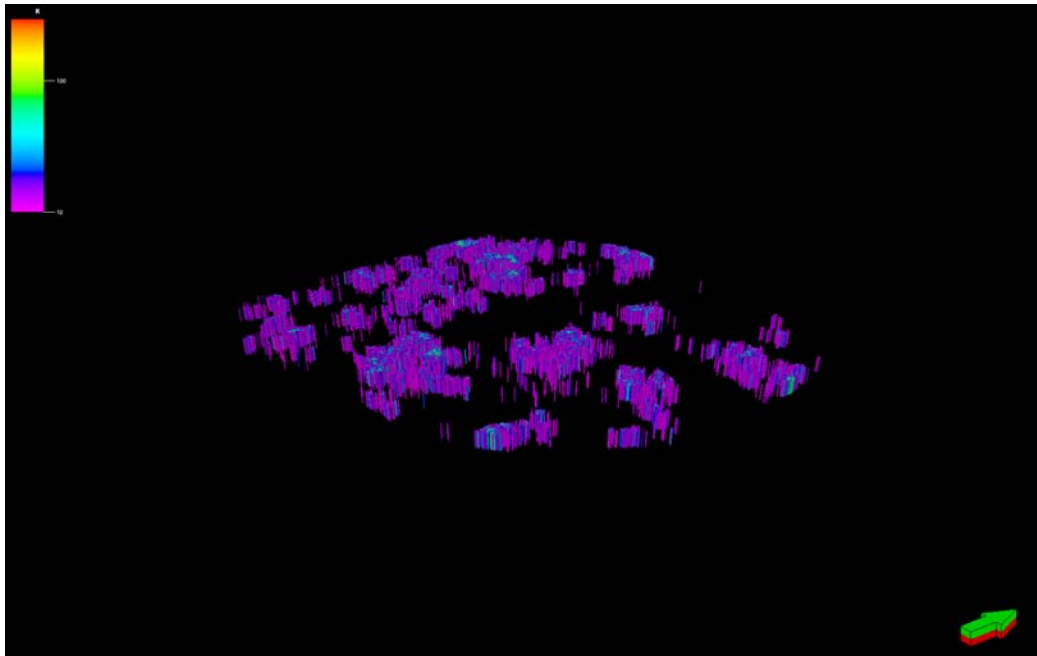


Figure 5.17b .Permeability (10-300 mD) distribution for SI Reservoir, pink color indicates low permeability, red color indicates high permeability

5.6.3 Lithofacies models

The histogram of facies distribution is illustrated in Figure 4.18. Figures 4.18a, 4.18b, 4.18c and 4.18d show the 3 D model of the different facies (channel lag, point bar and overbank) existing in this field.

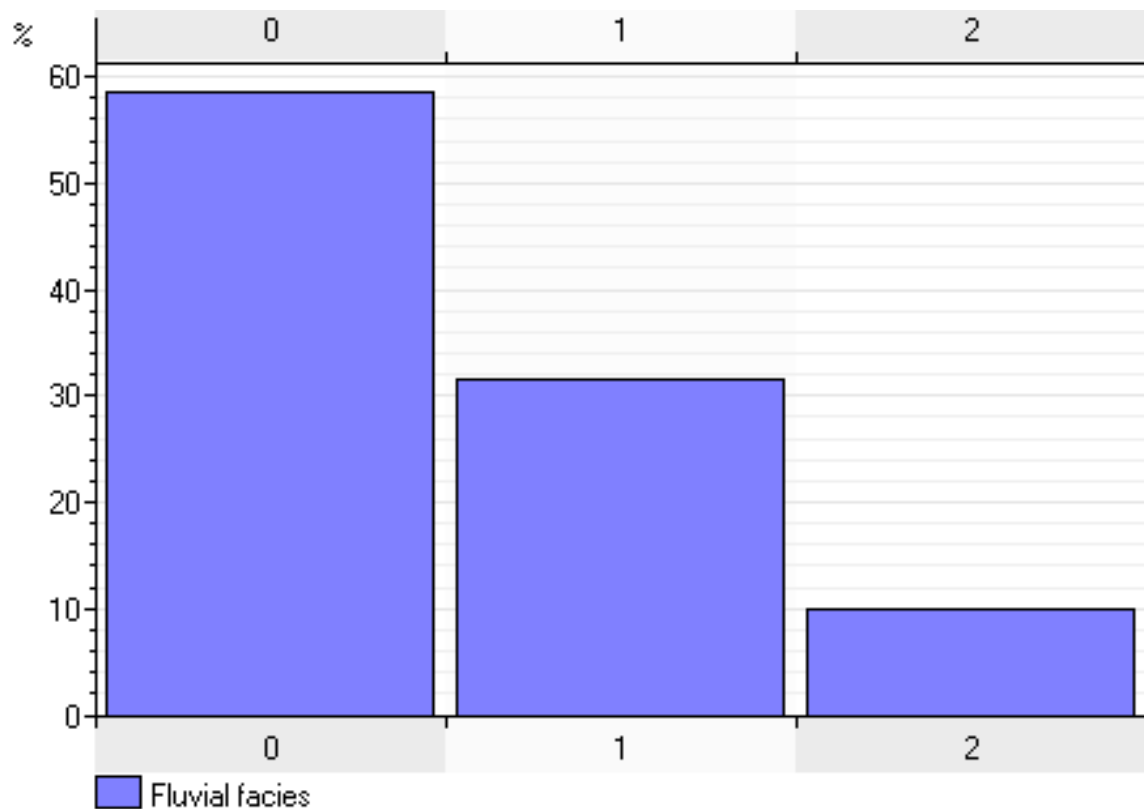


Figure 5.18 Histogram of facies distribution ,with 0 channel lag, 1 point bar and 2 overbank

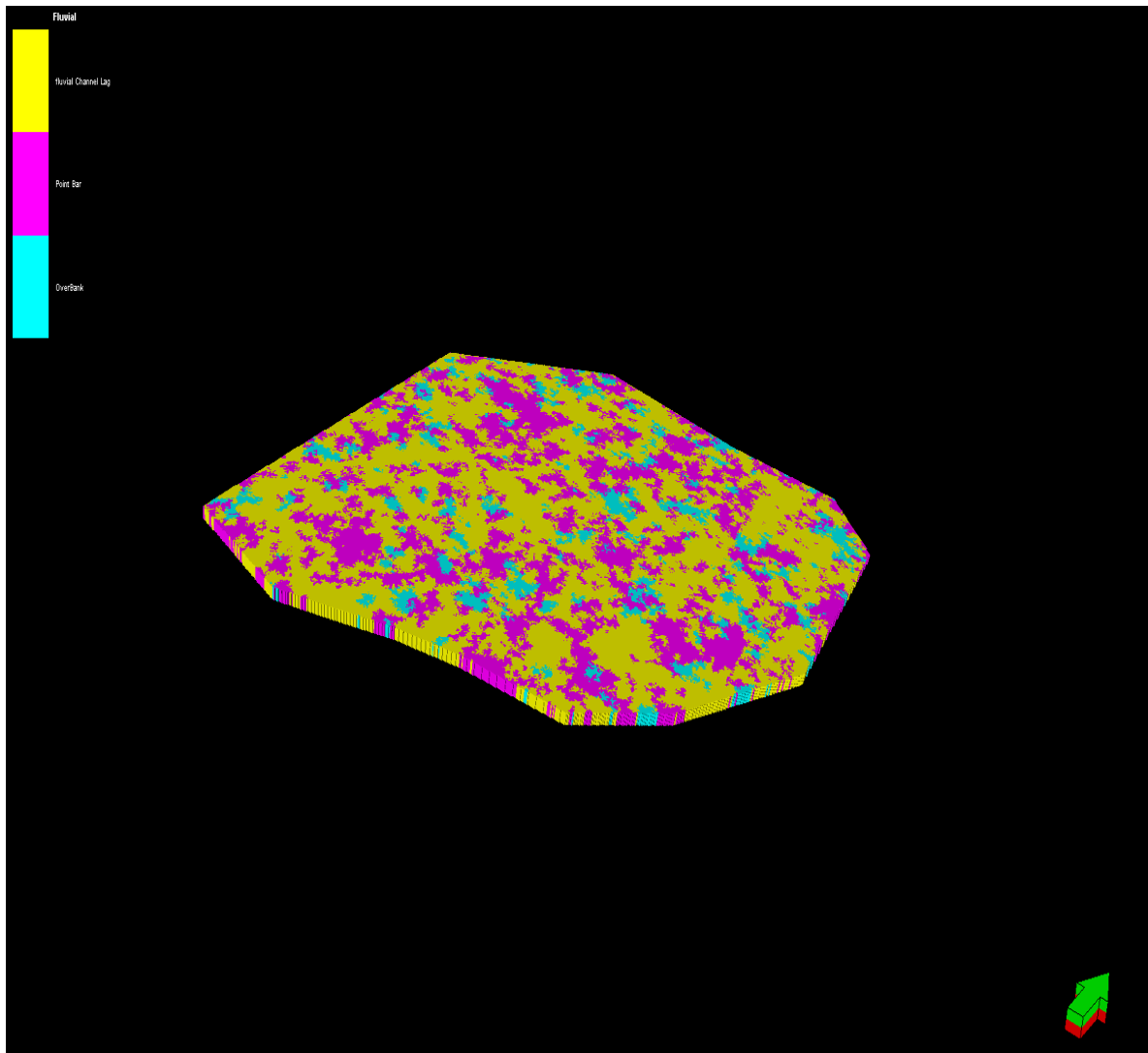


Figure 5.18a Facies model for SI Reservoir , blue color indicates overbank, pink color point bar and yellow indicates channel lag

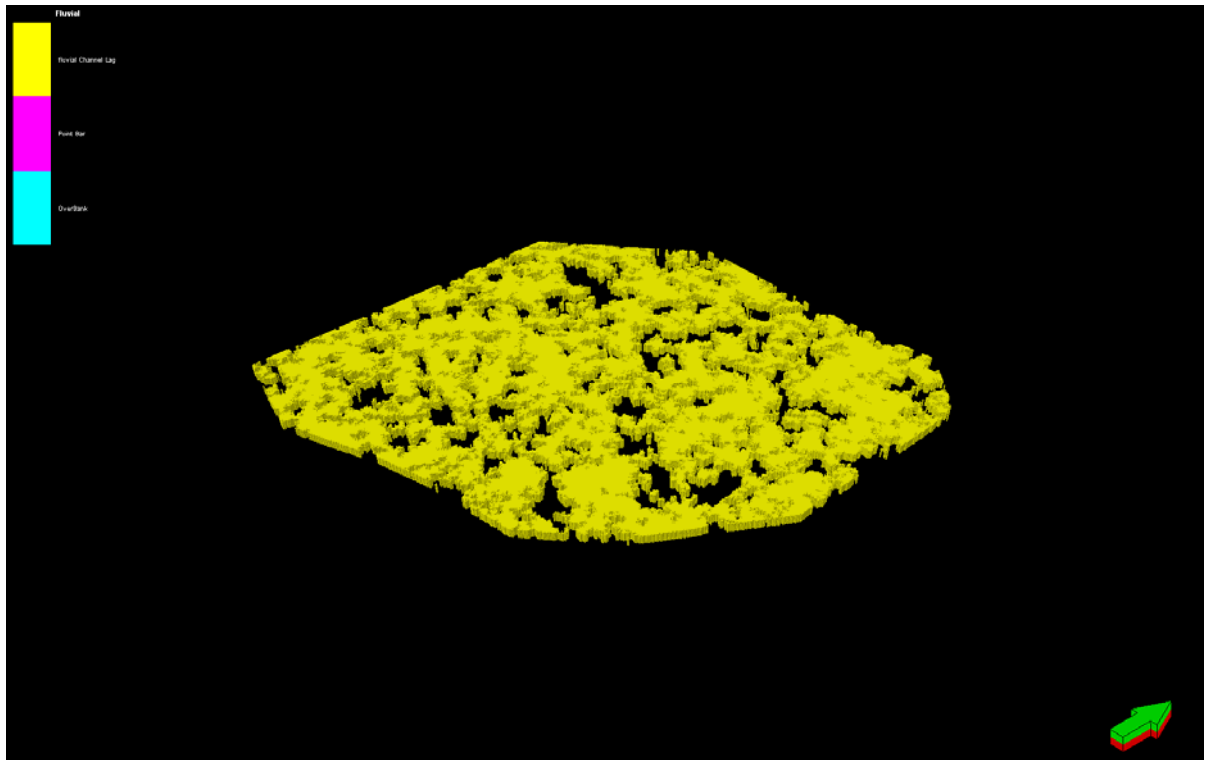


Figure 5.18b Channel lag distribution in SI Reservoir

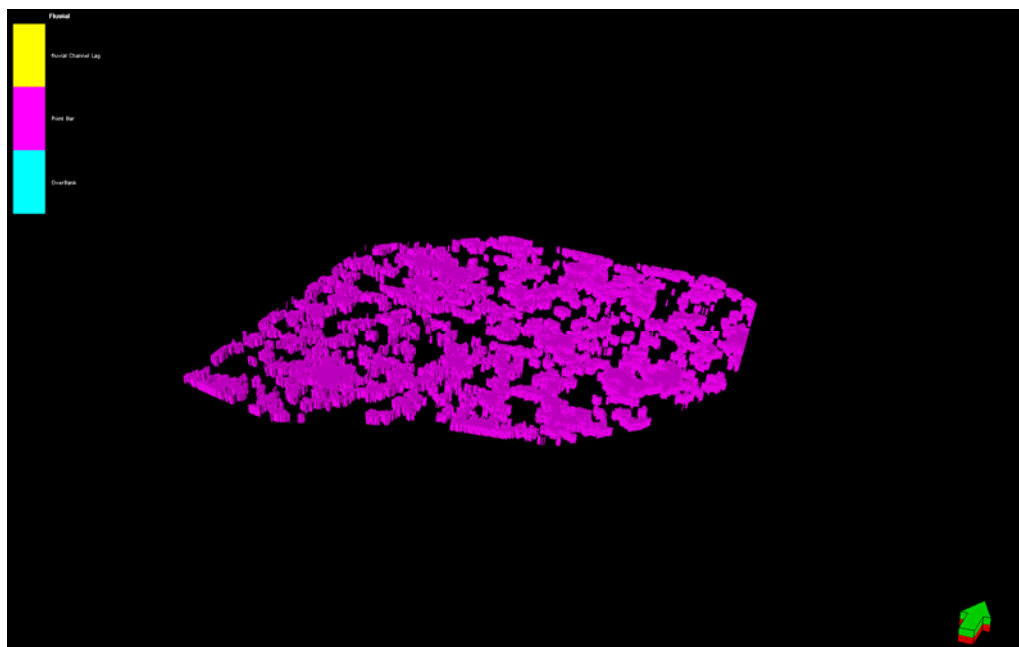


Figure 5.18. c. Point bar distribution for SI Reservoir

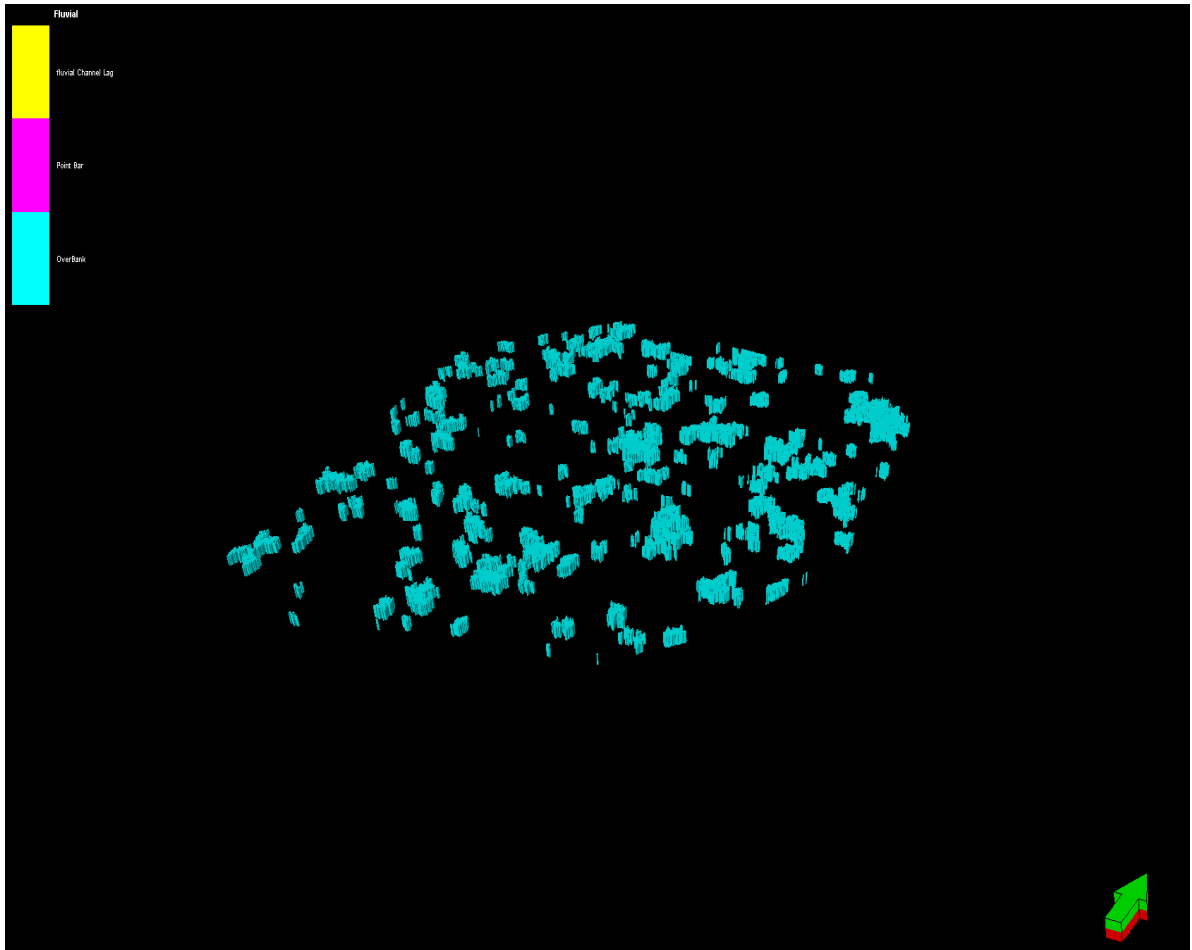


Figure 5.18d Over bank distribution for SI Reservoir

CHAPTER SIX

CONCLUSION AND RECOMMENDATIONS

6.1 Summary

This research work investigated the application of two paradigms in neural networks in developing accurate models for the prediction of reservoir properties (porosity, permeability and lithofacies).

The first part of this study focused on designing and investigating multilayer perceptron (MLP) and general regression neural networks (GRNN) for the prediction of these reservoir properties using well log data.

From the previous part we selected the best algorithm (GRNN) and we used it to predict porosity and permeability using seismic attributes derived from 3D seismic volume.

In the third part, we integrated seismic attributes with well log data for better prediction of reservoir properties.

The last part of this study was to build 3D models for the predicted properties (porosity, permeability and lithofacies).

6.2 Conclusions

Based on the research and analysis discussed previously in this work, the following conclusions are reached:

- Porosity, permeability and lithofacies can be easily predicted using well log data rather than coring every well in the field.
- The agreement between the core data and the predicted values by neural networks demonstrate a successful implementation and validation of the network's ability to map complex non-linear relationships between well logs, seismic attributes, permeability and porosity.
- Results from this study show how powerful general regression neural network (GRNN) is compared to multilayer perceptron (MLP).
- Multilayer perceptron (MLP) can have good generalization if there is enough time and knowledge of the network topology.
- The use of seismic attributes combined with well log data gave better prediction results and enhanced the results reached by using well logs only.
- The 3D geological models gave the full distribution of reservoir properties and indicated the appropriate zones for future well implementation.

6.3 Recommendations for Future Work

Although good results were obtained from the investigation carried out in this research work, better accuracy and generalization may be obtained from the following recommendations:

- Investigating using new development of neural network techniques such as function networks (FN) and Cascaded correlation neural network (CCNN).
- Using other techniques in artificial intelligence such as support vector machine (SVM) , fuzzy logic (FL) and neuro-fuzzy systems (NFL).
- Investigating combined networks in the form of committee machine or modular networks where different networks such as Ploynet, FN and GRNN are combined. These three models were suggested because of the unique results that can be obtained from them. However, many factors need to be considered in developing such architecture, including:
 - 1- There are several different methods of combining networks, depending on the task at hand.
 - 2- Determination of training strategy for different networks to achieve more accurate network model can be challenging. For example, do we train each network with the same data set, or different data sets, with overlapping or without overlapping?
 - 3- Determination of the techniques to combine is also not an easy task.
 - 4- Model complexity versus gained accuracy is another factor to consider.

It is also recommended to integrate more data for more accurate predictions such as petrography data (Grain size, Sorting , percentage of cements, grain shape...ect). It is hoped that implementation of these recommendations will lead to better models for the prediction of rock properties.

References

- 1) AL-Bazzaz, W. H, Y. W. Al-Mehanna, A. Gupta, Permeability Modeling Using Neural-Networks Approach for Complex Maaddud-Burgan Carbonate Reservoir *SPE* 105337, 2007.
- 2) Ali .K, Neural Networks: A New Tool for the Petroleum Industry, *SPE* 1994.
- 3) Aminzadeh, F. and Brouwer, F. Integrating Neural Networks and Fuzzy Logic for Improved Reservoir Property Prediction and Prospect Ranking. *SEG New Orleans 2006 Annual Meeting*.
- 4) Asquith, G. and Gibson, Ch., *Basic Well Log Analysis for Geologists. AAPG Methods for Exploration Series*, Number 3. 1982.
- 5) Basu Tanwi, Michel Claverie, and David Noland, Kamarolzaman B. Yahya and Mustafa Suleiman, Facies Analysis: Integration of Core and Log Data using a Neural Networks as Input for Reservoir Modeling in Betty Field, Malaysia. *The Leading Edge*, v. 23; no. 8; pp. 794-797, 2004.
- 6) Baldwin, J. L. , Bateman, A. R. M. , Wheatley, C. L. , 1990. Application of Neural Network to the Problem of Mineral Identification from Well Logs. *The Log Analyst* 3, pp. 279–293.
- 7) Balan, B. , Mohaghegh, S. , Ameri, S. , 1995. State-of-the-Art in Permeability Determination from Well Log Data: Part I. Comparative study, model development. *SPE Eastern Regional Conference and Exhibition*, West Virginia, pp. 17–21.
- 8) Bean M. and Jutten C., 2000. Neural Networks in Geophysical Applications. *Geophysics*, 65, pp. 1032-1047.

- 9) Bel F. and Demargne F,1996. Etude Géologique du Terminal ANRH, Alger, Algérie, pp. 22.
- 10) Bellaoueur. A, 2008. Etude hydrogéologique des eaux souterraines de la région de Ouargla soumise a la remontée des eaux de la nappe phréatique et perspectives de solutions palliatives. Mémoire de Magister, L'université El-Hadj lakhdar, Batna, Algerie.
- 11) Bhatt A. and Helle H. B, 2002. Committee Neural Networks for Porosity and Permeability Prediction from Well Logs. *Geophysical Prospecting*, 50, pp. 645-660.
- 12) Black, M.: Reasoning with Loose Concepts. *Dialogue* (2) 1–12 (1963).
- 13) Brown, A.R., 1996, Seismic attributes and their classification. *The Leading Edge*, 15, p.1090.
- 14) Brown, A. R., 2001, Understanding seismic attributes: *Geophysics*, 66, pp. 47-48.
- 15) Busson.G, 1970. Principes, Méthodes et Résultats d'une étude stratigraphique du Mésozoïque saharien. *Mémoire Muséum Histoire Naturelle Paris, série C XXVI* (1972), p. 441.
- 16) Chang H.C., Kopaska-Merkel D. C., Chen H.C. and Durrans S. R., Lithofacies Identification using Multiple Adaptive Resonance Theory Neural Networks and Group Decision Expert System, *Computers and Geosciences*, 26, Number 5, 1 June 2000, pp. 591-601.
- 17) Chen, Q. and Sidney, S.,1997, Seismic attribute technology for reservoir forecasting and monitoring. *The Leading Edge*, 16, No.5, pp. 445-450.

- 18) Cheng Dang Zou, Xi-Ling Wu, and Ju-An Cheng, Determination of Reservoir Properties using a Fuzzy Neural Network, *SPE* 26430, *68th Annual Technical Conference and Exhibition*, Houston, Texas, 3-6 October 1993.
- 19) Christian Perrin, Mohamed Rafik, Mahmoud Akbar, Samir Jain, Integration of Borehole Image to Enhance Conventional Electrofacies Analysis in Dual Porosity Carbonate Reservoirs, *SPE* 11622, *International Petroleum Technology Conference*, Dubai, UAE 4-6 December 2007.
- 20) Daniel J. Leiphart and Bruce S. Hart, Case History Comparison of Linear Regression and Probabilistic Neural Network to Predict Porosity from 3-D seismic Attributes in Lower Brushy Canyon Channel Sandstones, Southeast New Mexico, *Geophysics*, Vol.66, No. 5, 2001, pp. 1349-1358.
- 21) Djabbar Tiab and Erle. C. Donaldson, *Petrophysics. Theory and Practice of Measuring Reservoir Rock and Fluid Transport Properties*. 1996 Gulf Publishing Company, Houston, Texas.
- 22) Doyen, P. M., 1998, Porosity from seismic data -A geostatistical approach: *Geophysics*, 3, pp. 1263-1275.
- 23) Dubief, J., 1963. *Le climat du Sahara*. Memoire Institut des Recherches Sahariennes. Tome 1 & 2, Alger, 317 + 275 pp.
- 24) Eshafei, M. and Gharib, M., Neural Network Identification of Hydrocarbon Potential of Shaly Sand Reservoirs , *Technical Symposium SPE*, 2007 .
- 25) Fabre, J, 1976. *Introduction à la Géologie du Sahara algérien*. SNED, Alger, Algerie, 422 pp.

- 26) Fruhwirth R.K., Thonhauser, G. and W. Mathis, Hybrid Simulation using Neural Networks to Predict Drilling Hydraulics in Real Time. *SPE Paper* 103217, SPE Annual Technical Conference and Exhibition, San Antonio, Texas, U.S.A., 24–27 September 2006.
- 27) Garrouch, N. and Smaoui, H., An Artificial Neural Network Model for Estimating Tight gacs sand Permeability, *SPE* 39703, 1994.
- 28) Geology of Algeria, Sonatrach Exploration Division, Research and Development Centre and Petroleum Engineering and Development Division. pp 93.
- 29) Guangyi Hu, Xuri Huang, Mingxiang Mei, Li Gu and Chaozheng Xiao, Characterization of a Reef Reservoir Permeability using Well and Seismic Data, *SPE 110179*, SPE Annual Technical Conference and Exhibition, California, USA, 11-14 November, 2007.
- 30) Jeff Heaton, *Introduction to Neural Networks with Java*. Heaton Research, Inc., 2005.
- 31) Hampson, D.P., Schuelke, J.S., and Quirein, J.A., 2001, Use of multiattribute transforms to predict log properties from seismic data: *Geophysics*, v. 66, pp. 220-236.
- 32) Herrera, V.M., Russell, B., and Flores, A., Neural Networks in Reservoir Characterization, *The Leading Edge*, 25, no. 4 (2006): pp. 402-411.
- 33) Lianshuang Qi, Timothy R. Carr, Neural Network Prediction of Carbonate Lithofacies from Well Logs, Big Bow and Sand Arroyo Creek Fields, Southwest Kansas, *Computers and Geosciences* 32 (2006) pp. 947–964.
- 34) Lucia, F.J., *Carbonate Reservoir Characterization*. Springer, 1999 .

- 35) Mari, J.-L., GlanGeaud, F and Coppens F., *Signal Processing for Geologists and Geophysicists* . Édition Technip, Paris, 1997.
- 36) Masters, T., *Practical Neural Networks Recipes in C++* , Elsevier, 1993.
- 37) Matos, M.C., Osório, P.L.M. and Johann, P.R.S., Unsupervised Seismic Facies Analysis Using Wavelet Transform and Self Organization Maps, *Geophysics*, Vol. 72, No. 1 (2007); pp. 9-21.
- 38) Mial, A.D., *The Geology of Fluvial Deposits: Sedimentary Facies, Basin Analysis and Petroleum Geology*: Springer-Verlag, Berlin, 582 pp., 1996.
- 39) Mohaghegh S., Arefi R., Ameri S. and Rose D., Design and Development of an Artificial Neural Network for Estimation of Permeability, *SPE* 28237, SPE Petr. Computer Conference, Dallas, Texas, USA, July 31 – August 3, 1994.
- 40) Moline, G.R. and Bahr, J.M., Estimating spatial distributions of heterogeneous subsurface characteristics by regionalized classification of electrofacies. *Mathematical Geology* 27, pp. 3–22, 1995.
- 41) Osborne, D. A. Neural Networks Provide More Accurate Reservoir Permeability. *Oil and Gas Journal* , Sept., 1992, pp. 80-83.
- 42) Oss (2003a et b), Système aquifère du Sahara septentrional. Rapport interne. Annexes, Tunis, Tunisie, pp229.
- 43) Ouja M, 2003. Etude sedimentologique et paléobotanique du jurassique moyen-crétacé inférieur du bassin de Tataouine. Phd, Université Claude Bernard. Lyon, pp164.
- 44) Raiche, A., A Pattern Recognition Approach to Geophysical Inversion using Neural Nets. *Geophysical Journal International* 105, pp. 629–648, 1991.

- 45) Rivera Vega Nestor, *Reservoir Characterization using Wavelet Transforms*. Texas A and M University Thesis, 2003.
- 46) Rogers, S.J., Fang, J.H., Karr, C.L. and Stanley, D.A., Determination of lithology from well logs using a neural network. *American Association of Petroleum Geologists Bulletin* 76 (1992): pp. 731–739.
- 47) Russell, B., Vagueness. *Austrian Journal of Philosophy* (1) (1923) pp. 84-92.
- 48) Salan B., Mohaghegh S. and Ameri S., Permeability Determination from Well Log Data: A Comparative Study, Model Development. *SPE* 30978, 1995.
- 49) Saggaf, M.M., Toksöz, M.N. and Marhoon, M.I., Seismic Facies Classification and Identification by Competitive Neural Networks, *Geophysics* ,Vol. 68, No. 6 (November-December 2003); pp. 1984-1999.
- 50) Schutz, P.S Hattori, M and Corbett, C., 1994, Seismic guided estimation of log properties, parts 1,2, and 3: The Leading Edge,13,305-310,674-678, and 770-776.
- 51) Sheriff, R.E., 1992, *Reservoir Geophysics*, IG No.7, Edited By SEG, 408pp.
- 52) Sippel, M., Reservoir Characterization from Seismic and Well Control with Intelligent Computing Software, *AAPG Annual Convention*, Salt Lake City, Utah, May 11-14, 2003.
- 53) Soto, R.B., Bernal, M.C. and Silva, B., How to Improve Reservoir Characterization using Intelligent Systems. *SPE* 62938, 2000.
- 54) Soto, R., Torres, B.F., Arango, S. and Cobaleda, G., Improved Reservoir Permeability Models from Flow Units and Soft Computing Techniques. A Case Study, Suria and Reforma-Libertad, *SPE* 69625, 2001.

- 55) Taner, M.T., Koehler, F., and Sheriff, R.F., 1979, Complex seismic trace analysis. *Geophysics*, 44,1041-1063.
- 56) Taner, M.T., Schuelke, J.S., O'Doherty, R., Baysal, E., 1994, Seismic attributes revisited: 64th Annual Internal Mtg, SEG., Expanded Abstracts, 1104-1106.
- 57) Tamhane, P., Wong, M., and Aminzadeh, F., Soft Computing for Intelligent Reservoir Characterization, *SPE* 59397, 2000.
- 58) Trappe H and Hellmich C., 1998, Seismic characterization of Rotliegend reservoir; from bright spots to stochastic simulation: *First Break*, 16, pp. 79-87.
- 59) Van der Baan, M. and Jutten, Ch., Neural Networks in Geophysical Applications. *Geophysics*, Vol. 65, No. 4 (2000); pp. 1032-1047.

VITAE

Mohamed Sitouah was born on September 02,1978 in Bordj Menail Algeria. He graduated from Boumerdes University in 2002 with bachelor degree in Geophysics.

He then joined the Algerian Company of Geophysics (ENAGEO) as Geophysicist and worked there till January 2007. Mohamed Sitouah joined earth Sciences Department at King Fahd University of Petroleum & Minerals in February 2007, as a Research assistant and completed his Master of Science (MSc) majoring in Geophysics in June 2009.

His areas of research include:

- 1- Seismic acquisition & Quality Control.
- 2- Seismic Data Processing (Promax, SU).
- 3- Reservoir Characterization
- 4- Reservoir Geophysics
- 5- Reservoir Monitoring (4 D Seismic)
- 6- Well Logging Interpretation
- 7- Geostatistical Modeling
- 8- Geological Modeling